

# Fundamentals, present status and future perspective of TOPCon solar cells: A comprehensive review



Dibyendu Kumar Ghosh<sup>a</sup>, Sukanta Bose<sup>a</sup>, Gourab Das<sup>a</sup>, Shiladitya Acharyya<sup>a</sup>, Anupam Nandi<sup>a</sup>, Sumita Mukhopadhyay<sup>a\*</sup>, Anindita Sengupta<sup>b</sup>

<sup>a</sup> School of Advanced Materials, Green Energy and Sensor Systems (SAMGESS), Indian Institute of Engineering Science and Technology (IIEST), Shibpur, Howrah, India

<sup>b</sup> Department of Electrical Engineering, Indian Institute of Engineering Science and Technology (IIEST), Shibpur, Howrah, India

## ARTICLE INFO

**Keywords:**  
 Tunnel oxide  
 Polysilicon  
 Passivated contact  
 Interface passivation  
 TOPCon  
 POLO

## ABSTRACT

Solar photovoltaics researchers have devoted enough time to improve the performance of various types of high efficiency crystalline silicon based solar cells including passivated emitter rear cells, heterojunction with intrinsic thin-layer solar cells, interdigitated back contact solar cells, heterojunction with interdigitated back contact solar cells and tunnel oxide passivated contact solar cells. Out of these various high efficiency solar cells, tunnel oxide passivated contact (TOPCon) solar cells are gaining more interests due to possessing various advantages such as availability of raw material, easy process sequence, high efficiency potential etc. In this review article, we shall discuss the evolutionary development of this high efficiency TOPCon solar cell, the progress made by the researchers in various aspects to improve the cell efficiency, current status of commercialization and finally future scopes of works with possible challenges.

## 1. Introduction

Discovery of solar photovoltaic effect i.e., the direct conversion of sunlight into electricity is undoubtedly considered as one of the best findings in modern science [1]. Besides, successful development of first real solar cell by Bell Labs in 1954 has been able to endorse the research activities by a considerable margin for various explorations in the field of solar photovoltaics [2]. Consequently, different types of solar cell structures have been designed based on various semiconductor materials but standard Al BSF (Back Surface Field) crystalline silicon solar cells dominated the market share over a longer period of time due to possessing numerous advantages such as abundance of raw material, availability of easy fabrication technologies, high throughput, low maintenance, low running cost etc. [3,4]. However, two major drawbacks namely high back surface recombination velocities at p-p<sup>+</sup> interface and low back surface reflectance limit the efficiency potential of this structure [4]. As a result, the present day researches on crystalline silicon based solar cells are exclusively focusing to simplify the processing steps as well as maximize the power output of other high efficiency crystalline silicon based solar cells such as HIT (Heterojunction with Intrinsic Thin Layer) solar cells, IBC (Interdigitated Back Contact) solar cells, PERC (Passivated Emitter and Rear Contact) solar cells and

TOPCon (Tunnel Oxide Passivated Contact) solar cells [5]. Conceptually, 'TOPCon' may also be abbreviated as 'POLO' (Polysilicon on Oxide) [6].

A constant uptrend in the power conversion efficiency of these various crystalline silicon based solar cells has been thus observed. For an example, in 2015, Kaneka reported about the development of 25.1% ( $V_{oc} = 738$  mV,  $J_{sc} = 40.8$  mA/cm<sup>2</sup> and FF = 83.5%) HIT solar cells based on n-type CZ-Si wafers with an active cell area of 151.9 cm<sup>2</sup> [7]. On the other hand, SunPower also claimed almost similar result with a conversion efficiency of 25.2% ( $V_{oc} = 737$  mV,  $J_{sc} = 41.33$  mA/cm<sup>2</sup> and FF = 82.7%) for single junction IBC solar cells fabricated onto n-type CZ-Si wafers [8]. The corresponding cell area was 153.49 cm<sup>2</sup>. However, the latter provided superior  $J_{sc}$  due to no shading effect while the former demonstrated better  $V_{oc}$  and FF owing to the presence of amorphous silicon layer which offered high-quality surface passivation. Applying the concept of interdigitated back contact into HIT solar cells, in 2014 Sharp first developed HBC (Heterojunction Back Contact) solar cells with a conversion efficiency of 25.1% [9]. By applying the similar concept Panasonic developed HBC solar cells with a conversion efficiency of 25.6% ( $V_{oc} = 740$  mV,  $J_{sc} = 41.8$  mA/cm<sup>2</sup> and FF = 82.7%), the record efficiency at that time for crystalline silicon based solar cells [10]. The active cell area of the developed cells was 143.7 cm<sup>2</sup>. However, the

\* Corresponding author.

E-mail address: [4sumitam@gmail.com](mailto:4sumitam@gmail.com) (S. Mukhopadhyay).

record did not sustain over a longer time period because within two years, in 2016 Kaneka reported about the development of 26.3% ( $V_{oc} = 744$  mV,  $J_{sc} = 42.3$  mA/cm $^2$  and FF = 83.8%) efficient HBC solar cells with an active cell area of 180.4 cm $^2$  [11]. Shortly after, Kaneka further announced an improvement in the conversion efficiency of HBC solar cells as the best cell demonstrated a conversion efficiency of 26.6% ( $V_{oc} = 740$  mV,  $J_{sc} = 42.5$  mA/cm $^2$  and FF = 84.6%) with an active cell area of 179.7 cm $^2$  [12]. Recently, in October 2021 LONGi Solar has announced new record HJT solar cells with 26.3% efficiency based on M6 wafers [13]. In contrast, the highest reported efficiency for conventional PERC and TOPCon solar cells has been found to be 24.06% and 25.7%, respectively [14,15]. In 2018, ISFH, the eminent solar energy research institute located in Germany claimed that they developed 26.1% ( $V_{oc} = 726.6 \pm 1.8$  mV,  $J_{sc} = 42.62 \pm 0.4$  mA/cm $^2$  and FF = 84.28  $\pm$  0.59; active cell area of 4 cm $^2$ ) efficient c-Si solar cells by implementing both p $^+$ -POLO and n $^+$ -POLO structure at the rear side of a p-type c-Si wafer in an interdigitated pattern [16]. In the fabricated device, the passivated contacts i.e., n $^+$  and p $^+$  POLO layers were separated by an intrinsic poly-Si layer. Low parasitic absorption by doped poly-Si layer due to presence of passivated contacts at the rear side and no metal induced shading losses at the front side of the cell were the key features to realize such high efficiency value. Furthermore, they reported that laser ablation technique was used instead of photolithography process for the contact opening purpose; the use of which may facilitate to adopt screen printing based metallization technique during the cell fabrication process. Besides, through the Quokka2.0 simulation study Peibst et al. predicted that the power conversion efficiency of this (POLO) $^2$  IBC solar cells based onto standard p-type, FZ c-Si wafers may be as high as 27.8% (without photonic crystals) or even 29.1% (with photonic crystals) [17]. However, involvement of complex and expensive processing steps, less throughput etc. need to be addressed before going into mass production of IBC solar cells featuring (POLO) $^2$  structure at rear. On the other hand, The capital expenditure (CAPEX) for SHJ (Silicon heterojunction) solar cell is approximately RMB 400 million/GW whereas the same for PERC and TOPCon solar cell is nearly RMB 150–200 million/GW and RMB 250 million/GW [18]. Besides,

higher depreciated costs and use of expensive low temperature treated silver paste are major bottlenecks for wide commercialization of the SHJ solar cells.

According to the ITRPV 2021 report, the solar photovoltaics market is being exclusively dominated by cell concepts with diffused and passivated p-n junctions and passivated rear sides (PERC/PERL/PERT/TOPCON) [19]. The report has also predicted that BSF will be produced mostly on cost-efficient mc-Si wafers and will probably disappear after 2025. Most interestingly, the market share of PERC/PERL/PERT/TOPCON in 2020 slightly exceeds IHS Market assumptions as shown in Fig. 1. Besides, Fig. 2 illustrates that TOPCon solar cells will gradually grab the market share of approximately 50% (only PERC concept and TOPCon solar cells are considered) within next decade from its current market share of about 6%, indicating its dominancy in SPV industry. On the other hand, Si-heterojunction (HIT/HJT) solar cells will progressively gain a market share of about 10% in 2025 and about 18% in 2031. Fig. 1 again confirms the supremacy of double-sided contact cell concepts over other technologies concerning market share. It is assumed that rear-side contact cells have a change from  $\approx$  2% in 2020 to nearly 5% in 2031 in terms of market share. High cost, complex processing steps, requirement of significant modification of current cell processing technology, less throughput etc. may be responsible for lesser market share of HIT/HJT or IBC solar cells in the present scenario [4].

One of the major problems associated with the PERC solar cells is the rear side contact openings as the rear contact in PERC solar cell is realized by opening grooves in the passivating layers [5]. Therefore, bulk Si layer may get damaged during this opening process. Additionally, the photo-generated current has to flow the longer path due to the presence of localized metallic contacts. On the other hand, as the conventional monofacial TOPCon solar cells comprise of full area rear side metallic contact, therefore the problems like requirement of laser assisted contact openings or crowding of charge carriers at localized contacts are not there [17]. In general, the successful development of TOPCon structure is mainly dependent on four major processes; namely (i) development of ultra-thin SiO $_x$  tunneling layer, (ii) deposition of highly doped a-Si or a-Si:H layer onto the ultra-thin SiO $_x$  layer, (iii) high temperature thermal

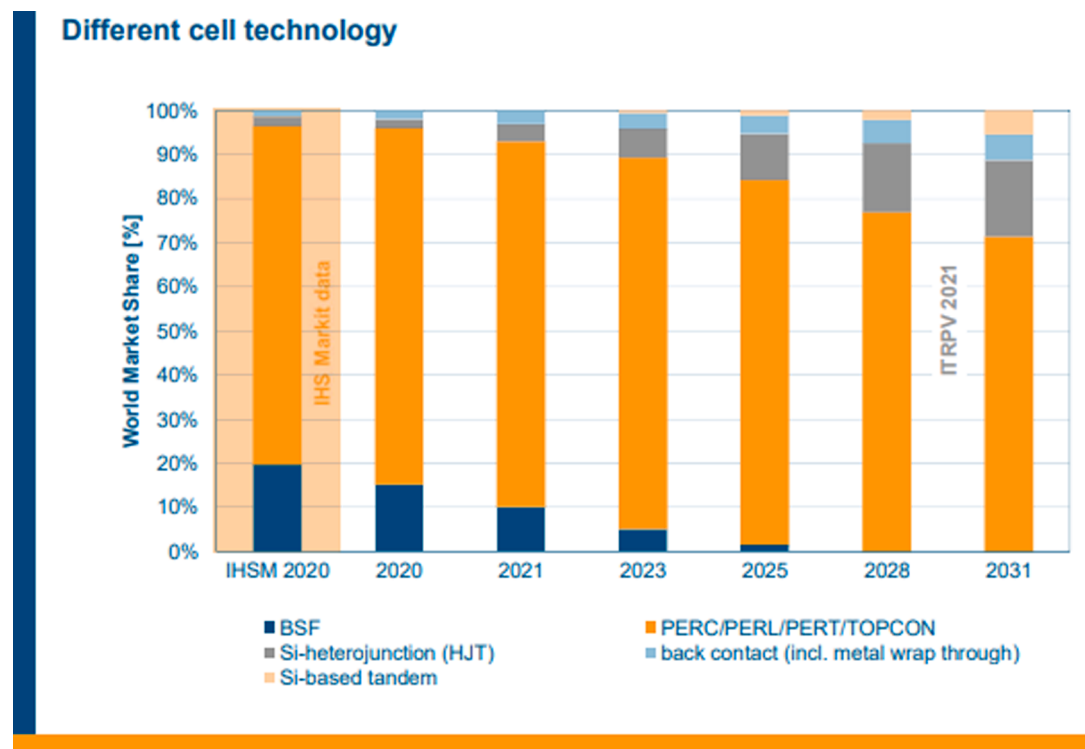
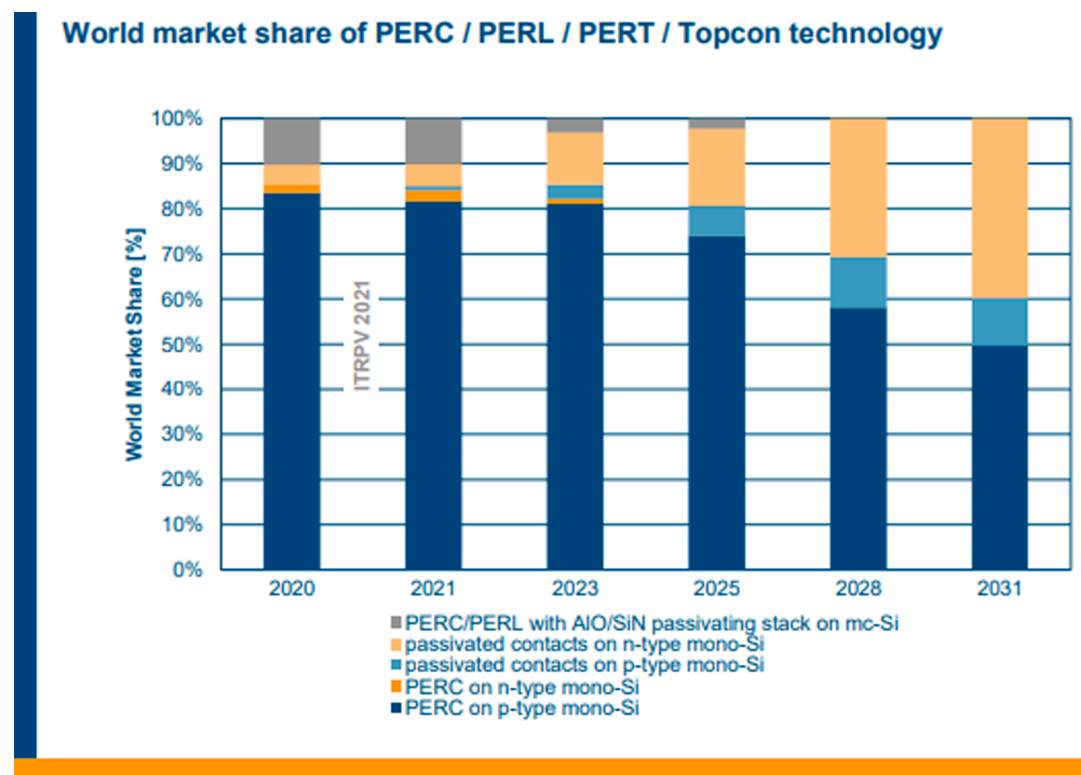


Fig. 1. Global market share for different cell technologies [19].



**Fig. 2.** Global market share of PERC/PERL/PERT and TOPCon solar cells [19].

annealing for dopant activation and crystallization of doped a-Si layer to make it polycrystalline, and (iv) post-annealing hydrogenation treatment to minimize the defect states within doped poly-Si layer [21]. Consequently, it is understood that the improvement in all of these processing steps may facilitate the fabrication of high efficiency TOPCon solar cells. Besides, rear side light management and use of selective emitter may also aid the power output of the TOPCon solar cells.

The average stabilized efficiency of the large area n-TOPCon solar cells in mass production has been found to be higher than the current market dominating p-PERC solar cells [19]. Recently, Chinese PV module manufacturer Jolywood has announced that they have developed 700W bifacial TOPCon solar modules with the maximum cell level efficiency of 25.4%, the highest reported efficiency so far for large area industrial TOPCon solar cells [22]. In addition, the module level efficiency has been found to be in between 21.73 to 22.53%; higher than the average stabilized efficiency of TOPCon solar modules in mass production. In contrast, LONGi, the other renowned solar module manufacturer has claimed the successful development of 25.19% p-type TOPCon solar cells based on commercialized monocrystalline CZ c-Si wafers, demonstrating the industrial viability of p-TOPCon solar cells [23]. However, the detailed information about the process through which they have realized such kind of high efficiency value has not been revealed yet [24].

In essence, the continuous progress of TOPCon solar cells since its development in 2013 by Fraunhofer ISE has motivated us to write this review article and the primary focus of this contribution is to understand the basic operation of TOPCon solar cells and its importance in PV industry. Next, the study reveals the fabrication of both-sided TOPCon solar cells with its merits and demerits. Besides, we shall observe how the use of TOPCon structure as rear emitter in p-type c-Si solar cells may eliminate the need of additional FSF (front surface field) layer without affecting the conversion efficiency by a considerable margin. The major part of this article is comprised of careful discussion on various research activities performed by researchers to improve the quality of ultra-thin  $\text{SiO}_x$  layer, doped poly-Si layer, post crystallization treatment,

metallization, rear side light management and front emitter related to TOPCon solar cells. Thereafter, various theoretical explorations especially focusing on various loss mechanisms involved in the highest reported TOPCon solar cell are going to be discussed. Furthermore, in this study, a special focus has been made to enlighten the development and commercialization of large area TOPCon solar cells including bifacial solar cells. The next part of discussion focuses on the possible technological options for developing the commercial grade TOPCon structure and various issues associated with the metallization of industrial TOPCon solar cells. After that, development of TOPCon solar cells based on cost-effective multicrystalline Si wafers has been pinpointed in details, followed by incorporation of TOPCon structure in hybrid or heterojunction solar cells. Finally, prior to conclusion, the future scope of works with possible challenges and their probable solutions have been analyzed.

## 2. Evolution of TOPCon solar cell and its importance in PV industries

As stated earlier that the passivated contact based solar cells will gain the highest market share in the near future. Consequently, the current researches in solar cell architectures are primarily focusing on PERC and TOPCon solar cells. However, due to the challenges like rear contact openings and carrier crowding at localized metallic contacts, market dominating PERC solar cells are likely to be replaced by TOPCon solar cells in the future. The first report on the development of TOPCon solar cells was published in 2013 by Fraunhofer ISE [20]. In the article, Feldmann et al. revealed that inserting of an ultra-thin silicon dioxide layer ( $\text{SiO}_2$ ) along with a phosphorous-doped poly silicon layer at metal-semiconductor interface may significantly reduce the surface recombination at the rear side of n-type crystalline silicon solar cells. The thickness of chemically grown silicon dioxide layer was kept as low as 1.4 nm so that current can tunnel through it easily and efficiently. Onto this ultra-thin oxide layer, a 20 nm phosphorous doped amorphous silicon layer was deposited by PECVD technique, followed by a high

temperature annealing process to transform this doped amorphous silicon layer into doped poly-crystalline silicon layer. Depending upon annealing conditions, a very good surface passivation was observed which in turn provided a very high implied open-circuit voltage ( $iV_{oc}$ ) of above 710 mV and a very low recombination current density ( $J_{0,rear}$ ) of about 9–13 fA/cm<sup>2</sup>. This novel approach was named as TOPCon (Tunnel Oxide Passivated Contact) structure and the solar cells which comprise of this TOPCon structure are known as TOPCon solar cells. The schematic diagram of a TOPCon solar cell is depicted in Fig. 3 which features tunnel oxide passivated rear contact and a diffused boron-doped p<sup>+</sup> emitter. To reduce the front side surface recombination, boron-doped p<sup>+</sup> emitter was passivated by a stack of atomic layer deposited (ALD) aluminium oxide (Al<sub>2</sub>O<sub>3</sub>) layer and plasma-enhanced chemical vapor deposited (PECVD) silicon nitride (SiN<sub>x</sub>) layer. Besides, it has been well established that silicon nitride (SiN<sub>x</sub>) layer also serves the purpose of anti-reflection coating (ARC) so that optical confinement inside the solar cell can be enlarged. Using this novel structure, apart from high implied voltage ( $iV_{oc}$ ), high implied fill factor (iFF) was also obtained in both maximum power point (MPP) and open-circuit (OC) conditions. In the cell fabrication process, front side metallic contacts were realized by thermally evaporated Ti/Pd/Ag seed layer and subsequent electroplating of Ag layer. The width of the metallic fingers was kept as 20 µm. On the other hand, thermally evaporated Ti/Pd/Ag stack was used as rear side metallic contact. Eventually, the best cell with an active cell area of 2 cm × 2 cm based onto 200 µm thick, <100> oriented, 1 Ω-cm, n-type FZ silicon wafers demonstrated a power conversion efficiency of 21.81% featuring a short circuit current density ( $J_{sc}$ ) of 38.4 mA/cm<sup>2</sup>, an open-circuit voltage ( $V_{oc}$ ) of 690.8 mV and a fill factor (FF) of 82.1%. In contrast, the best power conversion efficiency of 19.6% with  $V_{oc}$  of 638.3 mV,  $J_{sc}$  of 37.8 mA/cm<sup>2</sup> and FF of 81.1% was achieved for the identical solar cells without TOPCon structure at the rear side. Therefore, the importance of incorporating TOPCon structure at the rear side of the crystalline Si solar cells may be well understood. The process flow of TOPCon solar cell reported by Feldmann et al is given below:

- Step 1: Selection of shiny-etched 200 µm, <100> oriented, 1 Ω-cm n-type FZ Si wafers (2 cm × 2 cm)
- Step 2: Cleaning of wafers by standard RCA process
- Step 3: Diffusion of boron into random pyramid textured front side
- Step 4: Deposition of 1.4 nm SiO<sub>x</sub> layer (wet chemical process) and subsequent 20 nm phosphorous doped amorphous Si layer (PECVD process) at the rear side
- Step 5: High temperature annealing (optimized annealing temperature ~ 850°C) in N<sub>2</sub> atmosphere
- Step 6: Deposition of ALD coated Al<sub>2</sub>O<sub>3</sub> layer and PECVD coated SiN<sub>x</sub> layer onto front p<sup>+</sup> emitter

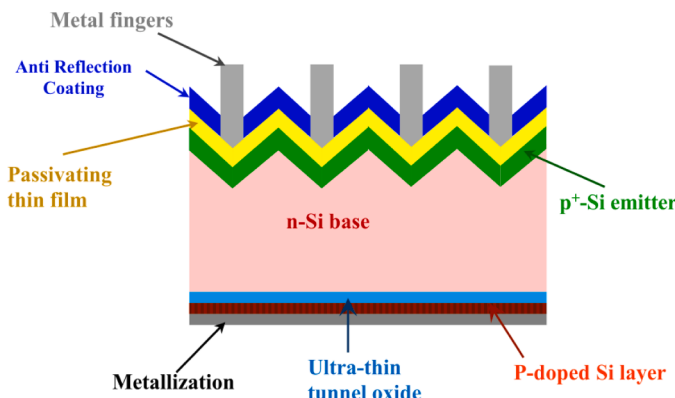


Fig. 3. Schematic diagram of tunnel oxide passivated contact (TOPCon) solar cell [20].

Step 7: Front side metallization by thermally evaporated Ti/Pd/Ag seed layer (finger width: 20 µm) and subsequent electroplating of Ag layer

Step 8: Rear side metallization by thermally evaporated Ti/Pd/Ag layer

However, for better light management, rear side Ti/Pd/Ag metallic stack was replaced by either a stack of lowly doped 200 nm ITO layer and 1 µm Ag layer or single 1 µm Ag layer. The use of ITO/Ag stack or single Ag layer provided higher  $J_{sc}$  compared to the cells featuring Ti/Pd/Ag as rear side metallic contact. However, the solar cells featuring ITO/Ag stack at the rear side suffered from achieving higher FF due to having higher series resistance value. In contrast, no decrement in the FF was observed for the solar cells featuring single Ag layer at the back side. Additionally, the authors also varied the metallized area fraction at the front electrode by choosing two different contact opening widths (5 and 20 µm). The reduction of metallized area fraction from 3% (20 µm contact opening) to 1.1% (5 µm contact opening) resulted in a decrement of recombination current density at front metal/semiconductor interface. As a result, significant improvement in  $V_{oc}$  was observed. Consequently, TOPCon solar cells featuring Ag single layer as the rear electrode and metallized area fraction of 1.1% at the front side demonstrated the highest conversion efficiency of 23.7% ( $V_{oc} = 703.3$  mV,  $J_{sc} = 41.0$  mA/cm<sup>2</sup> and FF = 82.2%) whereas relatively poor power conversion efficiency of 23.3% ( $V_{oc} = 693.0$  mV,  $J_{sc} = 41.4$  mA/cm<sup>2</sup> and FF = 81.2%) was obtained for the solar cells featuring Ag single layer as the rear electrode and metallized area fraction of 3% at the front side. The authors suggested that further improvement in the power conversion efficiency may be realized by reducing the recombination current density at front emitter. Consequently, Hermle et al. realized an enhancement in power conversion efficiency by placing selective emitter structure underneath the front side metallic contact [25]. Here, the best cell fabricated on n-type FZ c-Si wafer with an active cell area of 2 cm × 2 cm provided a power conversion efficiency of 24.9% with  $V_{oc} = 718$  mV,  $J_{sc} = 41.5$  mA/cm<sup>2</sup> and FF = 83.4%. The incorporation of selective emitter structure underneath the metallic contact resulted in a very low front sided recombination current density ( $J_{0,front}$ ) of 16 fA/cm<sup>2</sup> [14 fA/cm<sup>2</sup> due to the 150Ω/sq p<sup>+</sup>-emitter and 2 fA/cm<sup>2</sup> due to the selective emitter structure]. The authors further revealed that reduction in recombination current density at front p<sup>+</sup> emitter and enhancement of optical confinement of the incident light into the absorbing layers may lead to fabricate TOPCon solar cells with the power conversion efficiency of well above 25%. Eventually, in 2015, Glunz et al. announced about the development of TOPCon solar cells with a conversion efficiency of 25.1% ( $V_{oc} = 718$  mV,  $J_{sc} = 42.1$  mA/cm<sup>2</sup>, FF = 83.2%) [21]. The corresponding cell area was 2 × 2 cm<sup>2</sup>. Fig. 4 represents the band diagram of different interfaces such as a-Si/c-Si, poly silicon with tunnel oxide/c-Si and amorphous/poly silicon with tunnel oxide/c-Si (TOPCon). From these band bending diagrams, efficient and simplified separation of photo-generated carriers at the back side of n-Si base for a TOPCon solar cell can be well understood.

Almost one and half years later, in 2017 Richter et al. reported about the influential effect of wafer thickness and bulk resistivity on the power conversion efficiency of TOPCon solar cells [15]. In the study, 150, 200 and 400 µm thick n-type FZ Si wafers having a resistivity of 5 Ω-cm were used for the variation of thickness. In contrast, study of resistivity variation was conducted by choosing 200 µm thick n-type FZ Si wafers having three different resistivities of 1, 5 and 10 Ω-cm. Solar cells featuring all these variations demonstrated a conversion efficiency of about 25%. However, significant degradation in FF and pseudo-FF (PFF) was observed for the increment of the base resistivity. Quokka simulation study revealed that this reduction of FF may be caused due to the increment of Shockley-Read-Hall recombination losses in c-Si bulk. Simulation study also confirmed that the concentration of impurities in c-Si bulk is strongly dependent on the wafer thickness too. Finally, after optimizing the wafer thickness and resistivity, 25.7% ( $V_{oc} = 725$  mV,  $J_{sc}$

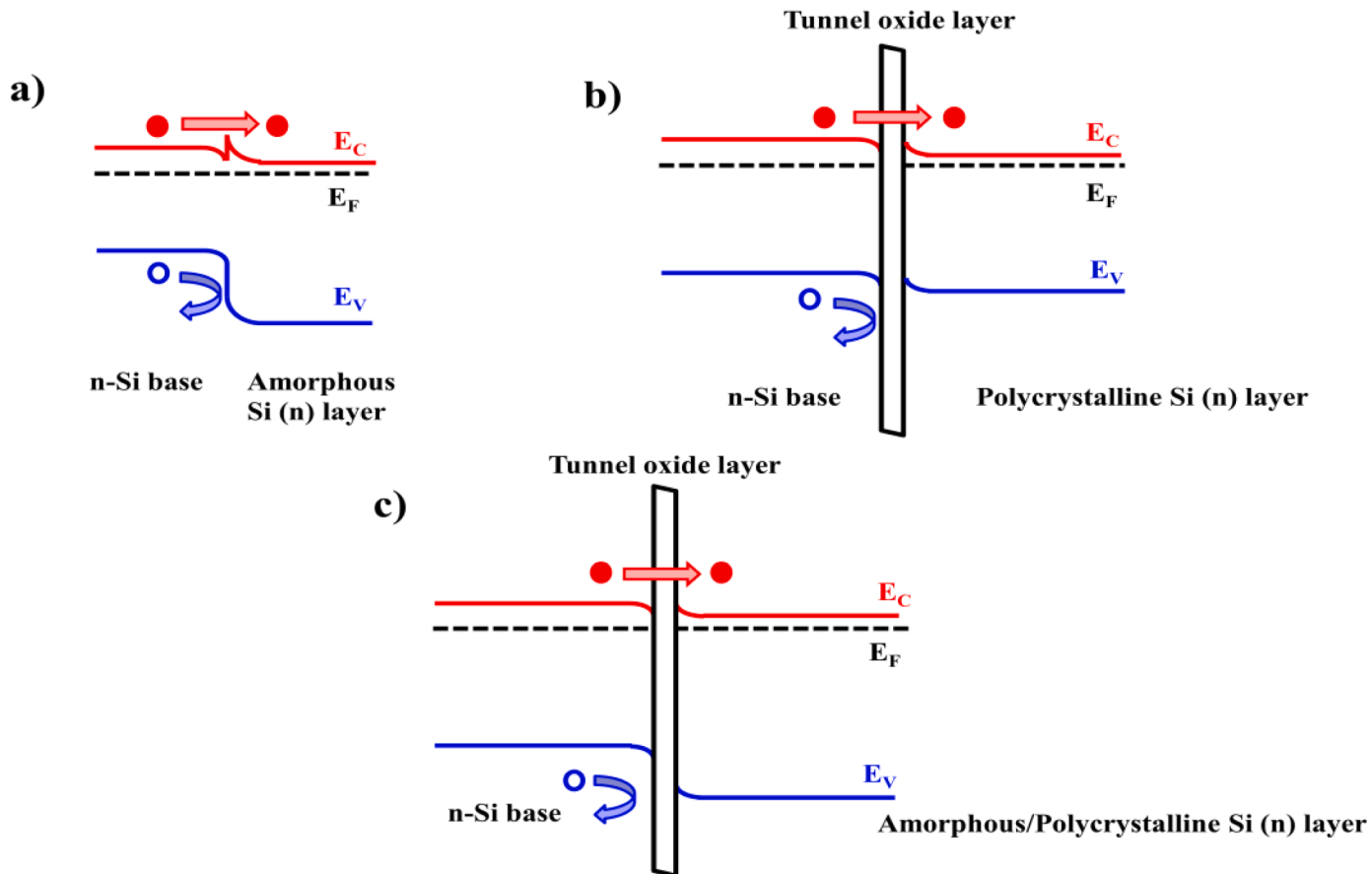


Fig. 4. Band diagram of different passivated contact technologies: (a) a-Si/c-Si heterojunction, (b) poly silicon with tunnel oxide, and (c) TOPCon [21].

$= 42.5 \text{ mA/cm}^2$  and  $\text{FF} = 83.3\%$ ) efficient TOPCon solar cells based on 1  $\Omega\text{-cm}$ , 200  $\mu\text{m}$  thick n-type FZ Si wafers were fabricated with an active cell area of  $2 \text{ cm} \times 2 \text{ cm}$ . Apart from the optimization of base resistivity and wafer thickness, the authors used a stack of PECVD grown 50 nm  $\text{SiN}_x$  layer and thermally evaporated 90 nm  $\text{MgF}_2$  layer as double-layer anti-reflection coating (DARC) to increase the optical confinement inside the solar cells. Therefore, after observing the above mentioned results, one may easily realize the importance of this high efficiency TOPCon solar cell in the PV industries. In the following section, we shall discuss about the both sided TOPCon solar cells.

### 3. Both sided TOPCon structure based on p-type c-Si wafers

In industrial perspective, p-type Si wafers are more common in comparison with n-type Si wafers due to their cost-effectiveness. Therefore, development of TOPCon structure based on p-type c-Si wafers may be an attractive approach. Consequently, Feldmann et al. developed symmetrical n-TOPCon and p-TOPCon structure based on planar, shiny-etched, 250  $\mu\text{m}$ , p-type, 1  $\Omega\text{-cm}$ ,  $<100>$  oriented FZ silicon wafers [26]. The study showed that the passivation quality of n-TOPCon structure was superior to its counterpart. Therefore, we may conclude that the interface passivation quality of n-TOPCon structure is good for both n-type (as mentioned in the section number 2) and p-type Si wafers. In contrast, symmetrical p-TOPCon structure served lower interface passivation ( $iV_{oc} = 680 \text{ mV}$ ) quality due to the presence of higher defect density in bulk Si layer as well as at  $\text{Si}/\text{SiO}_x$  interface. Finally, to understand the influence of incorporating carrier selective contacts on the cell performance, p-type Si solar cells (active cell area  $2 \text{ cm} \times 2 \text{ cm}$ ) were developed where n-TOPCon served as front emitter and p-TOPCon provided back surface field (see Fig. 5). The solar cells featuring amorphous Si emitter gave higher  $V_{oc}$  (693.5 mV) and higher

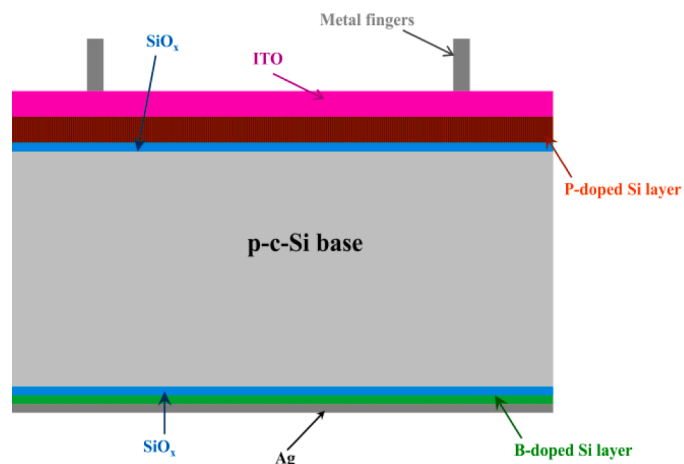
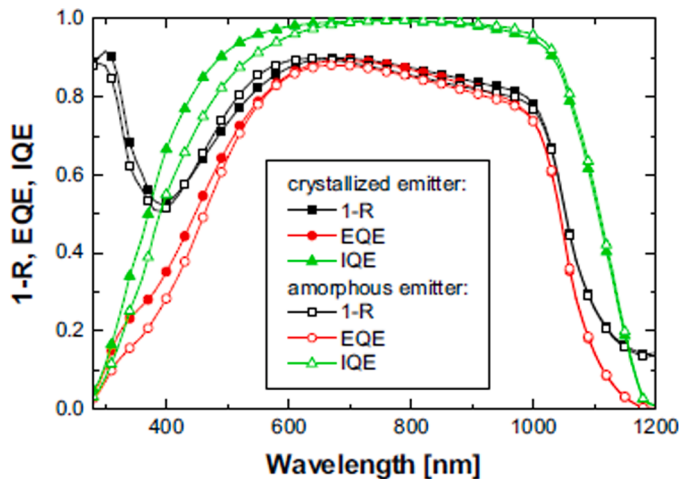


Fig. 5. Schematic diagram of both-sided TOPCon solar cell based on p-type c-Si wafer [26].

$\text{FF} (81\%)$  than the solar cells featuring semi-crystalline Si emitter. But the latter provided higher  $J_{sc}$  due to improved blue response. Consequently, the obtained efficiency of both cell groups was almost same (17.9% for amorphous silicon emitter and 17.8% for semi-crystalline silicon emitter). Nevertheless, improvement in the passivation quality of p-contact may lead to maximize the power conversion efficiency.

In addition, double-sided contact solar cells with n-TOPCon on textured front side and p-TOPCon on planar back side were also developed onto 250  $\mu\text{m}$  thick, shiny etched, 1  $\Omega\text{-cm}$ ,  $<100>$  oriented p-type FZ silicon wafers [27]. But here, the authors used atomic layer deposited



**Fig. 6.** External and internal quantum efficiency of the champion cells featuring an amorphous emitter and partially crystallized emitter, respectively. In addition, the 1-R curves representing the upper limit for the EQE are also given [26].

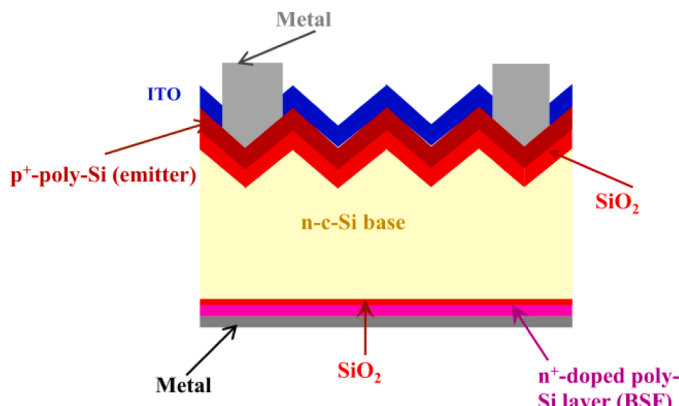


**Fig. 7.** Schematic diagram of both-sided TOPCon solar cell based on n-type c-Si wafer [28].

(ALD) 20 nm thin AZO (aluminium doped zinc oxide) or ZnO (zinc oxide) layer as an interfacial layer in between the n-TOPCon structure and sputter deposited ITO layer so that the sputter induced damage occurring onto the n-TOPCon layer during the development of ITO layer may be avoided. As a result, higher FF was realized which may be attributed to the reduced Schottky barrier height at n-TOPCon/AZO contact. Besides, an increment of 0.8% in the power conversion efficiency was also observed when AZO/ITO stack was used as front TCO layer instead of single ITO layer. On the other hand, TCOs having high work function such as  $\text{WO}_x$ ,  $\text{MoO}_x$  showed great potential to serve the purpose for contact layers to p-TOPCon. Development of both sided TOPCon structure on n-type Si wafers will be discussed in the next section.

#### 4. Both sided TOPCon structure based on n-type c-Si wafers

In 2018, Tao et al. reported about the fabrication of both sided TOPCon solar cells featuring p-TOPCon structure at the front side and n-TOPCon structure at the rear side [28]. Besides, the authors also studied the impact of ITO sputtering onto n-TOPCon and p-TOPCon structure which were fabricated symmetrically onto 3–8  $\Omega\text{-cm}$ , n type, double-side polished CZ c-Si wafers. The study revealed that the deposition of ITO layers onto p-TOPCon and n-TOPCon structure by rf-magnetron sputtering technique resulted in a strong degradation of the effective

minority carrier lifetime ( $\tau_{\text{eff}}$ ). However, significant recovery of  $\tau_{\text{eff}}$  was observed for p-TOPCon samples upon high temperature (500 °C) annealing after ITO deposition while n-TOPCon samples showed a partial recovery of  $\tau_{\text{eff}}$  upon thermal treatment. This contrast in recovery of  $\tau_{\text{eff}}$  may be attributed to the more improvement of the p-type poly-Si film quality upon thermal exposure. Besides, the study also revealed that deposition of ITO layers at relatively low rf power and room temperature may lead to maximize the recovery of  $\tau_{\text{eff}}$ . Initially, the solar cells featuring p-TOPCon on front and n-TOPCon at the rear showed a very low conversion efficiency of 16.05% with  $V_{\text{oc}} = 604$  mV,  $J_{\text{sc}} = 35.87$  mA/cm<sup>2</sup> and FF = 74.1% due to the damages occurred by sputter deposited ITO layer. However, thermal treatment after ITO deposition helped to raise the power conversion efficiency up to 18.55% having  $V_{\text{oc}} = 671$  mV,  $J_{\text{sc}} = 38.14$  mA/cm<sup>2</sup> and FF = 72.5%.

Lozac'h et al. also developed double-sided TOPCon solar cells based onto <100> oriented, 1–5  $\Omega\text{-cm}$ , 270  $\mu\text{m}$  thick, n-type textured FZ c-Si wafers with p-TOPCon structure at the front side and n-TOPCon structure at the rear side [29]. In this study, atomic layer deposition (ALD) technique was used for the deposition of ultra-thin  $\text{SiO}_x$  layer. TEM images revealed an excellent conformal growth of  $\text{SiO}_x$  layer even onto the textured wafers.

In addition, no pinhole was observed at  $\text{Si}/\text{SiO}_x$  interface and hence the transportation of the charge carriers through the ultrathin  $\text{SiO}_x$  layer would be governed by tunnelling process only. On the other hand, ALD technique also provides the facility of precise control of the thickness of ultra-thin  $\text{SiO}_x$  layer which featured an optimized thickness value of  $0.6 \pm 0.1$  nm. Furthermore, the diffusion profiles of boron and hydrogen at the p-side  $\text{SiO}_x/\text{c-Si}$  interface were also optimized for the improvement of solar cell performances. Eventually, the best cell with a boron concentration of about  $1.3 \times 10^{20}$  at/cm<sup>3</sup> at the front (p) stack and a hydrogen concentration of  $2 \times 10^{21}$  at/cm<sup>3</sup> near the p-side c-Si/ $\text{SiO}_x$  interface demonstrated a power conversion efficiency of 18.8% with an outstanding  $J_{\text{sc}}$  of above 39 mA/cm<sup>2</sup>. Besides, Lozac'h and Nunomura also carried out a comparative study on the performance of both sided TOPCon solar cells fabricated on polished (<100> and <111> oriented) and pyramid textured n-type FZ Si wafers, respectively [30]. The study revealed that the optimized thickness value of ALD coated ultra-thin  $\text{SiO}_x$  layer was  $1.1 \pm 0.1$  nm, irrespective of nature and orientation of the bulk Si surfaces. However, a gain in  $V_{\text{oc}}$  of almost 10 mV was realized when polished <100> oriented Si wafers were used for the development of double-sided TOPCon solar cells. This gain may be attributed to the presence of lower number of defect states at bulk c-Si/ $\text{SiO}_x$  interface. On the other hand, TOPCon structure based on <111> oriented polished Si wafers demonstrated a very low value of contact resistance of about 0.45  $\Omega/\text{cm}^2$ . Nevertheless, both-sided TOPCon solar cells based on textured Si wafers outperformed the both-sided TOPCon solar cells fabricated on polished Si wafers due to featuring higher value of  $J_{\text{sc}}$ . The highest reported efficiency was 19.1% for the both-sided TOPCon solar cells developed on textured Si surfaces. The other important application of TOPCon structure is to use it as rear emitter in p-type c-Si solar cells which is going to be discussed in the following section.

#### 5. TOPCon as rear emitter in p-type Si solar cells

The performance of p-type rear junction silicon solar cells with TOPCon rear emitter was investigated both theoretically and experimentally [31]. In this cell structure, front p<sup>+</sup> layer acts as front surface field (FSF) which improves the collection probability of holes with a greater extent. On the other hand, rear n-TOPCon layer behaves as electron contact. In front sided emitter solar cells, lateral current transport losses within the emitter are quite significant power losses. This power loss may be reduced efficiently in the rear junction TOPCon solar cell structure as it features full area metal contact underneath the doped poly-silicon layer. Lateral current transport within the front surface field (FSF) becomes less important because the transportation of majority carriers i.e., holes towards the local p<sup>++</sup> layer is significantly

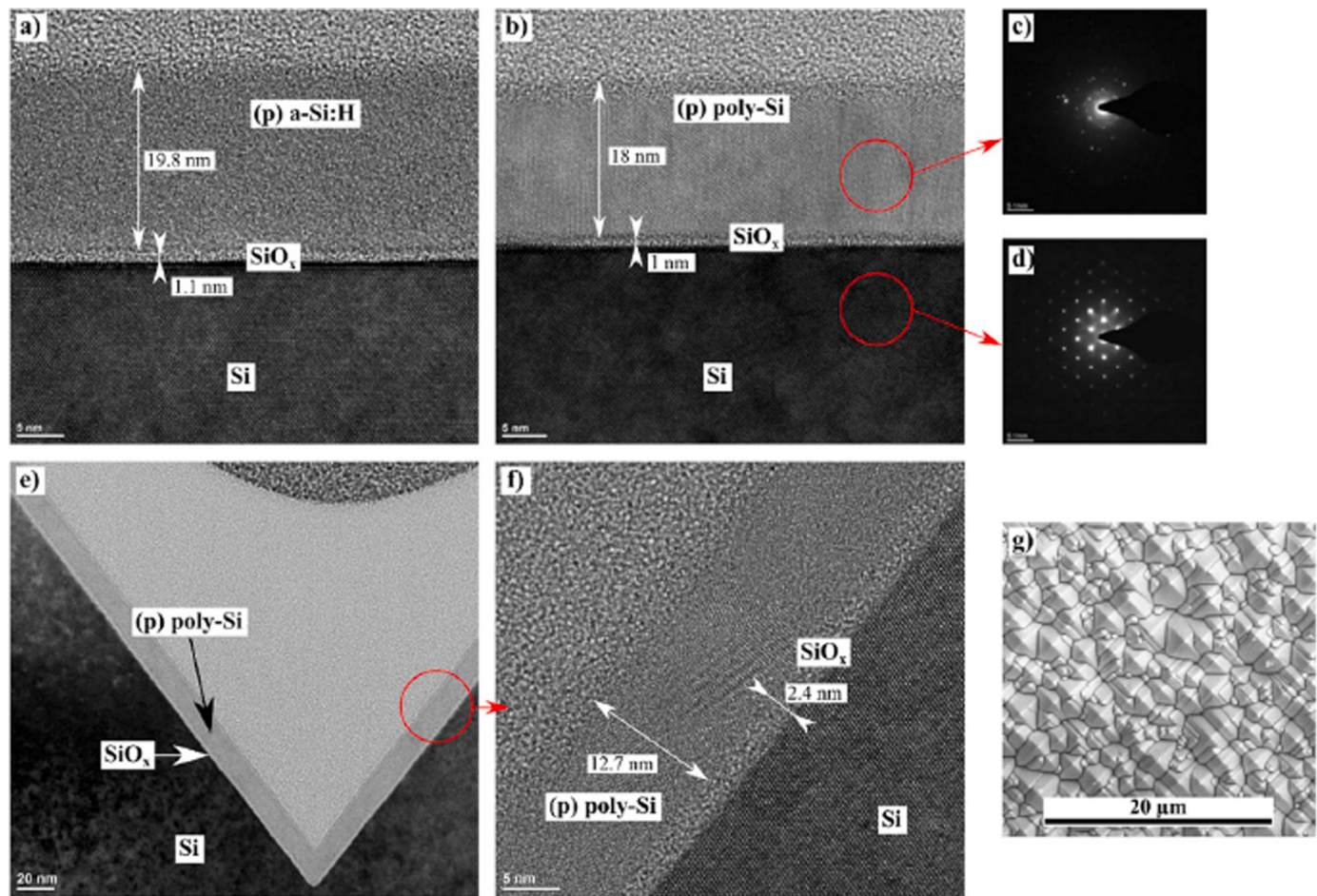


**Fig. 8.** TEM images of (a) (p) a-Si:H/SiO<sub>x</sub> on polished surface as deposited, (b) (p) poly-Si/SiO<sub>x</sub> on polished surface after high-T annealing. Diffraction patterns of (c) the (p) poly-Si compared to d) the bulk-Si by nano beam diffraction (NBD). TEM images of (e) (p) poly-Si/SiO<sub>x</sub> on textured surface after high-T annealing, (f) magnification of (e). (g) Plane view of the textured surface [29].

influenced by the p-type bulk silicon layer. Due to this simplified and efficient carrier transport mechanism, the sheet resistance of the front surface field (FSF) layer gets reduced. Even the omission of front surface field (FSF) as depicted in Fig. 9 may also lead to provide adequate result which in turns simplifies the processing steps of p-type Si solar cells with n-TOPCon structure as rear emitter. Finally, the influence of the lateral conductivity of the front surface field (FSF) on the performance of the solar cell was studied thoroughly. Simulation study demonstrated that the requirement of front surface field (FSF) depends on the bulk resistivity of Si wafer. According to the study, the device performance does not depend much on the sheet resistance of the front surface field (FSF) layer for a 1 Ω-cm Si wafer while for a 10 Ω-cm Si wafer, the power conversion efficiency of the solar cells may be affected by the sheet resistance of the front surface field (FSF) layer. Experimentally, two types of rear junction TOPCon solar cells i.e., with and without front surface field (FSF) were developed based on 10 Ω-cm, 250 μm, <100> oriented FZ Si wafers. The obtained power conversion efficiency was 23.9% ( $V_{oc} = 708.4$  mV,  $J_{sc} = 42.4$  mA/cm<sup>2</sup> and FF = 79.7%) and 24.3% ( $V_{oc} = 714.2$  mV,  $J_{sc} = 42.4$  mA/cm<sup>2</sup> and FF = 80.8%) for without and with front surface field (FSF) layer, respectively. The corresponding cell area was 4 cm<sup>2</sup>. The slight decrement of the power conversion efficiency of the solar cells without front surface field (FSF) may be attributed to the reasonable increment of the series resistance compared to its counterpart.

Gao et al. also studied the feasibility of using TOPCon structure as rear emitter in p-type c-Si solar cells [32]. In the contribution, to conduct the passivation study, symmetrical n-TOPCon structure was fabricated

by industrial feasible PECVD system based onto <100> oriented, 1-3 Ω-cm resistive, 170 μm thick, 4 × 4 cm<sup>2</sup> p-type CZ Si wafers. After RCA cleaning and removal of native oxide layer, the substrates were undergone into N<sub>2</sub>O plasma assisted oxidation treatment for 10 min inside the 13.56 MHz PECVD system to deposit the SiO<sub>x</sub> layer. Furthermore, same PECVD tool along with SiH<sub>4</sub>, H<sub>2</sub>, and PH<sub>3</sub> as the process gases were used for the development of P-doped hydrogenated a-Si layer onto the ultra-thin SiO<sub>x</sub> layer. The authors also optimized the post-deposition annealing temperature for the dopant activation and crystallization of P-doped a-Si:H layer. The optimized annealing temperature was observed to be in the range of 850 to 880 °C which was higher than the optimized annealing temperature (820°C) for the identical TOPCon structure featuring chemically grown SiO<sub>x</sub> layer and P-doped poly-Si layer. However, a correlation between the PH<sub>3</sub>/SiH<sub>4</sub> doping ratio during the deposition of P-doped a-Si:H layer and subsequent annealing temperature in N<sub>2</sub> atmosphere was noticed where a decrement in the optimized annealing temperature was realized for the increment of PH<sub>3</sub>/SiH<sub>4</sub> doping ratio. After the crystallization of poly-Si layer, forming gas annealing (FGA) was also performed for 30 min at 450°C to improve the passivation quality. In addition, to further improve the surface passivation properties, atomic layer deposited (ALD) Al<sub>2</sub>O<sub>3</sub> was used as capping layer, followed by a thermal annealing at 400°C. As a result, the developed TOPCon structure based onto p-type Si wafers demonstrated an excellent surface passivation quality with  $iV_{oc}$  (implied open-circuit voltage) = 742 mV,  $J_0$  (single-side saturated recombination current density) ~ 3 fA/cm<sup>2</sup>,  $\rho_c$  (contact resistivity) ~ 2–4 mΩ·cm<sup>2</sup>, and  $\tau_{eff}$  (effective minority carrier lifetime) = 1050 μs.

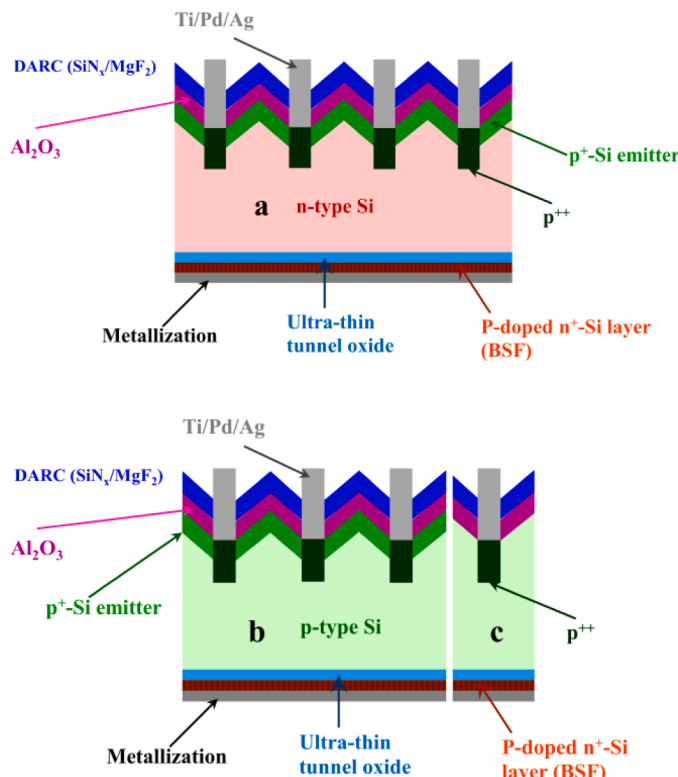


**Fig. 9.** Schematic diagram of (a) standard n-TOPCon solar cell, (b) p-type rear junction TOPCon solar cell with FSF and (c) p-type rear junction TOPCon solar cell without FSF [31].

Furthermore, from Quokka 2 and OPAL 2 simulation results, rear emitter TOPCon solar cells based on p-type solar grade CZ silicon wafers featured a conversion efficiency of  $\sim 22.8\%$  whereas the conversion efficiency for the front emitter p-TOPCon solar cells was 22.4%. Eventually, the study also revealed that the power conversion efficiency may be enhanced to  $\sim 24.9\%$  by using high quality c-Si wafers and optimized process parameters in R&D laboratories. In recent times, Richter et al. demonstrated that a conversion efficiency of as high as 26% ( $V_{oc} = 732.3$  mV,  $J_{sc} = 42.05$  mA/cm<sup>2</sup> and FF = 84.3%) with an active cell area of  $2 \times 2$  cm<sup>2</sup> was yielded for the TOPCon rear junction (without additional FSF layer) solar cells fabricated onto high quality 250  $\mu$ m thick, p-type, FZ Si wafers [33]. The realization of such high efficiency may pave the path for its commercialization process in coming years.

## 6. Advancement of different layers present in TOPCon solar cells

From the above discussions, it can be realized that similar to other high efficiency solar cells, the performance of TOPCon solar cells is highly dependent on efficient generation of electron-hole pairs upon light exposure and easy transportation of these photo-generated carriers into external circuit. In other words, improving the surface passivating quality and enhancing the optical confinement inside the absorbing layers of the solar cells may result in developing high efficiency TOPCon solar cells. The improvement in the passivating quality of TOPCon structure may be realized by improving the quality of ultra-thin SiO<sub>x</sub> tunnelling layer and doped poly-Si layer. Besides, reducing the recombination current density at front emitter is also important to obtain higher power conversion efficiency. The other way to maximize the value of  $J_{sc}$  and hence conversion efficiency is to reflect back the unabsorbed light from the rear side metallic contact into the absorbing layer of the solar cells. Therefore, in the following sections, we shall discuss about various observations which have been reported focusing on the improvement of the quality of ultra-thin SiO<sub>x</sub> layer, doped poly-Si

layer, front emitter and rear side light management.

### 6.1. Ultra-thin SiO<sub>x</sub> layer

The quality of ultra-thin SiO<sub>x</sub> layer may be recognised by its surface passivation quality, thermal stability and carrier tunnelling ability. As a result, different types of studies such as finding out the best possible route to develop high quality tunnelling layer, required properties for obtaining superior interfacial passivation and impact of presence of pinholes on carrier tunnelling have been carried out throughout the years.

#### 6.1.1. Formation of ultra-thin SiO<sub>x</sub> layer by different routes and its consequences

In 2014, Moldovan et al. reported that ultra-thin SiO<sub>x</sub> layers grown on planar Si surfaces in hot HNO<sub>3</sub> atmosphere and sub-sequent thermal treatment (after doped a-Si:H layer deposition) at very high temperature (up to 900°C) provided excellent surface passivation quality with an  $iV_{oc}$  of more than 720 mV [34]. However, an enormous degradation in the interface passivating quality was observed in case of textured Si surfaces at the same 900°C annealing temperature. This effect may be attributed to the formation of non-homogeneous tunnel oxide layer on the textured surfaces. On the other hand, UV/O<sub>3</sub> grown SiO<sub>x</sub> tunnelling layers demonstrated an outstanding interface passivation quality up to 900°C annealing temperature for both planar and textured samples with an  $iV_{oc}$  of higher than 720 mV and 710 mV, respectively. Moldovan et al. further carried out an investigation on the dependence of the passivating quality of ultra-thin SiO<sub>x</sub> tunnelling layer for different oxide development process such as hot nitric acid oxidation, photo-oxidation in ozonized DI-H<sub>2</sub>O (DIO<sub>3</sub>) process and UV/O<sub>3</sub> process [35]. The study showed that SiO<sub>x</sub> layers grown by either ozonized DI-H<sub>2</sub>O (DIO<sub>3</sub>) or UV/O<sub>3</sub> process were thermally more stable than the oxides layer developed by hot concentrated nitric acid. The authors further revealed that the passivating quality is strongly influenced by the stoichiometry of interfacial SiO<sub>x</sub> layer. Improved passivation quality was realized for more stoichiometric SiO<sub>2</sub> structure. Consequently, superior  $iV_{oc}$  was obtained for continuous and homogeneous UV/O<sub>3</sub> oxide layers compared to the oxide layers grown by other methods. Finally, n-TOPCon solar cells featuring full area passivated rear contact were developed by applying these differently grown ultra-thin SiO<sub>x</sub> layers for the formation of TOPCon structure [36]. A power conversion efficiency of 24.8% with a  $V_{oc}$  of 716 mV was achieved for HNO<sub>3</sub> reference process corresponding to an optimized annealing temperature of 800°C for the formation of TOPCon structure. In contrast, 24.9% efficient TOPCon solar cells with slightly more  $V_{oc}$  of 719 mV were developed for DIO<sub>3</sub> and UV/O<sub>3</sub> oxidation process with an optimized annealing temperature of 900°C. On the other hand, in 2018, Tong et al. reported that ultra-thin SiO<sub>x</sub> layer grown by three volumes of HNO<sub>3</sub> (68 wt%) acid and one volume of H<sub>2</sub>SO<sub>4</sub> (98 wt%) acid at 60°C demonstrated an excellent surface passivation quality with an average gain of  $iV_{oc}$  by 2–10 mV and a reduction of  $J_0$  by 1–7 fA/cm<sup>2</sup> in comparison with SiO<sub>x</sub> layer grown by only HNO<sub>3</sub> acid at same process temperature [37]. High oxidized state of Si in CNS (Concentrated nitric and sulphuric) acid grown SiO<sub>x</sub> layer may be the cause for this improvement in the passivation quality. Concurrently, requirement of low temperature (60°C) also helped to minimize the volatility and maintain the quality of the acid solution during the growth process. Furthermore, the obtained average efficiency was 20.5% ( $V_{oc} = 661$  mV,  $J_{sc} = 39.11$  mA/cm<sup>2</sup>, FF = 79.36%) for the solar cells featuring CNS acid grown SiO<sub>x</sub> layer whereas an average conversion efficiency of 20.35% ( $V_{oc} = 660.3$  mV,  $J_{sc} = 39.03$  mA/cm<sup>2</sup>, FF = 78.95%) was achieved for the solar cells featuring HNO<sub>3</sub> acid grown SiO<sub>x</sub> layer. Therefore, this straight forward gain of 0.15% in the power conversion efficiency may become fruitful in the mass production of TOPCon solar cells.

Various other methods for the formation of ultra-thin SiO<sub>x</sub> layer were applied to come across the best possible technique to deposit such thin

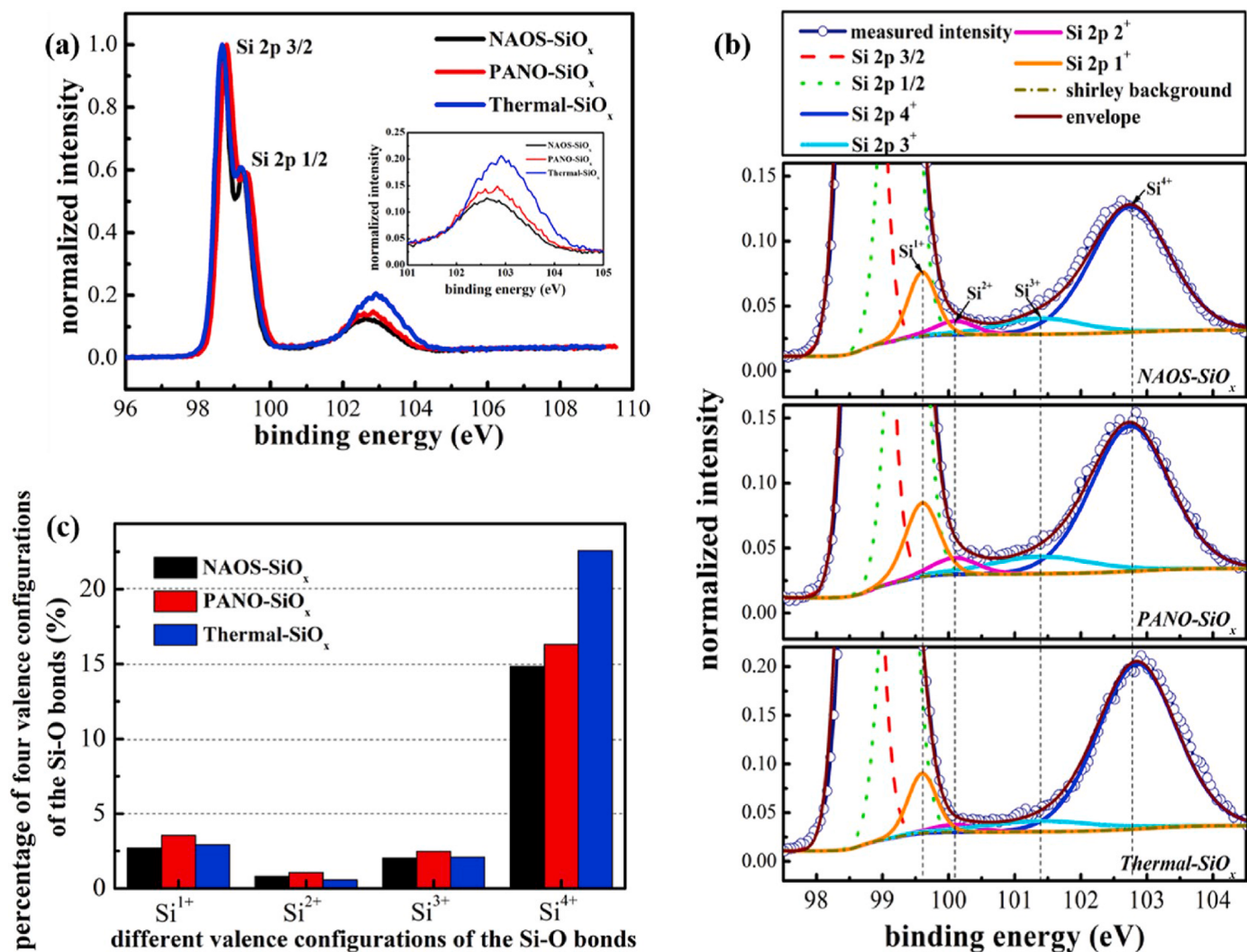


**Fig. 10.** (a) Comparison of XPS spectra of different SiO<sub>x</sub> samples (NAOS-SiO<sub>x</sub>, PANO-SiO<sub>x</sub> and Thermal-SiO<sub>x</sub>) after normalization. The small image as the inset is the energy spectrum comparison of 101 eV–105 eV after normalization. (b) Fractional fitting (Si 2p 3/2 and Si 2p 1/2, Si1<sup>+</sup>, Si2<sup>+</sup>, Si3<sup>+</sup> and Si4<sup>+</sup>) of XPS spectra of different SiO<sub>x</sub> samples. (c) Comparison of the percentages of four valence configurations of the Si–O bonds in the SiO<sub>x</sub> films obtained by fitting the Si 2p XPS spectra of the three kinds of SiO<sub>x</sub> samples [39].

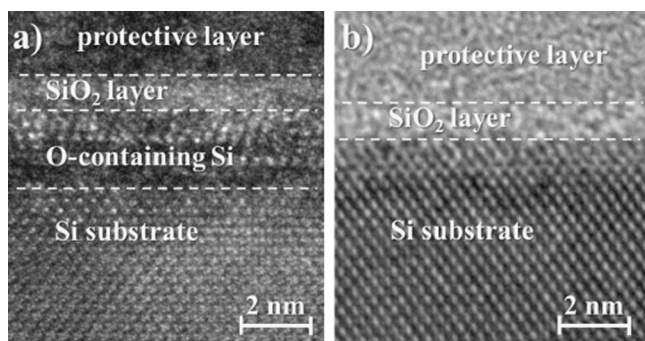


**Fig. 11.** TEM image of thin silicon oxide layer ( $d \approx 1.3\text{ nm}$ ) (a) before and (b) after annealing, the inhomogeneity in crystallinity almost disappears after the annealing step [42].

SiO<sub>x</sub> layer without compromising with its quality in terms of the passivation properties [32,38–40]. Huang et al. investigated the impact of using plasma assisted nitrous oxide gas oxidation (PANO) method instead of standard hot HNO<sub>3</sub> oxidation (NAOS) process for the formation of ultra-thin SiO<sub>x</sub> layer onto solar grade n-type CZ Si wafers [38].

After optimizing the process parameters and performing the crystallization process the developed n-TOPCon structure featured an excellent surface passivation quality with an  $iV_{oc}$  of as high as 730 mV; the corresponding value of  $J_0$  was found to be  $4.3 \text{ fA/cm}^2$ . Further improvement in the passivation quality with an  $iV_{oc}$  of 747 mV and  $J_0$  of  $2 \text{ fA/cm}^2$  was realized after performing AlO<sub>x</sub>/SiN<sub>x</sub> hydrogenation step. In contrast, prior to the hydrogenation step the developed n-TOPCon structure which comprised of NAOS-SiO<sub>x</sub> showed slightly inferior passivation quality to its counterpart PANO-SiO<sub>x</sub> as it offered an  $iV_{oc}$  of 727 mV and  $J_0$  of  $4.4 \text{ fA/cm}^2$ . The study also revealed that the optimized annealing temperature for the PANO SiO<sub>x</sub> and NAOS SiO<sub>x</sub> samples was different (880°C for PANO and 820°C for NAOS) which was found to be consistent to the study conducted by Gao et al. [32]. Huang et al. also extended their study to the device level and the best conversion efficiency of 21.01% with  $V_{oc} = 669 \text{ mV}$ ,  $J_{sc} = 38.70 \text{ mA/cm}^2$  and FF = 81.16% (cell area:  $4 \text{ cm}^2$ ) was yielded for the developed TOPCon solar cells featuring PANO-SiO<sub>x</sub> layer [38]. On the other hand, Guo et al. developed p-TOPCon structure onto  $3 \Omega\text{-cm}$ ,  $170 \mu\text{m}$ , n-type CZ c-Si wafers where the ultra-thin SiO<sub>x</sub> tunnelling layer was developed by three different ways: (a) a hot HNO<sub>3</sub> oxidation at 110°C for 15 min (NAOS-SiO<sub>x</sub>), (b) a plasma-assisted oxidation for 5 min in N<sub>2</sub>O atmosphere (PANO-SiO<sub>x</sub>), and (c) a thermal oxidation inside a tube-furnace

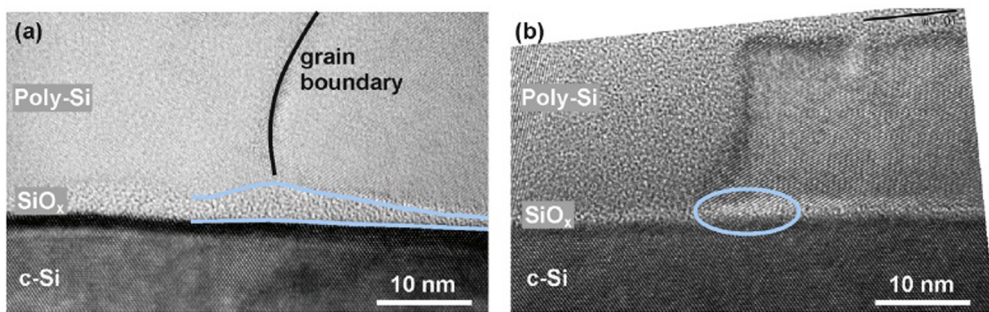


**Fig. 12.** High resolution TEM cross section images of  $n^+$  poly-Si/c-Si junctions after junction formation at 1050°C, showing (a) a local variation of the interfacial oxide thickness, and (b) a direct local contact of the lattice of the poly-Si and of the c-Si substrate, possibly indicating pinhole formation. Initial interfacial oxide thickness was  $\sim 2.4$  nm for (a) and  $\sim 1.7$  nm for (b). The  $J_0$  values are (a) 10 fA/cm $^2$  and (b) 20 fA/cm $^2$  [6].

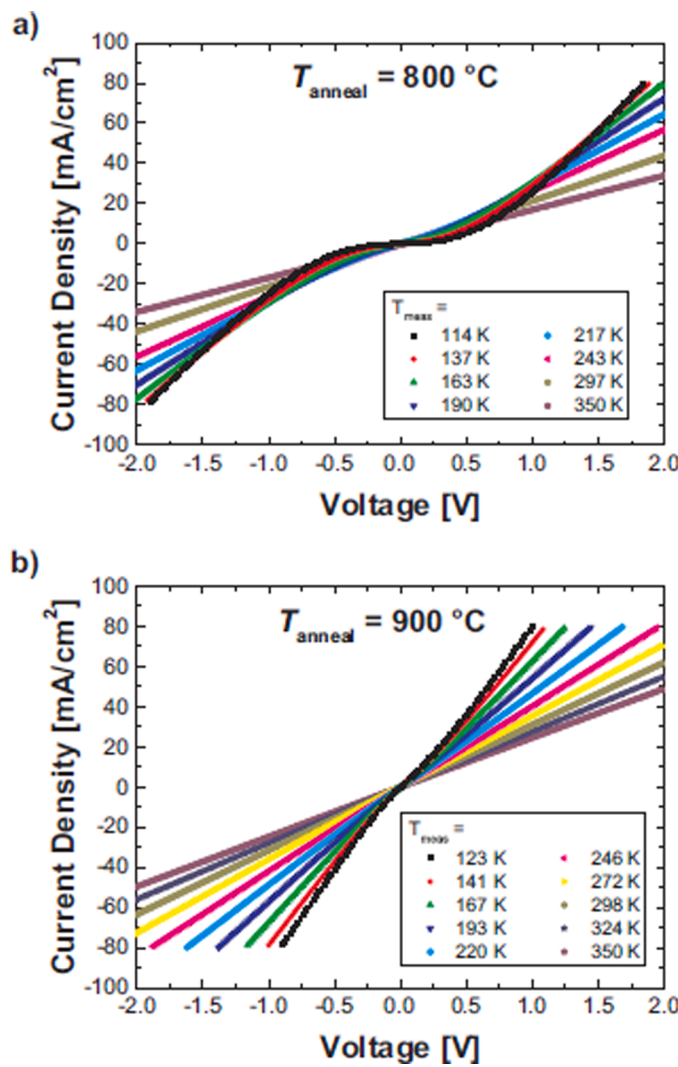


**Fig. 13.** Dark J-V characteristics of n-TOPCon samples annealed at (a) 800°C and (b) 900°C [45].

at 650°C for 20 min within N<sub>2</sub> and O<sub>2</sub> atmosphere (Thermal-SiO<sub>x</sub>) [39]. The result showed that the best passivation quality with  $iV_{oc} = 722$  mV,  $\tau_{eff} = 1.56$  ms for an injection level of  $1 \times 10^{15}$  cm $^{-3}$  and  $J_0 = 5.95$  fA/cm $^2$  was obtained for the thermally grown SiO<sub>x</sub> layer (Thermal-SiO<sub>x</sub>). In contrast, relatively poor passivation quality was observed for chemically grown SiO<sub>x</sub> layers (NAOS-SiO<sub>x</sub>) with  $iV_{oc} = 718$  mV,  $\tau_{eff} = 1.85$  ms for an injection level of  $1 \times 10^{15}$  cm $^{-3}$  and  $J_0 = 7.9$  fA/cm $^2$  and the worst

passivation properties were realized for plasma assisted SiO<sub>x</sub> layers (PANO-SiO<sub>x</sub>) with  $iV_{oc} = 703$  mV,  $\tau_{eff} = 1.65$  ms for an injection level of  $1 \times 10^{15}$  cm $^{-3}$  and  $J_0 = 18.5$  fA/cm $^2$ . Besides, the optimized annealing temperature for realizing the best passivation quality was found to be different for the differently grown SiO<sub>x</sub> layers (930°C for Thermal-SiO<sub>x</sub>, 820°C for NAOS-SiO<sub>x</sub> and 880°C for PANO-SiO<sub>x</sub>). Moreover, XPS spectra revealed that the samples with Thermal-SiO<sub>x</sub> possessed higher stoichiometric Si<sup>4+</sup> states and hence better passivation quality with lower number of interfacial defect states was revealed in comparison with the other ones. In addition, more stoichiometric Thermal-SiO<sub>x</sub> samples offered more resistance for B-diffusion during the thermal annealing process and due to which higher annealing temperature was required to optimize the B-diffusion profiles. In contrast, the authors assumed that the penetration of N into the ultra-thin SiO<sub>x</sub> layer during the plasma assisted N<sub>2</sub>O oxidation process resulted in realizing relatively poor passivation quality. Moreover, from the contact resistivity ( $\rho_c$ ) value of Thermal-SiO<sub>x</sub> samples was higher than its counterpart. But still the absolute value was quite low for enabling high efficiency TOPCon solar cells. Recently, Mandal et al. also reported that ultra-thin SiO<sub>x</sub> tunnelling layer grown by thermal oxidation method demonstrated superior surface passivation quality for both polished and textured monocrystalline CZ Si wafers (both n-type and p-type were used) compared to the oxide layer grown by either chemical oxidation or plasma oxidation method [40]. The supremacy of thermally grown ultra-thin SiO<sub>x</sub> tunnelling layer in terms of  $iV_{oc}$  and minority carrier lifetime ( $\tau$ ) may be attributed to the lesser number of Si/SiO<sub>x</sub> interfacial defect states. In addition, XPS results also confirmed that thermally grown SiO<sub>x</sub> layer featured the most number of Si<sup>4+</sup> oxidation states than the oxide layer developed by other methods.

Apart from the above mentioned methods, plasma enhanced atomic layer deposited (PE-ALD) was also used to develop ultra-thin hydrogenated silicon oxide layer (SiO<sub>x</sub>:H) [41]. In this study, passivation property of stack layers consisting of plasma enhanced atomic layer deposited (PE-ALD) ultra-thin hydrogenated silicon oxide layer (SiO<sub>x</sub>:H) and plasma enhanced chemical vapor deposited (PECVD) hydrogenated amorphous silicon [either intrinsic (a-Si:H) or doped (p-a-Si:H, n-a-Si:H)] layer was thoroughly investigated. The thickness of SiO<sub>x</sub>:H layer which was precisely controlled by ALD technique was kept below 2 nm and the post-deposition annealing temperature of the stacked layer was varied from 100 to 900°C with an interval of 50 to 100°C to realize the impact of the thermal treatment of the stacked layer onto its surface passivation properties. The study revealed that post deposition annealing of the stacked layer at 300°C for 30 min might provide notable surface passivation with an effective minority carrier lifetime of 0.5 ms. Probably diffusion of H atoms from a-Si:H layer into SiO<sub>x</sub>:H layer during low temperature thermal annealing facilitated to passivate the unfinished bonds present at the surface of c-Si wafer. As expected, improvement in the crystallization of doped a-Si:H layer was also observed when the samples were annealed at higher temperature. Additionally, the

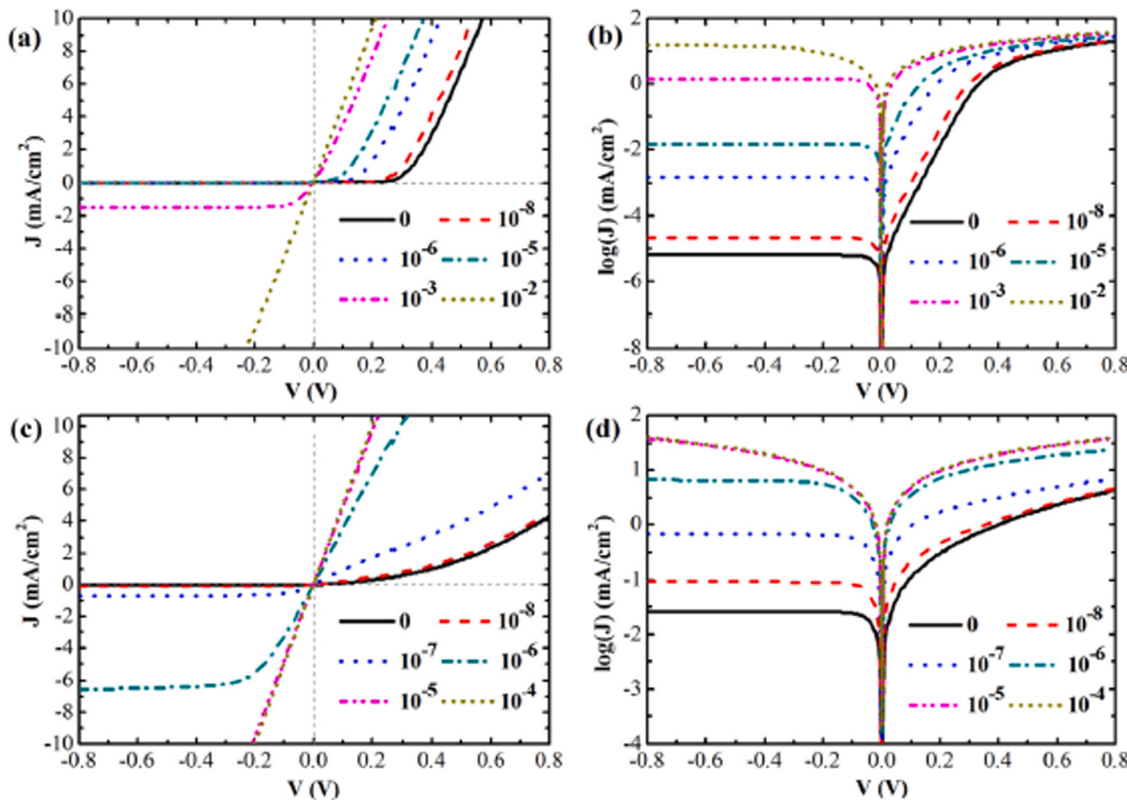


**Fig. 14.** Simulated J-V characteristics of (a, b) the GaIn/n-c-Si/SiO<sub>x</sub>/Al, and (c, d) GaIn/n-c-Si/SiO<sub>x</sub>/n+-poly-Si/Al structures with different magnitudes of transport possibility through pinholes, where the SiO<sub>x</sub> thickness is 1.4 nm, similar to what used in the real TOPCon solar cells [59].

stoichiometry of SiO<sub>x</sub> layer was also found to be increased due to the complete effusion of hydrogen atoms at such high temperature (~850°C) thermal treatment which in turn significantly enhances the passivation quality of SiO<sub>x</sub>:H/ p-a-Si:H or n-a-Si:H stacked layers. In essence, realization of notable surface passivation by SiO<sub>x</sub>:H/ a-Si:H stacked layer even after low temperature post-deposition thermal treatment may pave the path for further research to lower down the thermal budget.

#### 6.1.2. Effect of the properties of ultra-thin SiO<sub>x</sub> layer on the surface passivation quality

Carrier recombination losses at Si/SiO<sub>x</sub> interfaces are greatly influenced by structural and chemical properties of interfacial tunneling layers. Thickness, homogeneity and chemical compositions i.e., stoichiometry of tunneling oxides play a major role to improve the majority carriers collection and to reduce the recombination current density at metal-semiconductor interfaces. Therefore, thickness, chemical composition and electrical properties of ultra-thin SiO<sub>x</sub> tunneling layer were measured and analyzed by using different advanced characterization techniques [42]. In this study, the SiO<sub>x</sub> layers were grown by UV/O<sub>3</sub> oxidation process based on polished FZ c-Si wafers and some samples were undergone a subsequent annealing process in a tube furnace at 800°C to understand the impact of thermal treatment on the change of structural and chemical properties of the SiO<sub>x</sub> tunneling layers. TEM and angle-resolved XPS (X-ray Photoelectron Spectroscopy) were found to be the most suitable method for the measurement of the thickness of the ultra-thin 1.0–1.5 nm SiO<sub>x</sub> layers with an accuracy of 0.35 nm. On the other hand, an overestimation of the actual thickness was observed by using ToF-SIMS (Time-of-Flight Secondary Ion Mass Spectroscopy) technique and for spectral ellipsometry process, applied model has an influential role on the data interpretation.

Additionally, several high resolution techniques namely TEM (Transmission Electron Microscopy), ARXPS (Angle Resolved XPS) and

ToF-SIMS were used to understand the structural and chemical composition of the interfacial tunneling oxide layer. The effect of annealing on the homogeneity of the interfacial oxide layer was clearly visible in TEM investigation techniques. The study revealed that more homogeneity at Si/SiO<sub>x</sub> interfaces was obtained for the annealed samples whereas the non-annealed samples resulted the presence of inhomogeneity with a depth of about 5 nm. Besides, ToF-SIMS measurements demonstrated that the first few atomic layers in the Si substrate contained lower oxygen content. Finally, bias dependent specific transfer resistance perpendicular to the tunnel oxide layer was calculated and the value of specific transfer resistance was in the range of 1–3 Ω-mm<sup>2</sup> in the forward direction.

On the other hand, Wang et al. used three different thicknesses (1.55, 1.25 and 1.43 nm) of SiO<sub>x</sub> tunneling layer (formed in a tube furnace) to investigate its effect on the performance of the TOPCon solar cells which were fabricated onto n-type, 0.5–2 Ω-cm, 156.75 × 156.75 × 0.18 mm<sup>3</sup> CZ Si wafers [43]. The metallic contacts of the cells were realized by industrially feasible screen-printing technology. Eventually, the best cell featuring 1.55 nm thick SiO<sub>x</sub> tunneling layer demonstrated a power conversion efficiency of 22.43% with V<sub>oc</sub> = 689.4 mV, J<sub>sc</sub> = 40 mA/cm<sup>2</sup> and FF = 81.35%. The corresponding phosphorous doping concentration in the poly-Si layer was over 1 × 10<sup>20</sup> atom/cm<sup>3</sup>. As a result, high value of FF and a very low value of series resistance (R<sub>series</sub> = 4.34 mΩ) were obtained due to this high phosphorous doping concentration. In addition, the recombination current density (J<sub>0, rear</sub>) value was as low as 18 fA/cm<sup>2</sup> for the samples which possessed 1.55 nm thick homogeneous and dense SiO<sub>x</sub> tunneling layer. However, simulation study revealed that a power conversion efficiency of beyond 24% may be obtained by improving the passivation quality at the rear and by implementing a selective emitter to reduce the recombination current density at metal-semiconductor interface at the front side.

Again, as stated above that the passivation quality of the ultra-thin SiO<sub>x</sub> layer is strongly influenced by interface trap density (D<sub>it</sub>) which

again depends on the stoichiometry of the tunnelling layer. On the other hand, the stoichiometry of the ultra-thin oxide layer is dependent on the fabrication process and post deposition thermal treatment. A study to control the oxide stoichiometry by optimizing the post deposition annealing conditions was carried out by Kim et al. [44]. Blistering of thin films on flat Si substrate surfaces was observed at the time of thermal treatment of doped a-Si:H layers. This phenomenon may be caused by the effusion of hydrogen from a-Si:H layers. However, minimization of this phenomenon may be realized by controlling the surface morphology and annealing profile which in turn provide adequate time and path for the escape of hydrogen atoms. As a result, an implied  $V_{oc}$  ( $iV_{oc}$ ) of more than 700 mV was realized for p-type passivated contacts at an annealing temperature of 900°C. On the other hand, degradation in the passivating quality of the passivated contacts for the annealing temperature of beyond 900°C may be attributed to the local disruption of ultra-thin  $\text{SiO}_x$  layer and diffusion of phosphorous in n-type passivated contacts. Concurrently, electrical analysis demonstrated a decrement of the electrical resistivity of  $\text{SiO}_x$  layer for high temperature (greater than 900°C) annealing which was also shown by many reports [6,45]. Moreover, a very high implied  $V_{oc}$  ( $iV_{oc}$ ) of about 740 mV was realized for n-type passivated contact at an annealing temperature of 900°C [44]. Baek et al. claimed that post deposition ozone-treatment at 400°C demonstrated a significant improvement in the passivating quality of ultra-thin  $\text{SiO}_x$  tunneling layers which were grown in 70%  $\text{HNO}_3$  solution at 110°C for 5 min onto the CZ Si wafers [46]. Minimization of the sub-oxide states at Si/ $\text{SiO}_2$  interface due to the ozone-treatment might be the reason for realizing a very high implied open-circuit voltage ( $iV_{oo}$ ) of 740 mV for n-type passivated contacts. The authors further added that such high value of  $iV_{oc}$  was achieved for an optimized crystallization temperature of 875°C in  $\text{POCl}_3$  diffusion process for amorphous silicon layers.

#### 6.1.3. Formation of pinholes and its impact on the charge carrier transport mechanisms through ultra-thin $\text{SiO}_x$ tunneling layer

In 2016, Peibst et al. reported about various other notable observations apart from the lateral homogeneous tunneling at carrier selective passivated poly-Si/c-Si junctions [6]. Firstly, excellent passivation quality was realized at poly-Si/c-Si junctions irrespective of the tunneling barrier height ratio for the charge carriers. Secondly, TEM study demonstrated the change in the structural properties such as local thickness reduction, formation of pinholes at the interfacial  $\text{SiO}_x$  tunneling layer due to the thermal treatment, even for the samples featuring excellent passivation quality. Consequently, transportation of charge carriers at poly-Si/c-Si junctions might be affected due to the localized current flow through the pinholes and the region of reduced thickness of tunneling layer. Hence, one may conclude that the lateral homogeneous tunneling is not solely responsible for the flow of charge carriers through the ultra-thin tunnel oxide layer. Therefore, the authors recommended terming this passivated contacts as POLO (poly-silicon on oxide) junctions. Thirdly, suitable and sufficient thermal treatment may provide low junction resistance ( $2.4 \text{ m}\Omega\text{-cm}^2$ ) even for the samples possessing an interfacial oxide layer thickness of greater than 2 nm. Therefore, by realizing the findings, one may consider the poly-Si/c-Si junction as “classical, locally contacted emitter”.

Lancaster et al. also studied the formation and the influential effect of pinholes on the charge carrier transport mechanism through ultra-thin  $\text{SiO}_x$  layers [47]. C-AFM (conductive atomic force microscopy) measurements showed that increment of annealing temperature from 800°C to 950°C raised the density of pinholes by a factor of 3. This phenomenon may be attributed to the thermal degradation of the oxide layer at higher annealing temperature. Besides, Choi et al. also realized the reduction of the oxide layer thickness and formation of pinholes through the ultra-thin oxide layer at higher annealing temperature (beyond 800°C and upto 1000°C) which in turn lowered down the carrier selectivity of the passivated contact [48]. Accordingly, the authors suggested that the optimized thickness value of ultra-thin  $\text{SiO}_x$  oxide

layer should be in the range of 1.2 nm to 1.5 nm. Moreover, Tetzlaff et al. demonstrated that the pinholes might be present into the wet chemically grown ultra-thin oxide layer even after annealing of poly-silicon on oxide (POLO) junctions at relatively low temperature of 750°C [49]. The correlation of annealing temperature and the pinhole density was investigated and the magnitude of the pinhole densities was found to be increased with the increment of annealing temperature, converged well with the other reports [47,48]. Furthermore, Tetzlaff et al. revealed that pinhole densities had strong impact on the saturation current densities ( $J_0$ ) and  $J_0$  was found to be increasing in nature with the increment pinhole densities [49]. The trend of this increasing nature of  $J_0$  with pinhole densities was found to be more prominent at higher pinhole density values [6,50–52]. Huang et al. in their experiment observed the leaking current spots (part of which might be generated from pinholes) from c-AFM images and both the size and the density of leaking current spots were found to be increased with the increment of annealing temperature [38]. The presence of pinholes in ultra-thin  $\text{SiO}_x$  layer was also confirmed by various other research reports published at different times [53–58]. Folchert et al. developed two types of TOPCon structures (n-TOPCon based onto n-type and p-TOPCon based onto p-type Si wafers) and named as “pinhole samples” and “tunneling samples”, respectively to realize the % contribution of current flow caused by pinholes and quantum mechanical tunneling process in each of the samples [55]. In the “pinhole samples” the thickness of thermal oxide was kept as 2.1 nm and the annealing temperature for the formation of TOPCon structure was kept at 1050°C to facilitate the production of more pinholes at higher annealing temperature. In contrast, “tunneling samples” featuring  $(1.7 \pm 0.1)$  nm  $\text{SiO}_x$  layer grown by thermal oxidation process were annealed at relatively low temperature of 700°C so that possibility of pinhole formation could be minimized. Eventually, the study revealed that the maximum current transport through pinholes was  $\sim 94$  and  $\sim 35\%$  for “pinhole samples” and “tunneling samples”, respectively. According to Galleni et al., the dominant charge carrier transportation mechanism through the ultra-thin  $\text{SiO}_x$  layer was found to be dependent on the annealing temperature along with the formation process of  $\text{SiO}_x$  layer [57]. In the report, the authors revealed that relatively higher annealing temperature (850°C to 950°C) was required to enable the pinhole dominant transportation process of charge carriers through thermally grown 1.5 nm  $\text{SiO}_x$  layer. In contrast, an annealing temperature of 700 to 750 °C was found to be sufficient to realize pinhole dominant carrier transport through chemically grown 1.3 nm  $\text{SiO}_x$  layer. Besides, the dominant transport mechanism was found to be independent to the surface morphology of the base wafer; however, lower contact resistivity ( $\rho_c$ ) was obtained for the textured wafers in comparison to the planar ones. The effect of duration of high temperature annealing process on the formation of pinholes in the ultra-thin  $\text{SiO}_x$  layer was studied thoroughly by Yang et al. and it was observed that the pinhole density did not change much for prolonged thermal treatment of 180 min in compared to 30 min thermal annealing even at different annealing temperature [58]. For example, the magnitude of pinhole density at an annealing temperature of 820°C was found to be increased from  $3.2 \times 10^{-8} \text{ cm}^{-2}$  to  $3.5 \times 10^{-8} \text{ cm}^{-2}$  for increasing the annealing time from 30 min to 180 min. From the c-AFM measurement systems, the same trend was also noticed at 950°C annealing temperature where the pinhole density just got increased from  $2.0 \times 10^{-9} \text{ cm}^{-2}$  to  $2.1 \times 10^{-9} \text{ cm}^{-2}$  for increasing the time duration from 30 min to 180 min. However, the rapid heating/cooling process produced compressive/tensile stress and as a result, significant amount of pinholes were formed inside the  $\text{SiO}_x$  layer which also featured much lower thermal expansion coefficient in compared to bulk Si layer and doped poly-Si layer. Therefore, it may be stated that the formation of pinholes mostly depend upon the heating/cooling rate of the TOPCon/POLO structure rather than the duration of thermal treatment.

Feldmann et al. investigated the transport mechanisms of charge carriers through the passivating contacts with the help of temperature dependent current-voltage (J-V) measurements [45]. From the

4-terminal dark J-V measurements, an exponential rise in the contact resistance at lower temperature was observed for the passivating contacts featuring chemically grown homogeneous ultra-thin silicon oxide layer and phosphorous doped poly-Si layer. The corresponding annealing temperature for the dopant activation and crystallization was 800°C. This non-linearity in the J-V characteristics of the passivating contacts may be attributed to the MIS (metal-insulator-semiconductor) theory along with the charge carriers tunneling through the ultra-thin oxide layer. However, a linear J-V characteristic was observed for the TOPCon structures which were annealed at 900°C. This phenomenon may be attributed to the occurrence of transportation of the charge carriers through pinholes. Consequently, the authors concluded that the carrier transport mechanism in TOPCon structure with homogeneous or non-disrupted oxide layer is mainly dominated by the quantum mechanical tunneling process. As a result, TOPCon structures which were annealed at 800°C showed better surface passivation quality with higher  $V_{oc}$  at device level compared to the TOPCon structures which were annealed at 900°C. So, formation of pinholes at higher annealing temperature may be responsible for the degradation of the passivation quality of tunneling oxide layer and hence lower  $iV_{oc}$  was realized as shown in the Table 4.

Furthermore, the presence of pinholes in ultra-thin  $\text{SiO}_x$  layer and its impact on the charge carrier transport mechanism were investigated experimentally and by simulation [59]. From dark J-V and c-AFM measurements, the transportation of charge carriers through pinholes was confirmed. Besides, simulation study revealed some useful observations: (i) if the transportation of charge carriers occurs due to the tunneling process only, then the J-V characteristic will be non-linear, (ii) increment in both forward current and reverse saturation current will be observed if pinholes contribute only a small amount of transportation of charge carriers, (iii) J-V curve will show linearity or Ohmic behavior when a certain amount of charge carriers flow through the pinholes. These findings converged well with the observations made by Guo et al. [39]. Also, the simulation results demonstrated that suitable amount of carrier transport through pinholes may maximize the FF and thus the power conversion efficiency of the TOPCon solar cells (when the thickness of  $\text{SiO}_x$  layer is greater than 1.2 nm). Generally, for a thicker  $\text{SiO}_x$  layer solely quantum mechanical tunneling can't provide sufficient carrier transport channels and due to which series resistance ( $R_{series}$ ) value gets increased. This resulted in obtaining lower FF. However, too much transportation of charge carriers through pinholes resulted in lowering down the cell performance. Therefore, an optimized pinhole density and pinhole size may feature an improved cell performance, the process of which is a subject of further research.

## 6.2. Poly-Si layer

Apart from ultra-thin  $\text{SiO}_x$  tunnelling layer, doped poly Si layer also plays a significant role in the passivating quality of TOPCon structure. The characteristics of doped poly-Si layer depend upon various parameters such as fabrication process, doping concentration, thickness of the layer, annealing atmosphere, annealing time, annealing temperature, even post annealing treatments. The following section will deal with different measures taken for improving the quality of doped poly-Si layer.

### 6.2.1. Development of doped poly-Si layer

*Ion implanted doped poly-Si layer.* Plasma enhanced chemical vapor deposition (PECVD) and low pressure chemical vapor deposition (LPCVD) techniques are widely used for the development of a-Si layer or a-Si:H layer and different types of impurities into this a-Si or a-Si:H layer may be introduced by two processes, namely *in-situ* doping [15,20,21, 25–32,34–37,39,44,45,47,59] (where different types of doping gases such as  $\text{PH}_3$  for n poly-Si and  $\text{B}_2\text{H}_6$  or  $\text{B}(\text{CH})_3$  for p poly-Si are added

during the growth process) and *ex-situ* doping (ion-implantation) [60–63]. High temperature annealing is then performed for the dopant activation and crystallization of this doped a-Si:H layer. Despite obtaining excellent result by using *in-situ* doping process, many researchers preferred ion-implantation technique for doping purpose of amorphous silicon layer to form TOPCon structure due to possessing many advantages such as precise dose control, ability of localized doping i.e. controllability of the penetration depth of the dopant atoms into the base material etc. [60–63]. For an example, Feldmann et al. investigated the influential effect of using low energy ion implantation technique for the doping purpose of PECVD coated 20 nm thick undoped amorphous silicon layer [60]. In essence, the study was conducted to correlate the impact of ion energy and ion dose on the passivation quality of both phosphorous and boron doped TOPCon structures which were fabricated onto planar,  $<100>$  oriented, 200  $\mu\text{m}$ , 1  $\Omega\text{-cm}$ , n-type FZ Si wafers. Besides, the samples were annealed at two different annealing temperatures (800°C and 900°C) for 60 min to activate the dopant and crystallize the doped amorphous silicon layer. Excellent surface passivation was obtained for phosphorous implantation with an implied  $V_{oc}$  ( $iV_{oc}$ ) of greater than 720 mV at an annealing temperature of 800°C. Additionally, the samples which were annealed at 800°C showed little variations in  $iV_{oc}$  due to the change of ion doses. However, deterioration of  $iV_{oc}$  was observed with the increment of the ion doses for 900°C annealed samples. According to the authors, this inverse relationship was obtained due to the oxide's inability to inhibit the increment of phosphorous penetration from doped poly-Si layer into the bulk crystalline Si wafer at relatively higher annealing temperature of 900°C. As a result, Auger recombination ( $J_{0,\text{Auger}}$ ) rate got increased within the diffused c-Si region near the c-Si/ $\text{SiO}_x$  interface. Besides, increment of surface recombination velocity ( $S_{eff}$ ) at c-Si/ $\text{SiO}_x$  interface was also noticed which was also a strong reason for the decrement of the value of  $iV_{oc}$  at higher annealing temperature. On the other hand, contrary to n-contact, an enhancement of  $iV_{oc}$  was observed with the increment of ion doses for  $\text{BF}_2$ -implanted passivation contacts (p-contacts) at 800°C annealing temperature. However, poor passivation quality was obtained for the samples which were annealed at 900°C in spite of possessing low Auger recombination ( $J_{0,\text{Auger}}$ ) value which meant diffusion of boron atoms into c-Si layer was not the cause for realizing poor  $iV_{oc}$ . Therefore, high carrier recombination rate within the doped poly-Si layer and at c-Si/ $\text{SiO}_x$  interface owing to the clustering of boron atoms might be a valid reason for obtaining such poor results. The authors finally recommended that the understandings may lead to simplify the development of IBC solar cells featuring passivation contacts. On the other hand, Reichel et al. studied the impact of P implantations into PECVD coated 15 nm boron doped a-Si layers [61]. After optimizing the ion doses, the Suns- $V_{oc}$  samples demonstrated an outstanding  $iV_{oc}$  of greater than 700 mV (corresponding annealing temperature: 800°C) which in turn facilitated the development of IBC solar cells with ion implanted tunnel oxide passivated contacts based onto 1  $\Omega\text{-cm}$ , 200  $\mu\text{m}$  thick, n-type FZ silicon wafers. The fabricated solar cells with an active area of 2 cm × 2 cm featured the highest  $V_{oc}$  of 682 mV and the highest pFF (pseudo fill factor) of 82.1%. Nevertheless, the authors pointed out that further investigations focusing on efficient charge carrier extraction are required for improving the cell performance. Furthermore, in another contribution, Reichel et al. claimed that for n-type passivated contacts, an excellent  $iV_{oc}$  of 725 mV was obtained by implanting P into undoped a-Si layers while slightly less  $iV_{oc}$  of 720 mV was realized when P implantations was made into *in-situ* B-doped a-Si layers [62]. In contrast, p-type passivated contacts were realized by either implanting  $\text{BF}_2$  or B into intrinsic a-Si layers.  $\text{BF}_2$  implantation provided excellent passivation quality with an  $iV_{oc}$  of 690 mV where as poor passivation quality was obtained for B implantations with an  $iV_{oc}$  of 640 mV. Improvement in the passivating quality by implanting  $\text{BF}_2$  instead of B implantations may be attributed to the presence of F as it provides better interfacial passivation. However, a reduced FF was obtained for silicon solar cells featuring  $\text{BF}_2$  implantations into undoped a-Si layers. Formation of

non-ohmic Schottky contact may be responsible for this reduction in FF. On the other hand, the formation of this non-ohmic contact may be ascribed to: (i) the deactivation of B dopant atoms due to the formation of defect states at the surface of the poly silicon layer, and (ii) the increment of the effective thickness of  $\text{SiO}_x$  interfacial layer. Eventually, the both-side contacted solar cells featuring P implantations into undoped a-Si layers (to form electron contact) and *in-situ* B-doped hole contact demonstrated a  $V_{oc}$  of 690 mV and a FF of 79.1%. In contrast, the solar cells with P implantations into *in-situ* B doped a-Si layers featured a  $V_{oc}$  of 680 mV and a FF of 80.4%. The results and the understandings may smooth the progress of the fabrication of IBC solar cells with passivated contacts. Again, ion-implantation technique was used for the conversion of low pressure chemical vapor deposited (LPCVD) intrinsic a-Si layer into doped poly-Si layer for the formation of TOPCon structure [63]. In the contribution, the influential effect on the surface passivation properties of the ion implanted passivated contacts due to the variation of doping species, ion dose, and poly-Si thickness was investigated to facilitate the fabrication of both-sided contact solar cells with higher power conversion efficiency. The study revealed that superior surface passivation quality with very low recombination current density ( $J_0$ ) of 4.5 fA/cm<sup>2</sup> was realized for n-type poly-Si contacts and the corresponding thickness of the poly-Si layer was 34 nm. On the other hand, significantly higher recombination current density ( $J_0$ ) of 22 fA/cm<sup>2</sup> was obtained for p-type poly-Si contacts. The corresponding  $iV_{oc}$  value was 696 mV and the doped poly-Si layer was 34 nm thick. The other important observation was the realization of slight improvement in the passivation quality of p-type poly-Si contacts when BF was implanted for doping purpose instead of B. Finally, both sided poly-Si/ $\text{SiO}_x$  passivated contacts Si solar cells featuring  $n^+$ -poly-Si at the front side and  $p^+$ -poly-Si at the rear side with an active cell area of 2 cm × 2 cm were fabricated onto 250 μm thick, 1 Ω-cm, p-type FZ Si wafers. The best cell showed a  $V_{oc}$  of 709 mV and a FF of beyond 81%. But high sheet resistance for thinner poly-Si films and concurrently, limitations of achieving short-circuit current density ( $J_{sc}$ ) of beyond 40 mA/cm<sup>2</sup> for thicker poly-Si films are one of the major concerns of these both sided poly-Si/ $\text{SiO}_x$  solar cells (in spite of featuring higher  $V_{oc}$  than standard Si heterojunction solar cells).

**Other innovative approaches.** One may concern that use of low frequency industrial scalable direct plasma PECVD technique for depositing doped silicon layer onto ultra-thin  $\text{SiO}_x$  tunnelling layer may severely damage the oxide layer and hence the passivation quality will also be degraded with an immediate effect. However, excellent surface passivation quality with an implied  $V_{oc}$  ( $iV_{oc}$ ) of above 735 mV and an implied FF (IFF) of 87.9% was realized when industrial scalable low frequency plasma enhanced chemical vapor deposition (RF-PECVD) technique was used to deposit the doped amorphous silicon layer for the formation of TOPCon structure [64]. Besides, TLM (Transmission line measurement) technique revealed that the upper limit of the specific contact resistivities of the samples were in the range of 3–6 mΩ cm<sup>2</sup>. Moreover, a lifetime test based on 100 Ω-cm, n-type FZ silicon wafers showed a very high minority carrier lifetime of 190 ms. Additionally, the study further revealed that better result was obtained when the low frequency PECVD coated doped poly-Si layer was combined with thermally grown ultra-thin interfacial tunnel oxide layer instead of combining with chemically grown oxide layer. On the other hand, Polzin et al. also obtained almost similar results by using low frequency batch-type direct plasma PECVD tool to realize doped Si layer for the formation of TOPCon structure [65]. Recently, another approach on the transformation of PECVD (13.56 MHz) coated phosphorous doped a-Si:H layer into  $n^+$  poly-crystalline Si layer by means of rapid thermal annealing (RTA) process was reported where several parameters such as annealing time (50–950 s), annealing temperature (780–900°C), cooling time (5–600 s) and the thickness of phosphorous doped a-Si:H layer (40–120 nm) were varied to facilitate the surface passivation quality of n-type TOPCon

structure [66]. The study revealed that RTA method took very low time of about 15 min for the whole crystallization process where as more than 60 min was needed in conventional tube furnace annealing process for the same purpose. Besides, no blistering during the thermal treatment was observed when the thickness of a-Si:H layer was less than 40 nm. But the passivation quality provided by RTA process with an  $iV_{oc}$  of 712 mV and  $J_0$  of 12.5 fA/cm<sup>2</sup> was found to be slightly inferior to the passivation quality realized by using conventional tube furnace annealing process. However, a post-annealing treatment of hydrogenation with ALD coated  $\text{Al}_2\text{O}_3$  capping layer resulted in a significant improvement of the surface passivation quality of RTA processed samples with an excellent  $iV_{oc}$  of 727 mV and a very low  $J_0$  of 4.7 fA/cm<sup>2</sup>. Eventually, the best cell with an active cell area of 2 cm × 2 cm demonstrated a power conversion efficiency of 23.04% with  $V_{oc} = 679$  mV,  $J_{sc} = 41.97$  mA/cm<sup>2</sup> and FF = 80.86%.

Atmospheric pressure chemical vapor deposition (APCVD) was found to be another suitable way to develop intrinsic or doped poly-Si layer [67,68]. The first report of APCVD coated doped poly-Si layer for the formation of POLO structure was presented by Markle et al. in the 35th European Photovoltaic Solar Energy Conference and Exhibition (EU PVSEC) which was held in 2018 [67]. According to that report, after performing high temperature thermal treatment and subsequent hydrogenation step adequate surface passivation quality was obtained for both n-type and p-type passivated contacts which featured chemically or thermally grown ultra-thin  $\text{SiO}_x$  layer and APCVD coated doped silicon layer. Quantitatively, the hydrogenated n-type and p-type POLO contacts based on CZ Si wafers provided quite low  $J_0$  of 6 fA/cm<sup>2</sup> and acceptable  $iV_{oc}$  of 721 mV and 730 mV, respectively. The best p-POLO solar cell fabricated onto 156.75 mm × 156.75 mm, 1.6 Ω-cm, p-type CZ Si wafers offered a conversion efficiency of 19.5% with  $V_{oc} = 661$  mV,  $J_{sc} = 37.7$  mA/cm<sup>2</sup> and FF = 78.0%. The corresponding cell area was 92.7 cm<sup>2</sup>. Recently, in 2022, Mousumi et al. claimed to realize a very low  $J_0$  of 3 fA/cm<sup>2</sup> and an  $iV_{oc}$  of 712 mV for hydrogenated n-type passivated contacts in which the doped silicon layer was prepared by APCVD technique [68].

Physical vapour deposition (PVD) techniques such as sputtering were used for the development of doped silicon layer [69,70]. Yan et al. in their study developed *in-situ* boron doped silicon films to realize hole-selective passivated contacts by using a single co-sputtering system which comprised of undoped silicon (99.999% purity) and boron (99.999% purity) as target materials [69]. The stack of rf sputtered p-type silicon films and wet chemically grown ultra-thin  $\text{SiO}_x$  interlayer showed interesting passivation properties with a  $J_0$  of less than 20 fA/cm<sup>2</sup> after undergoing a high temperature annealing step in N<sub>2</sub> atmosphere. Eventually, 2 cm × 2 cm p-TOPCon solar cells featuring sputter deposited doped Si layer were fabricated onto 200 μm, 1 Ω-cm, monocrystalline, p-type FZ Si wafers; the best conversion efficiency was found to be as high as 23.0% with  $V_{oc} = 701$  mV,  $J_{sc} = 41.1$  mA/cm<sup>2</sup> and FF = 79.9%. On the other hand, David et al. developed phosphorous doped silicon layers onto ultra-thin  $\text{SiO}_x$  layer by using dc sputtering unit to form the n-type passivated contact [70]. Furthermore, symmetric lifetime samples based onto n-type c-Si wafers were fabricated and the highest value of  $iV_{oc}$  was found to be 695 mV whereas the median value was 680 mV. Therefore, from Ref. [69,70] we may conclude that both p-TOPCon and n-TOPCon structure may be developed with notable surface passivation quality by using simple sputtering process. Most importantly, use of toxic gases like silane, diborane and phosphine may be avoided if sputtering is used for the development of doped silicon layers. However, significant improvement in the passivating properties of the TOPCon structure comprising of sputter deposited poly-Si layer is yet to be realized to compete with the state-of-the-art TOPCon structure featuring chemical vapour deposited poly-Si layer.

So far we have realized that high temperature annealing is a necessary and very important step to for the dopant activation and crystallization of the doped silicon layer. However, involvement of such high temperature annealing step undoubtedly increases the thermal budget

during the fabrication of the solar cells. In this regard, several approaches have been initiated by the researchers to reduce the temperature of the required annealing process and/or find a suitable alternative method for fulfilling the purpose for which annealing is done [71,72]. For example, in 2018, Masuda et al. reported that reduction of crystallization temperature and time may be realized by using aluminium-induced crystallization (AIC) technique for the development of doped poly-Si layer to form p-TOPCon structure [71]. The authors further added that improvement in the carrier density in the p-type AIC poly-Si layer was realized by using B-doped Si target instead of a non-doped Si target during the deposition of a-Si layer. This high carrier density due to the successful incorporation of Al and B resulted in the reduction of the resistance of doped poly-Si layer. Eventually, enhancement in the power conversion efficiency with relatively higher  $V_{oc}$  and FF was noticed due to having lower series resistance and higher carrier density. However, further explorations are still required as the best cell featured a conversion efficiency of 13.5%. Recently, in 2020, Wilkes et al. claimed that the use of novel pulsed-laser processing method instead of high temperature annealing treatment for the dopant activation and crystallization of phosphorous doped a-Si:H layer in TOPCon solar cell structure provided excellent surface passivation quality [72]. Besides, an improvement in the surface passivation quality with an implied open-circuit voltage ( $iV_{oc}$ ) of 718 mV, an effective minority carrier lifetime ( $\tau$ ) of 2 ms and single-sided recombination current density ( $J_0$ ) of 8.6 mA/cm<sup>2</sup> was realized after depositing 60 nm SiN<sub>x</sub> layer by PECVD method onto this laser processed TOPCon structure. However, the authors opined that further optimization of laser process and the thickness of a-Si:H layer may lead to maximize the interfacial passivation quality.

#### 6.2.2. Protecting the ultra-thin SiO<sub>x</sub> tunneling layer from damages/blistering during the development of poly-Si layer

Another major problem associated with the development of TOPCon structure is the blister formation [73,74]. Blisters are generally formed due to the accumulation of hydrogen content at the interface of SiO<sub>x</sub> and doped a-Si:H layer. This accumulation of hydrogen takes place mainly at the time of high temperature annealing process as the doped a-Si:H layer releases its hydrogen content during the high temperature thermal treatment. Formation of blisters is responsible for the degradation of the passivating quality of the TOPCon structure as it introduces inhomogeneity inside the film morphology. Hence, minimization of the blisters formation is essential so that the quality of TOPCon structure is not compromised. Li et al. also claimed that requirement of high temperature annealing process after the deposition of doped amorphous silicon layer onto SiO<sub>2</sub> tunneling layer for initializing the crystallization may lead to damage the ultra-thin tunneling oxide layer along with bulk Si layer [75]. However, Raman study revealed that TOPCon structure featuring  $\mu$ -Si thin layer demonstrated higher crystallinity at relatively low annealing temperature (around 600°C) as depicted in Fig. 15. Therefore, to overcome the damage caused by high temperature annealing such as blistering or balling up of ultra-thin SiO<sub>x</sub> layer, use of thin microcrystalline silicon layer was proposed instead of thin amorphous layer for the formation of TOPCon structure. Besides, improvement in the solar cell performance was also realized in the simulation study due to higher doping efficiency of thin microcrystalline silicon layer.

[Group A and Group B represent the two groups of Si layers which were deposited onto quartz substrates in PECVD chamber by varying the gas mixture. The gas flow ratio for Group A samples were SiH<sub>4</sub>:H<sub>2</sub>:PH<sub>3</sub> = 40:10:16 and for group B it was SiH<sub>4</sub>:H<sub>2</sub>:PH<sub>3</sub> = 10:200:4].

However, Tao et al. observed that tunnel oxide passivated contact featuring ultra-thin SiO<sub>x</sub> layer and doped a-Si:H layer showed better passivation quality [76]. In contrast, passivated contacts formed by SiO<sub>x</sub> tunnelling layer layer in conjunction with doped  $\mu$ -Si:H layer demonstrated better crystallization and no blistering upon thermal treatment but obtained poor passivation quality compared to its counterpart.

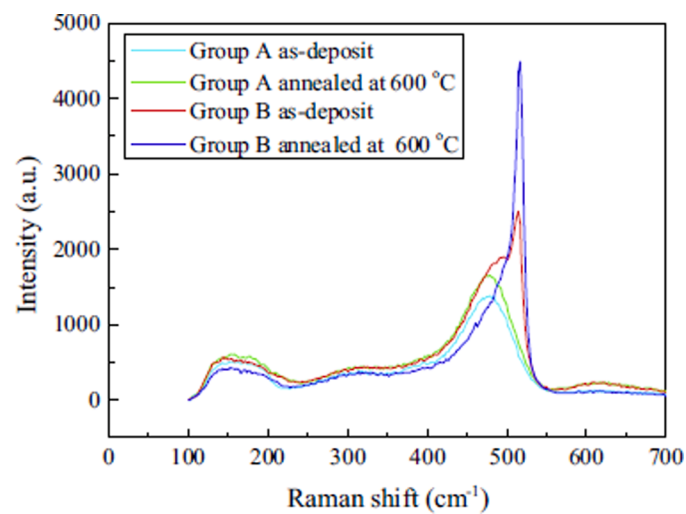


Fig. 15. Raman spectra of the Si layer as-deposited and after annealing at 600°C in nitrogen atmosphere for 60 min [75].

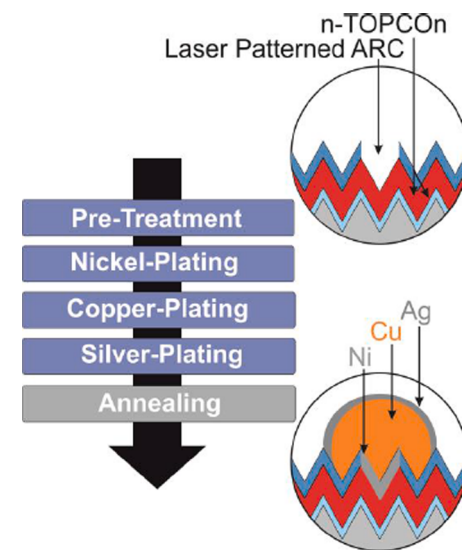


Fig. 16. Sequence of plating process used in this work [91].

Consequently, the authors used a-Si/ $\mu$ -Si:H hybrid layer for the formation of tunnel oxide passivated contact onto 3–8 Ω-cm, polished, n-type CZ Si wafers. This resulted an improvement in the passivation quality and contact properties by realizing an excellent minority carrier lifetime ( $\tau$ ) of 3.2 ms and an  $iV_{oc}$  of 716 mV. A significant improvement on the cell performance was also noted for the TOPCon solar cells featuring a-Si/ $\mu$ -Si:H hybrid layer at the back contact in comparison with the cells having only  $\mu$ -Si:H layer at the rear contact. Furthermore, simulation study revealed that a drastic improvement in the power conversion efficiency of the practical solar cells from 15.09% ( $V_{oc}$  = 600 mV,  $J_{sc}$  = 32.50 mA/cm<sup>2</sup>, FF = 77.4%) to 21.69% ( $V_{oc}$  = 694 mV,  $J_{sc}$  = 38.93 mA/cm<sup>2</sup>, FF = 80.29%) may be achieved by overcoming the front surface reflection and recombination losses.

The other ways to minimize the formation of blisters were described in a recent report by Choi et al. [77]. Firstly, fabrication of TOPCon structure onto the rough surface as the rough surface possesses higher adhesive force and consequently, chances of blister formation get reduced even after thermal annealing process. Secondly, high temperature deposition of doped a-Si:H layer may result in low hydrogen content inside the film. For an example, the authors observed almost no blistering of the annealed TOPCon structure when the doped a-Si:H layer

was formed by LPCVD technique at 580 °C. However, significant amount of blisters were found to be formed when the doped a-Si:H layer was deposited by PECVD technique at 300, 370 and 450 °C, despite low hydrogen content. This phenomenon may be attributed to the formation of porosity and increment of molecular-hydrogen tapping centres at higher substrate temperature.

Lin et al. claimed that use of PECVD coated carbon-doped poly-Si layer instead of doped poly-Si layer to form the TOPCon structure might be another suitable approach to restrain the effect of blistering [78]. Incorporation of carbon contents in poly-Si matrix (i) reduced the crystallization fraction of doped poly-Si layer; (ii) improved the bond strengths by forming stronger C-Si bonds; and (iii) formed C-H bonds which in turn reduced the possibility of H effusion from the passivated contacts during high temperature thermal treatment. In this way, carbon doped poly-Si layer could reduce the effect of blistering as well as preserve the passivating properties of the passivated contacts. Consequently, symmetrical lifetime based samples fabricated onto n-type CZ c-Si wafers featuring wet chemically grown ultra-thin SiO<sub>x</sub> layer and carbon doped poly-Si layer demonstrated an excellent surface passivation quality with an  $iV_{oc}$  of 750 mV,  $\tau_{eff}$  of more than 15 ms and a low  $J_0$  of 1.6 fA/cm<sup>2</sup>. In contrast, relatively poor result with an  $iV_{oc}$  of 739 mV,  $\tau_{eff}$  of 7.5 ms and a  $J_0$  of 2.2 fA/cm<sup>2</sup> was obtained for carbon free samples. In the device level (active cell area = 4 cm<sup>2</sup>), the best conversion efficiency was found to be as high as 24.27% ( $V_{oc} = 696.4$  mV,  $J_{sc} = 42.11$  mA/cm<sup>2</sup> and FF = 82.77%) for TOPCon solar cells featuring carbon doping poly-Si layer whereas the same was found to be 23.09% ( $V_{oc} = 688.2$  mV,  $J_{sc} = 41.80$  mA/cm<sup>2</sup> and FF = 80.28%) for the TOPCon solar cells featuring carbon free poly-Si layer. The improvement in  $V_{oc}$  and FF for carbon doped devices might be ascribed to the realization of superior passivation quality as stated above whereas the gain in  $J_{sc}$  might be attributed to the lower parasitic absorption of evanescent light due to the presence of wide band gap poly-SiCx layer. Furthermore, the study revealed the certified efficiency value of 23.82% for the TOPCon solar cells featuring carbon doped poly-Si layer, signifying the future application of poly-SiCx layer in the TOPCon/POLO devices. Zheng et al. also investigated the impact of carbon doping in boron doped poly-Si layer during the fabrication of double-sided passivated contacts solar cells (DPPCs) featuring p-TOPCon (SiO<sub>x</sub> + boron-doped poly-Si/boron-doped poly-SiCx) structure at the rear and n-TOPCon (SiO<sub>x</sub> + phosphorous-doped poly-Si) structure at the front side [79]. The solar cells were developed onto n-type, 1–5 Ω-cm CZ c-Si wafers with an active cell area of 2 cm × 2 cm. After optimizing the carbon doping concentration, thickness of boron doped poly-SiCx layer and post-deposition annealing temperature a conversion efficiency of 19.82% ( $V_{oc} = 694.7$  mV,  $J_{sc} = 36.28$  mA/cm<sup>2</sup> and FF = 78.63%) was yielded for DPPCs solar cell featuring boron doped poly-SiCx layer at the rear side whereas the similar cell structure featuring carbon free p-TOPCon structure showed quite inferior performance ( $V_{oc} = 671.5$  mV,  $J_{sc} = 36.16$  mA/cm<sup>2</sup> and FF = 56.12%,  $\eta = 13.63\%$ ) to its counterpart. Again, significant improvement in  $V_{oc}$  and FF was realized for the carbon doped samples due to preserving the passivation quality of p-TOPCon structure by suppressing the blistering effect upon thermal treatment.

#### 6.2.3. Variation of thickness and/or doping concentration of doped poly-Si layer

Feldmann et al. observed that an enhancement in free carrier absorption (FCA) at heavily doped poly-Si layer due to the increment of the doping concentration and thickness of poly-Si layer may play a vital role in the reduction of short-circuit current density ( $J_{sc}$ ) of TOPCon solar cells [80]. For example, solar cells with 145 nm thick doped poly-Si layer suffered from a  $J_{sc}$  loss of 0.53 mA/cm<sup>2</sup>. The corresponding doping concentration was as high as  $1.9 \times 10^{20}$  cm<sup>-3</sup>. Therefore, one may conclude that the thickness and doping concentration of doped poly-Si layer should be kept as low as possible to minimize the free carrier absorption loss. However, the authors suggested that the doping level of

doped poly-Si layer should not be decreased beyond  $1 \times 10^{20}$  cm<sup>-3</sup> so that the contact resistivity ( $\rho_c$ ) value can be kept as low as possible. Besides, the study revealed that the surface passivation quality was not found to be severely affected due to the decrement of the thickness of poly-Si layer, given the minimum thickness of 15 nm is maintained. But such thin layers may not be able to resist the penetration of Ag pastes into it during the screen printing and firing process and hence, degradation in the passivating quality may be realized. Therefore, the authors suggested that a proper balance should be maintained among different parameters such as passivating quality, contact resistivity and free carrier absorption losses during the design of poly-Si/SiO<sub>x</sub> contacts. Park et al. also studied the impact of phosphorous doping concentration on the passivation quality of poly-Si contacts grown by LPCVD technique [81]. Besides, the role of annealing temperature and annealing time on the passivation properties was also investigated. Excellent surface passivation quality with an implied open-circuit voltage ( $iV_{oc}$ ) of 734 mV was obtained for a doping concentration of  $2.1 \times 10^{19}$  cm<sup>-3</sup>. The corresponding annealing temperature and annealing time were 950°C and 60 min, respectively. Such high temperature treatment with increasing the annealing time from 10 min to 60 min helped to raise the poly-Si grain size from 13 nm to 40 nm which in turn provided high value of  $iV_{oc}$ . However, raising the annealing time from 10 to 60 min resulted in a reduction of  $iV_{oc}$  from 731 mV to 696 mV at higher phosphorous doping concentration of  $1.1 \times 10^{20}$  cm<sup>-3</sup>. Increment in the Auger recombination velocity from 9.3 fA/cm<sup>2</sup> to 21.6 fA/cm<sup>2</sup> due to phosphorous in-diffusion may be the reason for this shrinkage in  $iV_{oc}$ . The other parameter i.e.,  $\rho_c$  of the passivated contacts was also considered, prior to its application into the solar cells. Relatively high  $\rho_c$  of 394.27 mΩ-cm<sup>2</sup> was obtained for the poly-Si passivated contacts featuring a doping concentration of  $2.1 \times 10^{19}$  cm<sup>-3</sup>. In contrast, the poly-Si contacts with a phosphorous doping concentration of  $1.1 \times 10^{20}$  cm<sup>-3</sup> demonstrated quite low  $\rho_c$  along with high  $iV_{oc}$  of 731.5 mV, subjected to a thermal treatment at 950°C for 30 min. Therefore, highly doped poly-Si passivated contacts with identical annealing conditions were used to develop TOPCon solar cells based onto 180 μm thick, 1–2 Ω-cm, n-type CZ Si wafers. The best cell with an active cell area of 2 cm × 2 cm confirmed a conversion efficiency of 21.1% with  $V_{oc} = 665$  mV,  $J_{sc} = 40.6$  mA/cm<sup>2</sup> and FF = 78.3%. On the other hand, Chowdhury et al. investigated the change in the surface passivation quality of the TOPCon structure developed onto <100> oriented, 200 ± 30 μm, n-type CZ wafers due to the variation of LPCVD coated poly-Si layer thickness, PH<sub>3</sub> flow rate during the development of doped Si layer and the temperature of subsequent annealing process [82]. Finally, the best result with a very high  $iV_{oc}$  of 733 mV along with a very low  $J_0$  of 5.2 fA/cm<sup>2</sup> was obtained for 113 nm thick poly-Si layer at a PH<sub>3</sub> flow rate of 40 sccm with the corresponding subsequent annealing temperature of 900°C. However, additional improvement in the surface passivation quality and carrier selectivity with an  $iV_{oc}$  of 742 mV and a  $J_0$  of 2.5 fA/cm<sup>2</sup> were realized after the deposition of 10 nm Al<sub>2</sub>O<sub>3</sub> layer by ALD process on the front side of the symmetrical TOPCon structure. Actually, the incorporation of Al<sub>2</sub>O<sub>3</sub> layer not only provided field effect passivation but it also eased the minimization of the interfacial defect states and facilitated the formation of the carrier collection layer. Furthermore, by implementing the optimized parameters obtained from the experimental results the authors performed a simulation study with the help of Quokka 3 simulation tool and the study revealed that a very high conversion efficiency of beyond 25% may be achieved with their proposed cost-effective cell structure.

#### 6.3. Post-crystallization treatment

The post-crystallization treatment is mainly a process of hydrogenation which may be realized by several ways such as treatment in remote hydrogen plasma [21,26,29,30,34–36,47,61–63,77], forming gas annealing at moderate temperature [28,32,37,64,65,71] and deposition of hydrogen containing layer onto doped poly-Si layer, followed

by a thermal treatment at moderate temperature [32,39,64,75,80,82]. The purpose of this hydrogenation process is to improve the passivating quality of the TOPCon structure by minimizing the c-Si/SiO<sub>x</sub> interfacial defect states. Accordingly, Zhang et al. investigated the effect of thermal treatment in different atmospheres on the passivation quality of crystallized TOPCon structures [83]. The study showed that post-crystallization annealing of TOPCon structure at 450°C in nitrogen and water vapor atmosphere provided an outstanding surface passivation quality with  $iV_{oc} \approx 730$  mV,  $J_0$  (single-side reverse saturated recombination current density) = 3.8 fA/cm<sup>2</sup>, and contact resistivity  $\approx 5\text{m}\Omega\text{-cm}^2$ . Besides, secondary ion mass spectroscopy (SIMS) measurement revealed that reduction of defect density at Si/SiO<sub>2</sub> interface due to the incorporation of hydrogen content from the water vapor annealing might be responsible for realizing this improvement in the surface passivation quality. Further improvement in the passivation quality was observed when the crystallized c-Si/SiO<sub>x</sub>/n<sup>+</sup>-Si structures were coated by ALD Al<sub>2</sub>O<sub>3</sub> and/or PECVD SiN<sub>x</sub>:H layers, followed by thermal annealing at moderate temperature [84]. Consequently, a very high  $iV_{oc}$  (implied open-circuit voltage) of 747 mV, a very low  $J_0$  (single-side reverse saturated recombination current density) of 1.9 fA/cm<sup>2</sup> and a high  $\tau_{eff}$  (effective minority carrier lifetime) of 4.07 ms were obtained due to may be the minimization of defect states at Si/SiO<sub>2</sub> interface. Eventually, the solar cells fabricated onto n-type CZ Si wafers and featuring the optimized TOPCon structure demonstrated a power conversion efficiency of 22.15% ( $V_{oc} = 681.04$  mV,  $J_{sc} = 40.36$  mA/cm<sup>2</sup>, FF = 80.60%) with an active cell area of 2 cm × 2 cm. In addition, quite reasonable conversion efficiency of 21.4% was achieved for relatively large area (15.6 cm × 15.6 cm) solar cells.

Screen printing and co-firing in the fabrication process of large area TOPCon solar cells is an important step to achieve the cost-effectiveness, high throughput, industrial viability etc. [85,86]. Hence, maintaining the passivation quality of the TOPCon structure even after high temperature firing process is a challenging task. To conquer this challenge Polzin et al. investigated the thermal stability of both hydrogenated (by various ways) and non-hydrogenated TOPCon structure and the study revealed that hydrogenated TOPCon structure which featured no capping layer might lose some part of its passivation quality upon thermal treatment [87]. This phenomenon might be ascribed to the effusion of hydrogen entities from the TOPCon structure. However, the authors further revealed that insertion of ALD coated 15 nm thick AlO<sub>x</sub> layer in between doped poly-Si layer and PECVD coated SiN<sub>x</sub> capping layer might offer higher thermal stability along with better passivation quality by impeding the effusion of hydrogen atoms from Si/SiO<sub>x</sub> interface and/or doped poly-Si layer during the high temperature firing process (can protect the passivation quality up to 825°C).

#### 6.4. Metallization and rear side light management

Passivating quality of TOPCon structure should not be altered due to the realization of metal contacts onto it. Hence, metal contacts on the TOPCon structure should be deposited in such a way so that the possibility of damages due to the metallization gets reduced. Therefore, Feldmann et al. first used thermally evaporated Ti/Pd/Ag stack for realization of metal contacts at the rear side of the TOPCon solar cells [20]. On the other hand, the other limiting factor of achieving high efficiency of crystalline silicon based solar cells is the weak absorption of the incident sunlight at higher wavelength region i.e. NIR region. Therefore, to maximize the value of  $J_{sc}$ , the unabsorbed light should be reflected back into the absorbing layer as much as possible from the rear side metallic contact. But as Titanium is a very loose metal, it can't reflect back the evanescent light in the longer wavelength region. Consequently, the authors used either a stack of lowly doped 200 nm ITO and 1 μm Ag or single 1 μm Ag layer as the rear side metallic contact to offer better reflection of the light in the higher wavelength region. Significant improvement in  $J_{sc}$  was thus observed in both the cases. However, the solar cells featuring ITO/Ag stack as the rear side metallic

contact suffered from obtaining higher FF value due to the impact of high value of series resistance. In contrast, FFs above 82% was realized for the solar cells which contained only Ag layer at the back. Apart from Feldmann et al., Tutsch et al. also investigated the impact of inserting ITO layer in between the doped poly-Si layer and metal contacts [90]. The study revealed that lightly doped 100 nm dc magnetron sputtered ITO layer may be sufficient enough to realize significant improvement in the optical reflection for poly-Si/ITO/Ag stack in comparison with poly-Si/Ag stack. However, surface passivation quality of TOPCon structure may be degraded due to ITO sputtering on doped poly-Si layer. But high thermal stability of TOPCon structure allowed the authors to carry out the thermal treatment of poly-Si/ITO/Ag stack at relatively high temperature (~400°C) to regain the passivation properties. The high temperature annealing in ambient air however may be responsible for the formation of an interfacial oxide layer which in turn increased the contact resistivity of TOPCon/ITO/Ag stack. Nevertheless, the contact properties may be improved by increasing the thickness and doping level of n<sup>+</sup> Si layer but it increases the free carrier absorption (FCA) as well. Therefore, optimization of sputtering and annealing process was performed to realize acceptable passivation ( $iV_{oc}$  of well above 715 mV) and contact properties ( $\rho_c \sim 40$  mΩ·cm<sup>2</sup>). On the other hand, Grübel et al. reported about an industrially feasible approach of laser structuring and electroplating of Ni/Cu/Ag stack to realize the metallic contacts onto the rear side of standard TOPCon solar cells [91]. Further studies on contact adhesion, contact resistance, contact recombination and reflection from the rear side metallic contacts were also carried out to understand the impact of using electroplated Ni/Cu/Ag stack as the rear side metallic contact on the cell performances. 2 × 2 cm<sup>2</sup> TOPCon solar cells based on shiny etched, 1 Ω-cm, n-type, 4" (wafer area: 103.23 cm<sup>2</sup>) FZ Si wafers featuring full area rear side electroplated Ni/Cu/Ag stack as the metallic contact demonstrated a power conversion efficiency of 22.7% with  $V_{oc} = 690$  mV,  $J_{sc} = 39.9$  mA/cm<sup>2</sup> and FF = 82.4%. However, a slightly better conversion efficiency of 23.1% with  $V_{oc} = 694$  mV,  $J_{sc} = 41$  mA/cm<sup>2</sup> and FF = 81% was observed for the solar cells featuring PVD-Ag as full area rear metal contact. The loss in  $J_{sc}$  may be attributed to the inferior light reflection ability of Ni compared to Ag. Furthermore, electroplated metallic contacts were found to be less adhesive on planar TOPCon surfaces where as better adhesion was observed for the textured TOPCon surfaces, especially the samples which were annealed after Ni plating as depicted in Fig. 17. In addition, according to the transfer length method (TLM) analysis, contact resistance ( $\rho_c$ ) for locally plated metallic contacts on TOPCon structure were found to be in the range of  $(0.2 \pm 0.1)$  mΩ·cm<sup>2</sup>. Concurrently, no loss in

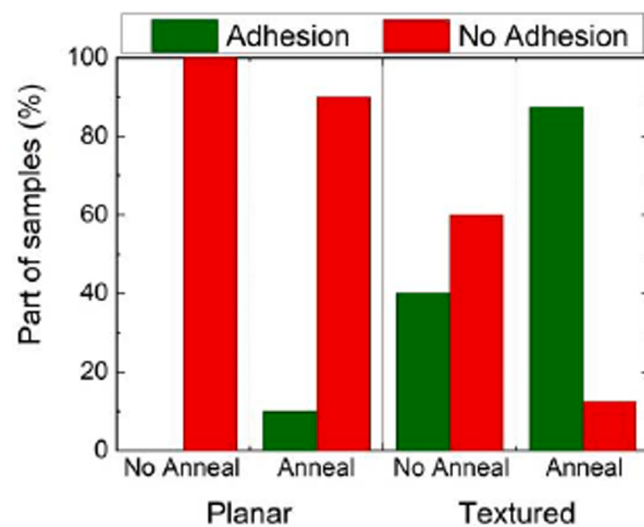
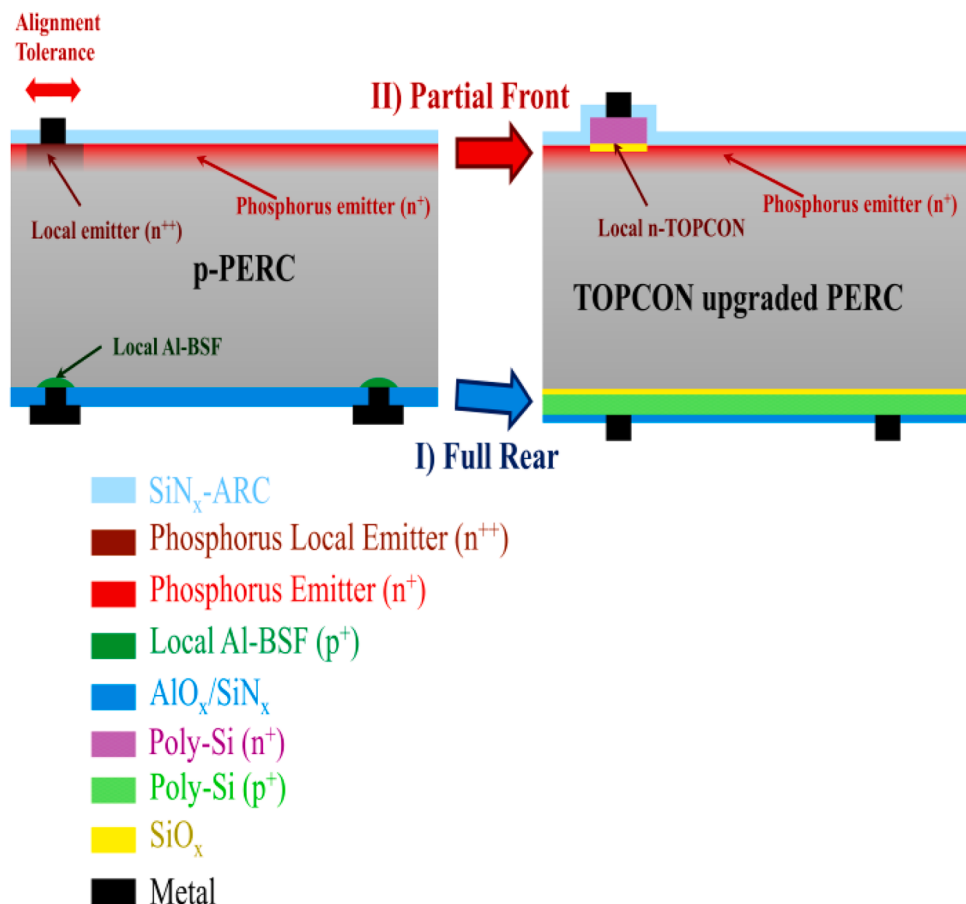


Fig. 17. Contact adhesion of planar and textured samples depending on the surface topography and annealing step [91].



**Fig. 18.** Investigated cell architectures. On the left: A standard industrial PERC cell as reference. On the right: Two TOPCon upgrade architectures: (I) Full Rear: Full-area rear p-type TOPCon with rear dielectric and local contact openings. (II) Local Front: n-type TOPCON locally aligned to front contacts. (III) Combination of I and II; the texturing of the front surface is not depicted [107].

$iV_{oc}$  was noticed due to openings of TOPCon layers by laser ablation technique. Therefore, to overcome the loss in  $J_{sc}$  and to obtain better power conversion efficiency, full area metal contacts may be replaced by laser ablated and electroplated local metal contacts based onto textured TOPCon surfaces.

In 2015, Eisenlohr et al. revealed that use of hexagonal sphere gratings at the rear side of the solar cells may significantly enhance the internal reflection of the passing light at higher wavelength region [92]. Electrical separation in between the solar cell base and sphere gratings was realized by inserting an ultra-thin tunnel oxide passivating contact (TOPCon) layer at the interface. Keeping planar front surface with double-layer anti-reflecting coating, a significant gain in current density of about  $1.4 \text{ mA/cm}^2$  was observed when sphere grating was used at the flat rear side of the solar cell. As a result, the best TOPCon cell showed a power conversion efficiency of 22.1% with  $V_{oc} = 710 \text{ mV}$ ,  $J_{sc} = 38.1 \text{ mA/cm}^2$ , and  $FF = 81.9\%$ . Moreover, notable improvement in the efficiency potential of Si based tandem solar cells may also be realized due to the presence of sphere grating at the planar rear side of the cells.

So far we have observed that reflecting back the passing i.e. the unabsorbed light from the rear side into the absorbing layer of TOPCon solar cells may maximize the value of  $J_{sc}$  which in turn provides more power output. However, the other major issue which needs to be addressed during the rear side light management of TOPCon solar cells is to reduce the parasitic absorption of the evanescent light inside the TOPCon structure, specifically, inside the heavily doped poly-Si layer [80,93,94]. As mentioned earlier in the Section 6.2.3, the thickness and the doping concentration of doped poly-Si layer should be optimized wisely in order to preserve a proper balance in between the contact properties and the surface passivation quality [80]. Furthermore, the

design of doped poly-Si layer should be kept in such a way so that the penetration of rear side metallic paste into doped poly-Si layer can be inhibited during the screen printing and paste firing process so that the passivation quality of the TOPCon structure can be maintained [80]. To preserve the passivation quality of the TOPCon structure even after high temperature paste firing process use of additional capping layer underneath the doped poly-Si layer may be a viable solution [87]. Besides, use of wideband gap poly- $\text{SiC}_x$  layer instead of poly-Si layer may also facilitate to triumph over the challenge of parasitic absorption even in lower wavelength region of the light [95].

#### 6.5. Front emitter management

Minimization of carrier recombination velocities at front emitter/metal interface is another way to enhance the performance of the TOPCon solar cells. Therefore, fabrication of both sided passivated contact solar cells is an appealing approach for the researchers as discussed in the earlier section [26–30]. However, both sided tunnel oxide passivated contact based solar cells generally suffer from parasitic absorption of light particularly at lower wavelength region due to presence of doped poly-Si layer at the front side. Therefore, as mentioned in the earlier section, recombination current density at the front emitter/metal interface was reduced by some other means such as implementation of selective emitter underneath the front metal contact [15,21,25,96,97]. According to Feldmann et al., use of selective emitter in n-type TOPCon solar cells resulted in reduction of the front side recombination current density by a considerable margin [96]. As a result, significant improvement in the power conversion efficiency of TOPCon solar cells was observed where the best cell having an active cell area of  $2 \text{ cm} \times 2$

cm demonstrated a power conversion efficiency of 24.4% with  $V_{oc} = 715.1$  mV,  $J_{sc} = 41.5$  mA/cm<sup>2</sup> and FF = 82.1%. Furthermore, according to Rohatgi et al., a power conversion efficiency of 23.8% ( $V_{oc} = 712$  mV,  $J_{sc} = 41.2$  mA/cm<sup>2</sup> and FF = 81.1%) was achieved by implementing selective boron emitter at the front side and tunnel oxide passivated contact at the rear side of the c-Si solar cells which were fabricated onto n-type FZ silicon wafers [97]. The corresponding cell area was 4 cm<sup>2</sup>. In addition, 2D Sentaurus simulation results revealed that by improving the wafer quality, optimizing the metal contacts design, and further reducing the recombination velocities at the front emitter and at rear TOPCon structure, a conversion efficiency of 26% may be realized with this cell structure. Additionally, with the help of Sentaurus device model Chen et al. also claimed that 23.2% efficient single sided TOPCon solar cells may be developed on 10 Ω-cm, 3 ms CZ wafers by implementing the selective emitter at the front and keeping the width of the screen printed front-sided metal fingers as 40 μm [98].

On the other hand, 23.3% TOPCon solar cells featuring RVD (rapid vapour-phase direct doping) grown boron emitter based on 1 Ω-cm, n-type, FZ Si wafers were fabricated with  $V_{oc} = 687$  mV,  $J_{sc} = 41.8$  mA/cm<sup>2</sup>, FF = 81% [99]. Less time requirement, single sided processing, flexibility in doping profile design were realized in RVD emitters compared to standard BBr<sub>3</sub> tube furnace emitters. Moreover, very low emitter saturation current density of less than 16 fA/cm<sup>2</sup> was also obtained for lifetime samples featuring single sided RVD emitter. Three years later in 2018, Kühnhold-Pospischil et al. also reported the development of TOPCon solar cells with RVD grown boron emitter [100]. In this case, the best cell showed a power conversion efficiency of 24% with  $V_{oc} = 697.6$  mV,  $J_{sc} = 41.8$  mA/cm<sup>2</sup> and FF = 82.1%. Moreover, the reasons behind obtaining lesser  $V_{oc}$  and lesser  $J_{sc}$  in comparison with standard reference cells (featured BBr<sub>3</sub> tube furnace emitters) were also explored. The loss in  $V_{oc}$  may be attributed to the degradation of the effective minority carrier lifetime. Now, the deterioration of carrier lifetime was ascribed to the increment of RVD surface dopant concentration and dopant depth. On the other hand, flattening of solar cell surfaces at higher diffusion temperature of beyond 980°C may be the cause of realizing lesser  $J_{sc}$ . Hence, to maximize the cell parameters two-step diffusion process was suggested.

## 7. Theoretical exploration

The following section will deal with various theoretical works performed for exploring several aspects of maximizing the power output of TOPCon solar cells. In 2017, Zeng et al. reported about using AFORS-HET (Automat FOR Simulation of HETerostructures) software to investigate the path for achieving higher power conversion efficiency of TOPCon solar cells by obtaining excellent surface passivation and efficient charge carrier collection [101]. According to the result obtained by the study, high  $iV_{oc}$  of 745 mV and low recombination current density of 9.5 fA/cm<sup>2</sup> for an injection level ( $\Delta n$ ) =  $5 \times 10^{15}$  cm<sup>-3</sup> may be realized by developing high quality TOPCon structure onto 1 Ω-cm, 200 μm n-type Si wafers. The influential effect of SiO<sub>2</sub> tunnelling oxide layer thickness on tunnelling current was also studied and it was observed that an increment of 0.2 nm oxide layer thickness may reduce the tunnelling current by more than one magnitude. However, improvement in the collection probability of electrons was noticed for increasing the doping level in n<sup>+</sup>-Si layer. This may simplify the mass production of TOPCon solar cells featuring thicker (1.4 nm–1.6 nm) tunnel oxide layer and highly doped poly-Si layer. Moreover, the study also revealed that a very high FF of beyond 84% may be obtained if the minimum forward bias tunnelling current for Si/ SiO<sub>2</sub>/n<sup>+</sup>-Si structure is about 0.01 A/cm<sup>2</sup> (however 0.1 A/cm<sup>2</sup> is more favourable). Besides, with the help of same AFORS-HET simulation software, Anand et al. also made an effort to optimize the major two parameters of TOPCon structure i.e., the thickness of ultra-thin tunnelling SiO<sub>x</sub> layer and the doping concentration of doped poly-Si layer [102]. The study revealed that a conversion efficiency of 25% ( $V_{oc} = 760$  mV,  $J_{sc} = 43$  mA/cm<sup>2</sup> and FF = 80%) may be

obtained for the TOPCon solar cells featuring thickness of SiO<sub>x</sub> layer as 1 nm and doping concentration of n<sup>+</sup> poly-Si layer as  $10^{19}$  cm<sup>-3</sup>. On the other hand, by using ATLAS TCAD simulation tool, Verma et al. also observed that the distribution of electric field in the tunnel oxide region in TOPCon solar cells is strongly dependent on the thickness of the ultra-thin tunnel oxide layer [103]. In the study, the thickness of SiO<sub>x</sub> tunnel oxide layer was varied from 0.2 nm to 1.4 nm and the electric field was found to be increased upon decreasing the oxide layer thickness. Actually, the reduction of oxide layer thickness resulted in increasing the number of carrier transport channels i.e. the number of pinholes which in turn maximized the electric field through the ultra-thin SiO<sub>x</sub> layer. Consequently, the highest electric field was obtained when the thickness of SiO<sub>x</sub> layer was kept as 0.2 nm. This enhancement in the electric field in the tunnel oxide layer resulted in maximizing the efficiency potential of TOPCon solar cells up to 29.03% with  $V_{oc} = 985$  mV,  $J_{sc} = 39.46$  mA/cm<sup>2</sup> and FF = 82.5%. However, the obtained result, especially realization of such high  $V_{oc}$  for 0.2 nm SiO<sub>x</sub> tunnelling layer has been found to be inconsistent to some other reports [6, 17, 53].

In 2019, Mitra et al. reported about the development of an analytical model to study the change in  $V_{oc}$  in TOPCon solar cells due to the variation of emitter saturation current density ( $J_{oe}$ ), surface recombination velocity (SRV), substrate thickness and doping density of poly-silicon layer [104]. The study revealed that a very high  $V_{oc}$  of 750 mV may be obtained for 180 μm thick substrate with  $J_{oe} = 2$  fA/cm<sup>2</sup> and doping density of poly-Si layer >  $10^{21}$  cm<sup>-3</sup>, considering the rear surface recombination velocity as zero. Keeping the other parameters unchanged, further improvement in  $V_{oc}$  (= 766 mV) was noticed for a 50 μm thick substrate due to lesser bulk recombination for thinner substrates. On the other hand, improvement in  $V_{oc}$  due to the increment in doping density of poly-Si layer from  $10^{19}$  to  $5 \times 10^{21}$  cm<sup>-3</sup> may be attributed to the restriction of minority carrier flow from the n-c-Si substrate to n<sup>+</sup> poly-Si layer. However, the dependence of  $V_{oc}$  on poly-Si doping density was found to be pronounced only for very low rear surface recombination velocity. The authors also added that use of same thick other tunnelling layers such as SiC or Si<sub>3</sub>N<sub>4</sub> instead of SiO<sub>2</sub> may provide lower  $V_{oc}$  due to featuring lower barrier height for the flow of minority carriers. Besides, the observations explored from the analytical model matched well with the results obtained from AFORS-HET v2.5simulation tool. In contrast, Quan et al. used numerical simulation tool AFORS-HET to study the influential effect of using low work function electron selective collection (ESC) layer instead of heavily doped n-type poly-Si layer at the rear side of the TOPCon solar cells [105]. The study revealed that the TOPCon solar cells featuring less defective tunnel oxide layer with a thickness of 1.2–1.4 nm and an electron selective collection (ESC) layer having a work function of < 3.6 eV showed a very high implied  $V_{oc}$  ( $iV_{oc}$ ) of 742 mV and a FF of 86%. The authors also investigated the effect on the surface passivation properties and carrier transport due to presence of defective transition layer (DTL) in between ultra-thin tunnel oxide layer and electron selective collection (ESC) layer. Therefore, selection of suitable electron selective collection (ESC) layer, minimizing the defects in the ultra-thin oxide layer, and reducing the thickness and defect density of the defective transition layer were recommended to improve the power conversion efficiency of TOPCon solar cells featuring electron selective collection (ESC) layer at back.

Recently, with the help of Sentaurus 2D simulation tool, Sugiura et al. demonstrated that n-type TOPCon solar cells outperformed the p-type TOPCon solar cells with 15% larger current density owing to featuring higher bulk lifetime, lower defect density, smaller minority carrier tunnelling through ultra-thin tunnel oxide layers and wider range of effective tunnelling oxide thickness [106]. On the other hand, Messmer et al. demonstrated a way out of upgrading the screen printed, busbarless bifacial p-PERC solar cells into bifacial p-TOPCon solar cells by introducing local n-TOPCon structure at the front and full area p-TOPCon structure at the rear side of the cell [107]. According to the simulation study, the TOPCon upgraded p-PERC solar cells showed

almost 1% more conversion efficiency in comparison with the conventional p-PERC cells. The study further revealed that improving the quality of p-type c-Si bulk and phosphorous doped front emitter may be a solution to enhance the efficiency potential of these TOPCon upgraded p-PERC solar cells.

#### Loss analysis

Richter et al. investigated the various loss mechanisms involved in the high efficiency (25.8%) TOPCon solar cells to realize the further scope of improvement in the cell performance [108]. With the help of Quokka3 simulation tool and FELA (free energy loss analysis) technique, it was observed that surface recombination losses at front emitter and Auger recombination losses at crystalline silicon bulk possessed a major contribution in the net electrical power losses. The occurrence of other significant electrical power losses may be attributed to the lateral movement of the charge carriers towards the front contacts and recombination of the charge carriers in the perimeter of the solar cell. However, carrier recombination losses and resistive power losses at the rear side of the cell were found to be less significant due to the excellent surface passivation provided by the TOPCon structure. The contribution of different electrical loss mechanisms occurring inside the champion TOPCon solar cells was depicted in Fig. 19. On the other hand, the study revealed that the escape reflection and IR parasitic absorption were the major part of the optical losses. Hence, to maximize the power output, the authors performed a simulation study to optimize the base material, front emitter and light trapping mechanisms. The study demonstrated that increment in base resistivity from  $1 \Omega\text{-cm}$  to  $10 \Omega\text{-cm}$  resulted in an efficiency improvement irrespective of the wafer thickness, for an example an efficiency increment of  $0.2\%\text{abs}$  was observed for  $200 \mu\text{m}$  thick wafers when the base resistivity was increased from  $1 \Omega\text{-cm}$  to  $10 \Omega\text{-cm}$ . Improvement in the cell performances was also realized for increasing the wafer thickness, particularly from  $100 \mu\text{m}$  to  $200 \mu\text{m}$  while a very little enhancement in the conversion efficiency was observed when the wafer thickness was increased from  $200 \mu\text{m}$  to  $300 \mu\text{m}$ . The study further revealed that for high impurity concentration, the high resistive silicon wafers featured lower conversion efficiency. The SRH defect levels obtained from experimental results were not altered while performing the simulations. Finally, the authors pointed out that for low impurity concentration, higher power conversion efficiency may be attained if the wafer thickness and base resistivity are kept higher than  $150 \mu\text{m}$  and  $1 \Omega\text{-cm}$ , respectively. On the other hand, minimization of the carrier recombination losses at the surface of the emitter may be realized by reducing the doping concentration at the emitter. In contrast, high doping concentration is required to obtain high lateral conductivity. Therefore, to reduce the power losses at the front emitter, the

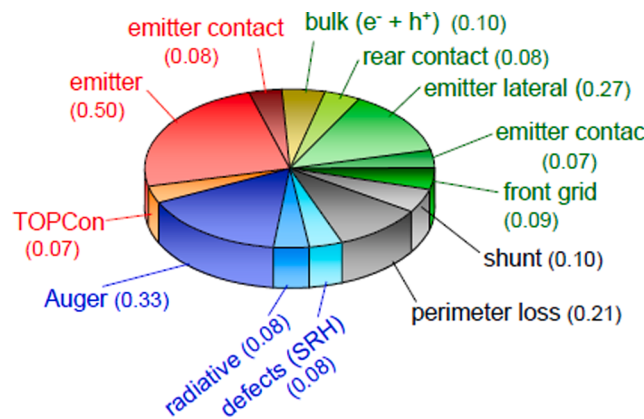


**Fig. 19.** Electrical power losses resulting from the FELA based on the 3D full-area simulations. The losses in the silicon bulk are shown in blue, surface recombination losses in red, current transport losses in green and other losses in gray. The power losses in brackets are given in  $\text{mW}/\text{cm}^2$  which equivalent to an efficiency loss in  $\%\text{abs}$ . [108].

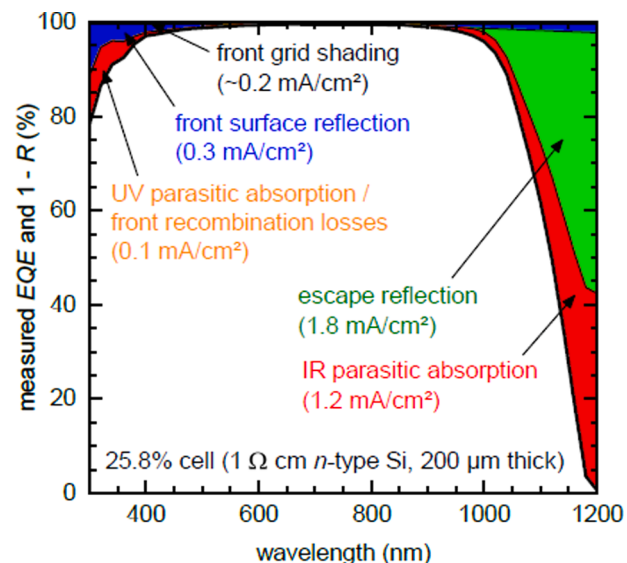


**Fig. 20.** Optical loss analysis for the 25.8% cell based on measured EQE and reflectance data. The values in brackets are current losses calculated from integration of the AM 1.5 g photon flux density. [108].

authors tried to optimize the emitter sheet resistance along with the distance between the metal fingers. Finally, the simulation results showed that an efficiency improvement of  $0.4\%\text{abs}$  may be realized by using the highly resistive boron emitter combined with triangular-shaped front metal fingers with a reduced finger pitch of  $0.5 \text{ mm}$ . Optical simulations study performed with OPTOS revealed that textured rear in combination with  $\text{SiO}_x/\text{Ag}$  mirror resulted a gain of  $0.5 \text{ mA}/\text{cm}^2$  in  $J_{\text{sc}}$  by enhancing the optical confinement inside the solar cells. However, to implement this advanced light trapping mechanisms at the rear sides of the TOPCon cells, full area metal contacts are to be replaced by local contacts. In essence, the authors demonstrated the pathways to fabricate both sides contacted solar cells featuring TOPCon structure at the back with a power conversion efficiency of beyond 26%.

On the other hand, numerical simulation tool Quokka 2 was used to evaluate the influential effect of p-type and n-type passivated contact on the efficiency potential of the industrial standard p-type Si solar cells [109]. Especially, a focus on the role of the front-structure design, the wafer resistivity and bulk lifetime, the carrier selectivity and the contact resistivity of the poly-Si passivated contact was made for improving the cell performances. Additionally, the energy loss of the p-type passivated contact solar cells was realized by FELA (free energy loss analysis) technique. The study revealed that the solar cells featuring p-type passivated contact as BSF are more beneficial when the bulk carrier lifetime is less than  $350 \mu\text{s}$ . Eventually, the pathway towards achieving a power conversion efficiency of more than 23% based on p-type CZ Si wafers with p-type or n-type passivated contact was presented. Recently, Zheng et al. reported about the detailed loss mechanisms occurred in large area 24.8% ( $V_{\text{oc}} \approx 714.6 \text{ mV}$ ,  $J_{\text{sc}} \approx 41.59 \text{ mA}/\text{cm}^2$  and FF  $\approx 83.43\%$ ) efficient n-TOPCon solar cells fabricated onto n-type,  $0.3\text{--}2.1 \Omega\text{-cm}$ , monocrystalline, CZ Si wafers with an active cell area of  $267.7 \pm 1.1 \text{ cm}^2$  [110]. According to the report, a total  $J_{\text{sc}}$  loss of about  $5 \text{ mA}/\text{cm}^2$  was realized due to the occurrence of various types of optical losses as mentioned here: (i) infrared parasitic absorption losses occurred in bulk and rear side of the cell (corresponding  $J_{\text{sc}}$  loss =  $1.8 \text{ mA}/\text{cm}^2$ ), (ii) infrared escape reflection losses (corresponding  $J_{\text{sc}}$  loss =  $1.4 \text{ mA}/\text{cm}^2$ ), (iii) front grid shading losses (corresponding  $J_{\text{sc}}$  loss =  $1.2 \text{ mA}/\text{cm}^2$ ), (iv) parasitic absorption of the incident light at the front side of the cell (corresponding  $J_{\text{sc}}$  loss =  $0.4 \text{ mA}/\text{cm}^2$ ) and (v) front surface reflection losses (corresponding  $J_{\text{sc}}$  loss =  $0.2 \text{ mA}/\text{cm}^2$ ). By analyzing the contribution of different kinds of optical losses it was realized that the improvement of the optical confinement specifically in the infrared

## Bifacial cell in world market

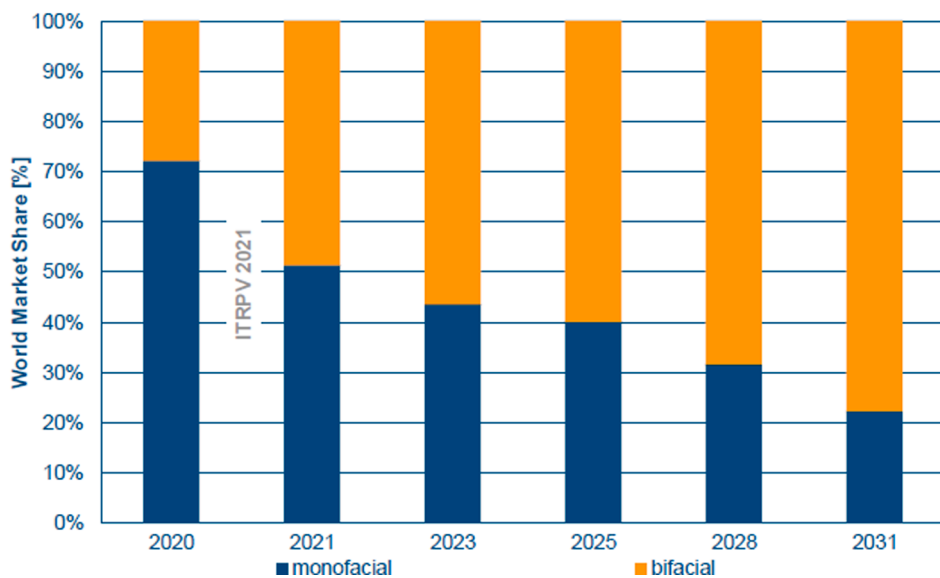


Fig. 21. Market share of monofacial and bifacial cell technology [19].

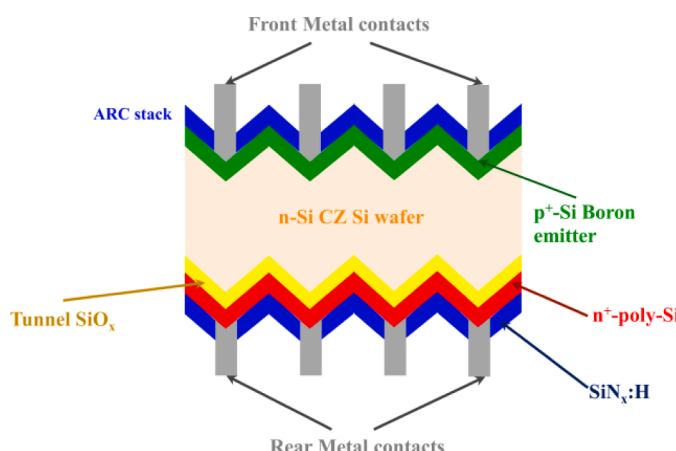


Fig. 22. Schematic diagram of i-TOPCon solar cells fabricated on n-type monocrystalline silicon wafers [120].

region of the incident light may improve the power conversion efficiency of the solar cells. Besides, the rear surface topology, doping concentration and thickness of the doped poly-Si layer needs to be optimized to minimize the parasitic absorption of the evanescent light. However, the electrical properties such as recombination current density and/or contact resistivity should not be compromised during the optimization of the poly-Si layer. Apart from optical losses, contribution of various types of electrical losses (resistive and recombination losses) was also analyzed with the help of free energy loss analysis (FELA) technique. The major electrical loss contributing 63% of the total electrical losses was found to be originated from boron-diffused emitter region. This in turn reduced the total power density of about  $1.19 \text{ mW/cm}^2$  (recombination at the metal/semiconductor interface at the front side =  $0.42 \text{ mW/cm}^2$ , lateral hole transport losses in the emitter region =  $0.39 \text{ mW/cm}^2$ , carrier recombination at the front surface passivated region =  $0.24 \text{ mW/cm}^2$  and front contact resistance losses =  $0.14 \text{ mW/cm}^2$ ). The next major power loss accounting for  $0.38 \text{ mW/cm}^2$  was found to be produced at the bulk. However, the authors opined that elimination of bulk SRH recombination may provide a gain of about

$0.1 \text{ mW/cm}^2$  in the power output. Lastly, the rear side electrical losses were calculated as  $0.27 \text{ mW/cm}^2$ . The presence of passivated contacts at the rear side facilitated to experience relatively lower power losses. Further optimization of the emitter region and front side grid pattern are required to enhance the possibility of receiving more power output.

### 8. Large area TOPCon solar cells

To promote the fabrication of industrial standard large area TOPCon solar cells various investigations have been carried out since the development of TOPCon solar cells [43,86,111–126]. Firstly, in 2016, Tao et al. claimed that large area ( $239 \text{ cm}^2$ ) TOPCon solar cells with ion-implanted homogeneous boron emitter based on industrial grade n-type CZ wafers were fabricated with a power conversion efficiency of 21.4% having  $V_{oc} = 674 \text{ mV}$ ,  $J_{sc} = 39.6 \text{ mA/cm}^2$ , and  $FF = 80.0\%$  [111]. The authors further added that carrier recombination at front metal/p<sup>+</sup> interface limits the efficiency potential of this cell structure. However, 2D simulation study revealed that application of fine line metallization and selective emitter technology may significantly maximize the conversion efficiency of these large area TOPCon solar cells. Just one year later, in 2017, Feldmann et al. reported that large area ( $10 \text{ cm} \times 10 \text{ cm}$ ) TOPCon solar cells were fabricated with a power conversion efficiency of 22.9% ( $V_{oc} = 694 \text{ mV}$ ,  $J_{sc} = 40.8 \text{ mA/cm}^2$  and  $FF = 81\%$ ) based on  $1 \Omega\text{-cm}$ , n-type, shiny etched FZ silicon wafers [113]. In the cell development process, laser ablation technique was used for the contact openings at the front side and realization of the front metallic contact was done by plating of NiCuAg. However, the authors opined that further improvement in the cell performance may be observed by optimizing the front metallic contact area and minimizing the damage occurred during the laser contact opening (LCO) process. On the other hand, according to Steinhäuser et al., 23.4% TOPCon solar cells featuring  $V_{oc} = 697 \text{ mV}$ ,  $J_{sc} = 41.4 \text{ mA/cm}^2$  and  $FF = 81.2\%$  were fabricated with a cell area of  $100 \text{ cm}^2$  [114]. To form the TOPCon structure, the heavily doped poly-Si layer was deposited onto the thermally grown ultra-thin tunnel oxide layer by means of industrial scalable low frequency plasma enhanced chemical vapor deposition (PECVD) technique. Here, the front contacts were also realized by laser contact opening (LCO) process and subsequent plating of NiCuAg. However, a conversion efficiency of 24.5% ( $V_{oc} = 713 \text{ mV}$ ,  $J_{sc} = 41.4 \text{ mA/cm}^2$  and

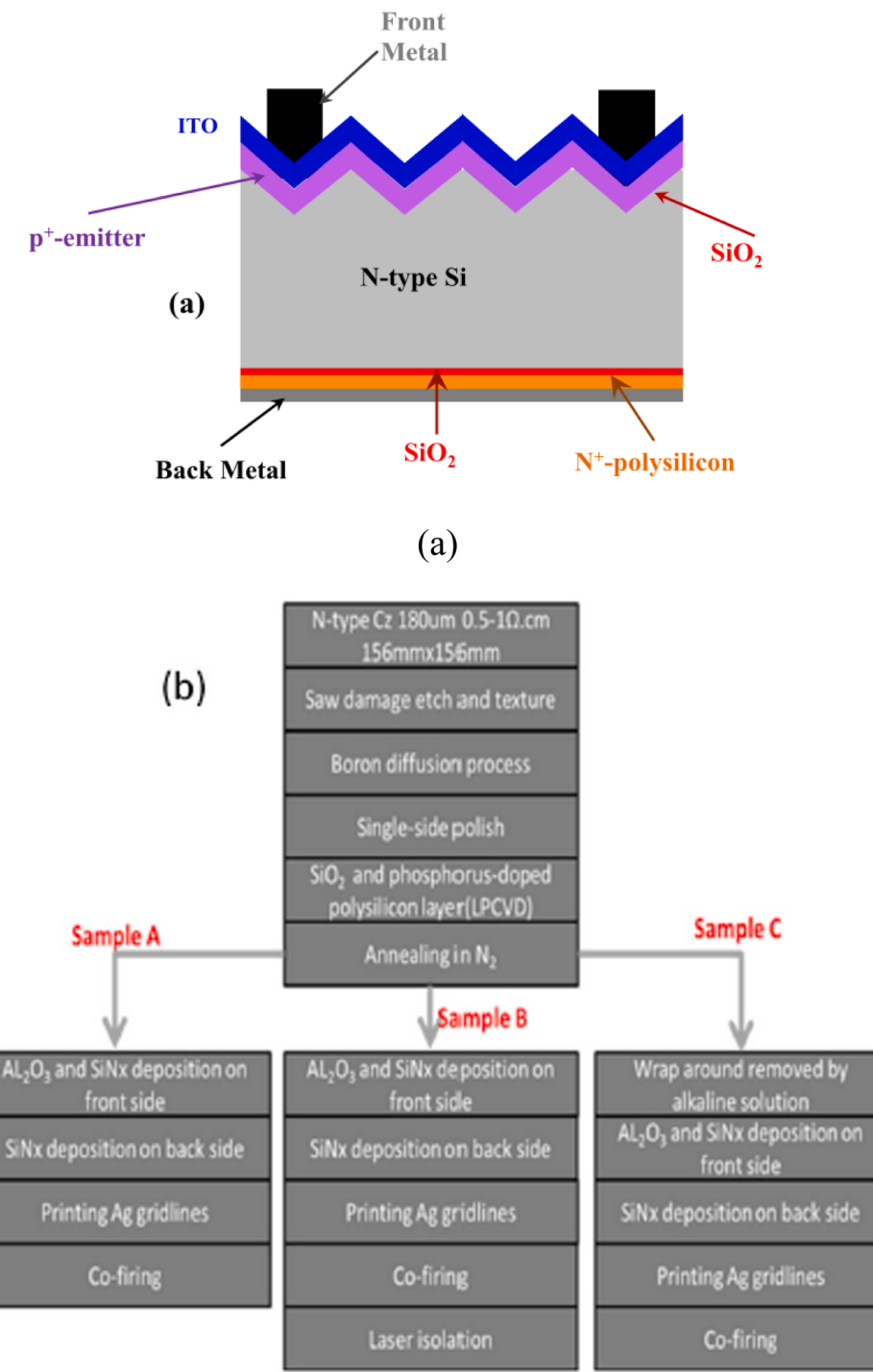


Fig. 23. (a) Schematic diagram and (b) the fabrication process sequence of the bifacial TOPCon solar cells [122].

FF = 83.1%) was achieved when the front contacts were opened with the help of lithography. The former suffered from relatively lower V<sub>oc</sub> and inferior FF due to the laser induced damage and higher contact fraction at the front side of the solar cells. Therefore, the authors suggested that using smart wire cell interconnection and minimizing the possibility of damage occurring during laser contact opening process may be a solution to triumph over these challenges. Again, in 2019, Feldmann et al. reported that thick TOPCon layers were developed by using industrial grade low frequency PECVD tool [115]. The developed TOPCon structure provided excellent surface passivation upon hydrogenation at low temperature. Eventually, the best solar cell based on n-type, M2-sized, 4Ω·cm CZ Si wafer showed a power conversion efficiency of 22.5%

with V<sub>oc</sub> = 691.2 mV, J<sub>sc</sub> = 40.4 mA/cm<sup>2</sup> and FF = 80.7%. In contrast, Huang et al. used LPCVD technique for the development of TOPCon structure in the large area TOPCon solar cells [116]. According to the report, TOPCon structure featuring HNO<sub>3</sub> grown ultra-thin (1.5 nm) SiO<sub>x</sub> layer in conjunction with LPCVD coated 100 nm n<sup>+</sup> poly-Si layer, followed by thermal annealing at 875°C demonstrated an outstanding surface passivation quality with J<sub>0b</sub> (rear side saturation current density) ~ 5 fA/cm<sup>2</sup> even after firing the screen printed metal contacts onto n<sup>+</sup> poly-Si layer through PECVD coated SiN<sub>x</sub> capping layer. The corresponding effective metal coverage area on the rear side of the solar cell was 9%. Finally, large area (239 cm<sup>2</sup>) TOPCon solar cells with ion-implanted homogeneous boron emitter based on industrial quality

## Average stabilized efficiency values for Si solar cells in mass production

Measured with busbars (no BB-less measurement) and front side STC

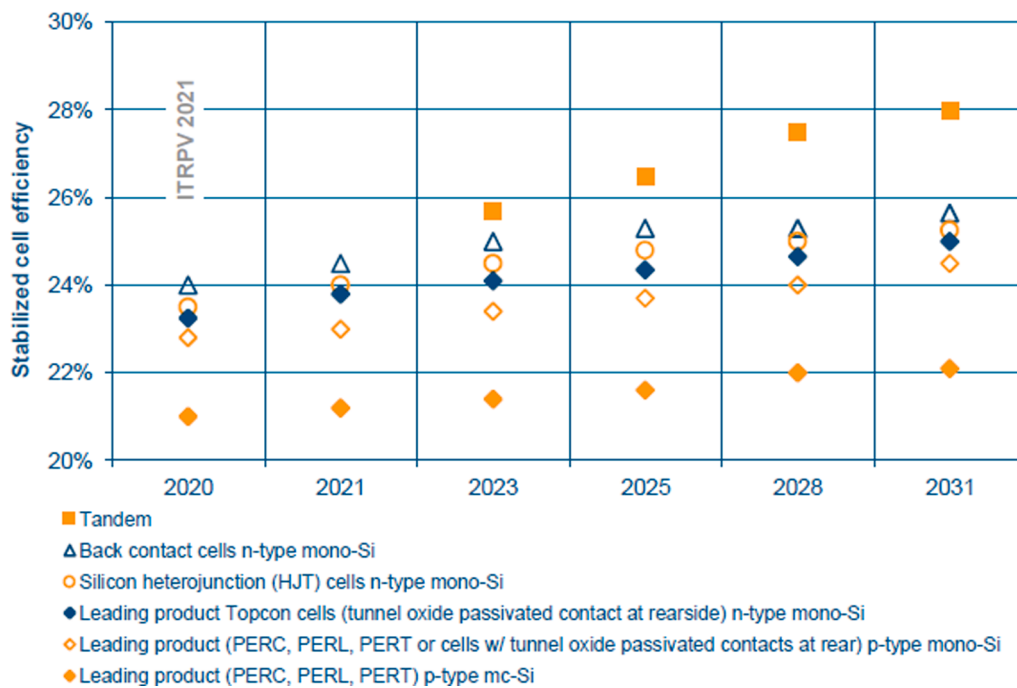


Fig. 24. Expected trend of average stabilized efficiency values for Si solar cells in mass production [19].

n-type CZ wafers were developed with a power conversion efficiency of 21.6% ( $V_{oc} = 676$  mV,  $J_{sc} = 39.7$  mA/cm $^2$ , FF = 80.40%). Besides, the solar cells having an effective cell area of 100 cm $^2$  showed slightly improved conversion efficiency of 22%. Furthermore, the simulation study using Sentaurus2D device model revealed that use of selective boron emitter along with floating front bus bars may lead to raise the conversion efficiency to beyond 23%.

### Bifacial TOPCon solar cells

Bifacial c-Si solar cells have drawn the attention of the researchers over the years to facilitate the goal of achieving grid parity and hence according to the latest ITRPV report, the bifacial solar cells will gradually gain a market share of about 80% within the next ten years [19]. This shows the importance of bifacial solar cells in the PV industry. In case of TOPCon solar cells, in 2016 Stodolny et al. first reported about the development of bifacial TOPCon solar cells (Though they termed the cells as "PERPoly" i.e. "Passivated Emitter and Rear Poly-silicon") by using industrial manufacturing tools [117]. These large area and screen-printed TOPCon solar cells were fabricated onto 6" n-type CZ wafers where the best cell demonstrated a conversion efficiency of 20.7% with  $V_{oc} = 675$  mV,  $J_{sc} = 38.8$  mA/cm $^2$  and FF = 79.1%. Since then, many reports have been published regarding the development of bifacial TOPCon solar cells which will be discussed in the subsequent section.

In 2018, Nandakumar et al. claimed to develop 22.8% efficient bifacial, large area and screen printed TOPCon solar cells based on M2 sized, 244.32 cm $^2$ , n-type CZ Si wafers [86]. Within one year, Chen et al. also reported about the development of the bifacial and industrial scalable TOPCon (i-TOPCon) solar cells based on n-type 6-inch CZ wafers [118]. According to the report, the average front side efficiency was obtained more than 23% with an open circuit voltage ( $V_{oc}$ ) of greater than 700 mV while the best cell demonstrated the power conversion efficiency as high as 23.57%. Finally, 120 pieces of half-cut pseudo square i-TOPCon solar cells with 9 bus-bar arrangement were used to develop bifacial i-TOPCon solar modules. The best module power was found to be higher than 355 W while the average module power was

greater than 345 W. The process sequence to realize the industrial grade TOPCon solar cells is as follows:

- Step 1: Double-sided texturization of wafers in alkaline solution to form the pyramid shape structure.
- Step 2: Diffusion of p<sup>+</sup> boron.
- Step 2: Removal of p<sup>+</sup> boron from the rear side of the wafers with the help of single-side inline wet bench.
- Step 4: Realization of (thermal oxidation + *in-situ* i-poly with a thickness value of 200 to 300 nm) by LPCVD method.
- Step 5: Doping of *in-situ* i-poly layer to convert it into n<sup>+</sup> poly layer by POCl<sub>3</sub> diffusion.
- Step 6: Removal of wrap around n<sup>+</sup> poly-Si layer by single-side etcher, followed by wet chemical cleaning.
- Step 7: Realization of surface passivation of the front boron emitter by using thin film stack.
- Step 8: Development of SiN<sub>x</sub>H layer onto rear side n<sup>+</sup> poly-Si layer by PECVD technique for surface passivation and capping purpose.
- Step 10: Screen printing and firing to realize the metallic contacts at the front and at the back side of the cells.

On the other hand, n-type bifacial TOPCon solar cells with an average efficiency of 23.04% ( $V_{oc} = 701$  mV,  $J_{sc} = 40.66$  mA/cm $^2$ , and FF = 80.80%) were fabricated by Chinese solar giant Jolywood enterprise [119]. In this case, the best cell demonstrated an outstanding conversion efficiency of 23.15% with an excellent  $V_{oc}$  of 703 mV,  $J_{sc}$  of 40.53 mA/cm $^2$ , and FF = 81.25%. However, based on free energy loss analysis (FELA), the authors observed that significant improvement in the power conversion efficiency may be realized by minimizing mainly the emitter recombination losses and resistive losses. In addition, the authors reported about the development of n-type bifacial TOPCon modules with an output power of 331 W and 392 W featuring 60 cells and 72 cells, respectively where these high efficiency modules showed an average bifaciality of 85%, a temperature coefficient of -0.32%/K and quite low degradation coefficient of -0.4%/year. Furthermore, Chen

et al. reported about the improvement in the performance of large-area ( $156.75 \times 156.75 \text{ mm}^2$ ) n-type bifacial i-TOPCon solar cells as the best cell featured a conversion efficiency of 24.58% while the median efficiency of the developed cells was 23.91% with  $V_{oc} = 712 \text{ mV}$ ,  $J_{sc} = 40.80 \text{ mA/cm}^2$ , and  $FF = 82.23\%$  [120]. The recombination current density ( $J_0$ ) at the rear side passivating contact was measured as low as  $7 \text{ fA/cm}^2$ . The authors further observed that in the 6% metallized region at the back side of the cells,  $J_0$  was about  $50.7 \text{ fA/cm}^2$ . In contrast, remaining 94% non-metallized area comprised of very low  $J_0$  of about  $3.4 \text{ fA/cm}^2$ . Furthermore, the authors opined that improvement in the conventional emitter design and metallization paste may maximize the power output. Concurrently, intensive research on the development of industrial scalable transparent passivating contacts along with simplification of the processing steps of poly-Si passivating contacts may play a significant role in the industrial evolution of high efficiency bifacial TOPCon solar cells. The developed i-TOPCon bifacial modules featured a straight forward gain of 6.5% in comparison with the other modules installed in a 100 KW solar system situated over a lake at Changzhou in China [121]. The data was monitored over two years.

Recently, Zhou et al. reported about the fabrication of large area ( $244.32 \text{ cm}^2$ ) bifacial TOPCon solar cells featuring n-type TOPCon structure at the back and boron diffused emitter at the front based onto  $180 \mu\text{m}$ ,  $0.5 - 1 \Omega\text{-cm}$ , n-type CZ Si wafers [122]. In the study, the ultra-thin ( $1.5 \text{ nm}$ )  $\text{SiO}_x$  layer and phosphorous doped poly silicon layer ( $100 \text{ nm}$ ) were developed by LPCVD tube, followed by a thermal treatment at  $850^\circ\text{C}$  for 10 min in  $\text{N}_2$  atmosphere to improve the passivation quality and dopant activation. However, despite of its necessity only at the back side, the deposition of LPCVD coated poly-silicon layer took place at the edges and at the front side of the wafers due to the wrap-around. Consequently, a path for the flow of leakage current was formed. As a result, the cell suffered with low shunt resistance ( $R_{sh}$ ) value and hence very low power conversion efficiency of 18.16% with  $V_{oc} = 665.7 \text{ mV}$ ,  $J_{sc} = 38.74 \text{ mA/cm}^2$  and  $FF = 70.41\%$  was obtained. To minimize the effect of poly-silicon wrap-around and to increase the value of shunt resistance ( $R_{sh}$ ), two methods namely, laser isolation process (laser wavelength:  $540 \text{ nm}$ ) and chemical etching process were adopted. Laser isolation process was carried out after the metallization where as in alkaline solution etching process, samples were immersed in KOH solution in between the  $\text{N}_2$  annealing process and  $\text{Al}_2\text{O}_3$  deposition process. The cells which were undergone the laser isolation process for reducing the effect of poly-silicon wrap around featured a conversion efficiency of 19.65% with  $V_{oc} = 669.4 \text{ mV}$ ,  $J_{sc} = 38.6 \text{ mA/cm}^2$  and  $FF = 76.01\%$ . On the other hand, a power conversion efficiency of 21.49% with  $V_{oc} = 675.88 \text{ mV}$ ,  $J_{sc} = 39.68 \text{ mA/cm}^2$  and  $FF = 80.12\%$  was achieved by implementing alkaline etching process instead of laser isolation process. The improvement in  $J_{sc}$  may be attributed to the weakening of the parasitic absorption of the incident light which was caused by the wrap-around of poly-Si thin films. However, after optimizing the process parameters further improvement in the cell performance with an efficiency value of 22.81% ( $V_{oc} = 702.6 \text{ mV}$ ,  $J_{sc} = 39.78 \text{ mA/cm}^2$  and  $FF = 81.62\%$ ) was achieved.

Besides, in another report, Zhou et al. claimed that use of thick BSG layer ( $> 50 \text{ nm}$ ) may inhibit the occurrence of damage into front  $p^+$  emitter during the removal process of wrap-around poly-Si layer developed by LPCVD technique [123]. Additionally, the study also revealed that uniform  $p^+$  emitter layer with acceptable sheet resistance may be developed by maintaining low pressure ( $300 \text{ mbar}$ ) at the time of thermal diffusion of  $\text{BCl}_3$  (boron trichloride) into textured,  $0.5 - 1 \Omega\text{-cm}$ ,  $<100>$  oriented, n-type CZ c-Si wafers. Finally, n-type large area ( $244.32 \text{ cm}^2$ ) TOPCon solar cells featuring optimized boron diffused emitter (the sheet resistance was  $70 - 90 \Omega/\text{sq}$  and BSG thickness was  $\sim 100 \text{ nm}$ ) demonstrated significant conversion efficiency of 22.14% with  $V_{oc} = 683.4 \text{ mV}$ ,  $J_{sc} = 39.53 \text{ mA/cm}^2$  and  $FF = 81.96\%$ . On the other hand, Huang et al. used masking process to etch out the LPCVD coated doped poly-Si layer from the front side of the bifacial TOPCon solar cells which were fabricated onto  $180 \mu\text{m}$  thick,  $2 \Omega\text{-cm}$ , n-type CZ wafers

[124]. The cells featured homogeneous ion-implanted boron emitter and the best cell demonstrated a power conversion efficiency of 22.6% with an effective cell area of  $239 \text{ cm}^2$ . Besides, TOPCon structure with  $\text{SiN}_x$  capping layer provided an excellent surface passivation quality with a very low  $J_{0,\text{TOPCON}}$  of  $\sim 5 \text{ fA/cm}^2$ , even after metallization (metal coverage area  $\sim 13\%$ ) through industrial screen printing process. In contrast, very low emitter recombination current density of  $\sim 31 \text{ fA/cm}^2$  was obtained (after the metallization process) for ion-implanted boron emitter which was passivated with ALD coated  $\text{Al}_2\text{O}_3$  layer and capped with PECVD coated  $\text{SiN}_x/\text{SiO}_x$  double-layer antireflection coating. However, according to the model calculations, a power conversion efficiency of 24% may be achieved after improving the bulk lifetime and implementing the selective boron emitter and multiwire contacts on the front.

## 9. Technological options for the mass production of TOPCon solar cells

Improvement in the conversion efficiency of the large area, industrial scalable TOPCon solar cells is undoubtedly facilitating its path to turn out to be a very tough competitor to the present state-of-the-art PERC/PERL/PERT solar cells. Recent report of ITRPV has also revealed that the average stabilized efficiency of n-type TOPCon solar cells in mass production has been higher than any type of p-type silicon based solar cells (including PERC/PERT/PERL and p-TOPCon) [19]. Besides, the continuous enhancement in terms of the power conversion efficiency has also been predicted, thanks to the improvement of individual processing steps involved in the cells fabrication technology. Most importantly, this improvement will not be restricted within the cells level only, as shown in Fig. 25. The expected average stabilized efficiency of TOPCon solar modules in mass production will reach  $\approx 23\%$  in 2031 from its current level of 21.2%, clearly surpassing the current market dominating p-PERC solar modules. The expected efficiency value is also comparable with the solar modules comprised of HJT or IBC solar cells. On the other hand, silicon based tandem solar cells with its expected average stabilized efficiency of 28% in cell level and 26% in module level within 2031 may become one of the key players in SPV industry in the long-term future. However, the mass production of Si-based tandem solar cells has not been started yet; expected to be initiated from 2023. Therefore, it has to pass through various stages such as simplification of the processing steps, enhancing the throughput and cost-effectiveness before replacing the current market dominating PERC-concept and TOPCon solar cells. Hence, as of now we may consider that TOPCon solar cells have the highest probability to become the mostly produced solar cells in the mass production in this decade. Thereafter, comparative study on various technological routes which are favourable for the mass production of the ultra-thin  $\text{SiO}_x$  tunneling layer and doped poly-Si layer is going to be pinpointed in the following section. Besides, the different issues associated with the metallization process in the mass production of TOPCon solar cells have also been enlightened.

**(a) Mass production of ultra-thin  $\text{SiO}_x$  layer:** In Section 6.1.1, the dependence of the surface passivation quality of the ultra-thin  $\text{SiO}_x$  tunnelling layer on its synthesis process has been summarized. Besides, in Table 1 the surface passivation quality of ultra-thin  $\text{SiO}_x$  layer grown by different routes on various types of substrates (wafers) has also been demonstrated. The rigorous research revealed that development of ultra-thin silicon oxide layer by thermal oxidation process had outperformed its counterpart i.e. the chemically grown or plasma-grown oxides in terms of surface passivation and thermal stability of the developed oxides [39,40]. Thermal stability of ultra-thin  $\text{SiO}_2$  oxide layer is an important parameter to consider always because the oxide layer must maintain its stoichiometry (the oxidation state of Si must be close to  $\text{Si}^{4+}$ ) during the thermal treatment of doped poly-Si layer for its dopant activation and crystallization purpose. Thermal oxide grown in LPCVD tube is mostly used for the mass production of TOPCon solar cells [117,118–123,127]. The comparative analysis of the various routes

## Module efficiency trend for modules in mass production with different c-Si based cell technologies

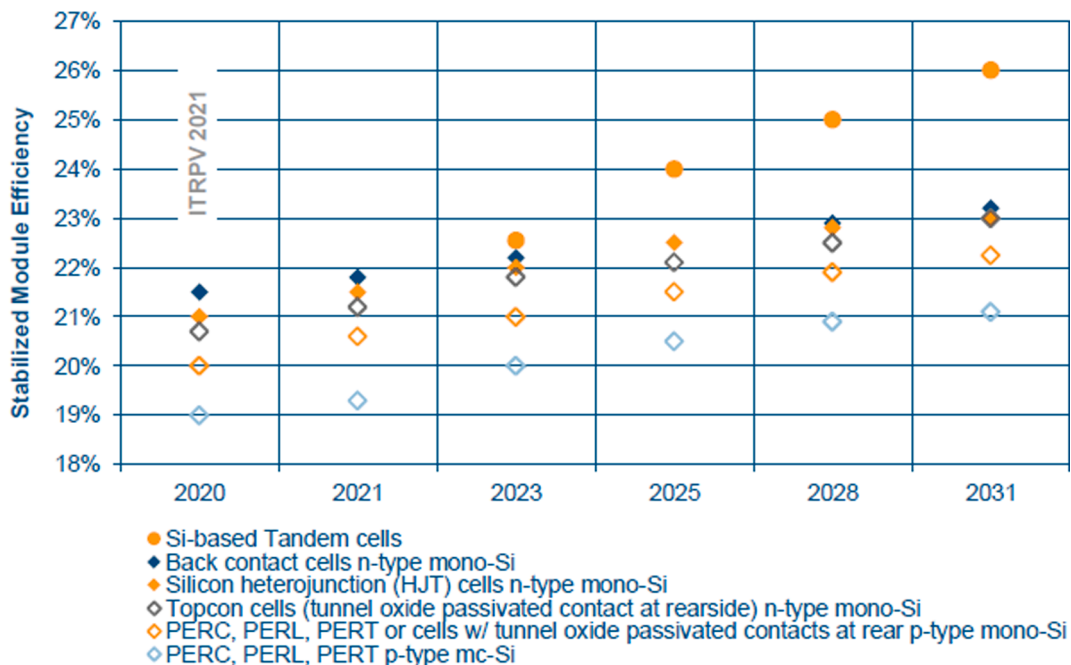


Fig. 25. Expected trend of average stabilized efficiency values for solar modules comprised of various c-Si solar cells [19].

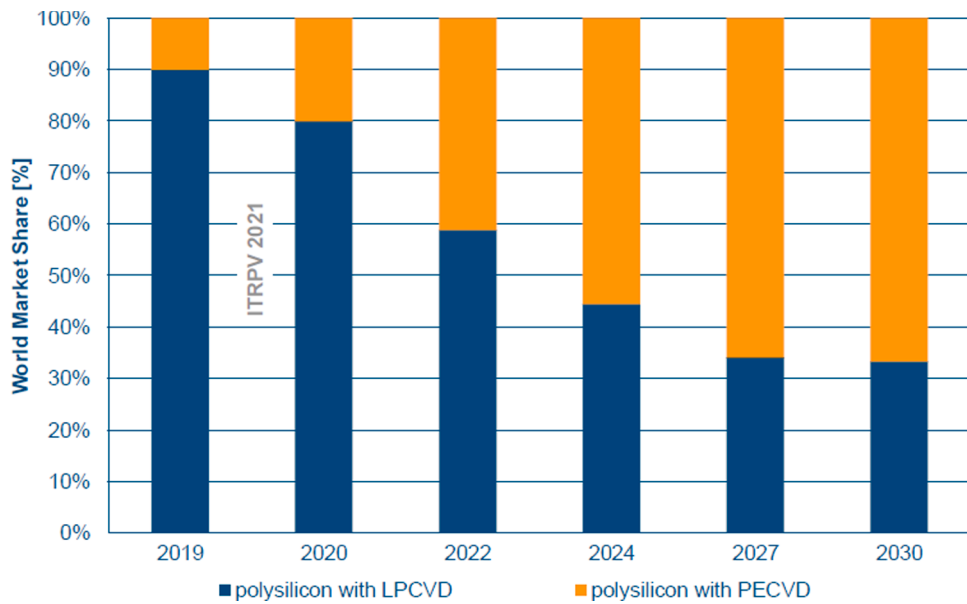


Fig. 26. Expected trend of poly-Si layer formation for TOPCon contacts [19].

available for the mass production of the ultra-thin tunnel oxide layer has been shown in Table 10.

(b) **Mass production of poly-Si layer:** poly-Si layer of first ever TOPCon solar cell was developed by PECVD process [20]. Later on, either LPCVD or PECVD has been used mostly for the development of the poly-Si layer [19]. However, for the mass production of amorphous-Si/poly-Si layer; LPCVD has been used widely due to possessing numerous advantages such as excellent uniformity of thickness along the wafer and the boat, formation of pin-hole free layers, high purity, high throughput etc. [127]. The other major advantage of LPCVD process is the opportunity to develop either intrinsic a-Si/poly-Si layer,

followed by an *ex-situ* diffusion process in  $\text{POCl}_3$  tube for the formation of n-type poly-Si layer (TOPCon *ex-situ*) or the development of *in-situ* doped a-Si/poly-Si layer, followed by a thermal annealing in  $\text{N}_2$  atmosphere (TOPCon *in-situ*). However, the latter has been found to be more cost-effective due to featuring lesser number of processing steps. Apart from LPCVD process, PECVD is also considered to be one of the most promising routes for the development of a-Si layer due to its higher deposition rate compared to the LPCVD process, availability of *in-situ* doping without comprising with the deposition rate and the layer uniformity, ability of single-sided deposition and hence no possibility of wrap-around of the developed a-Si layer. Nandakumar et al. showed that

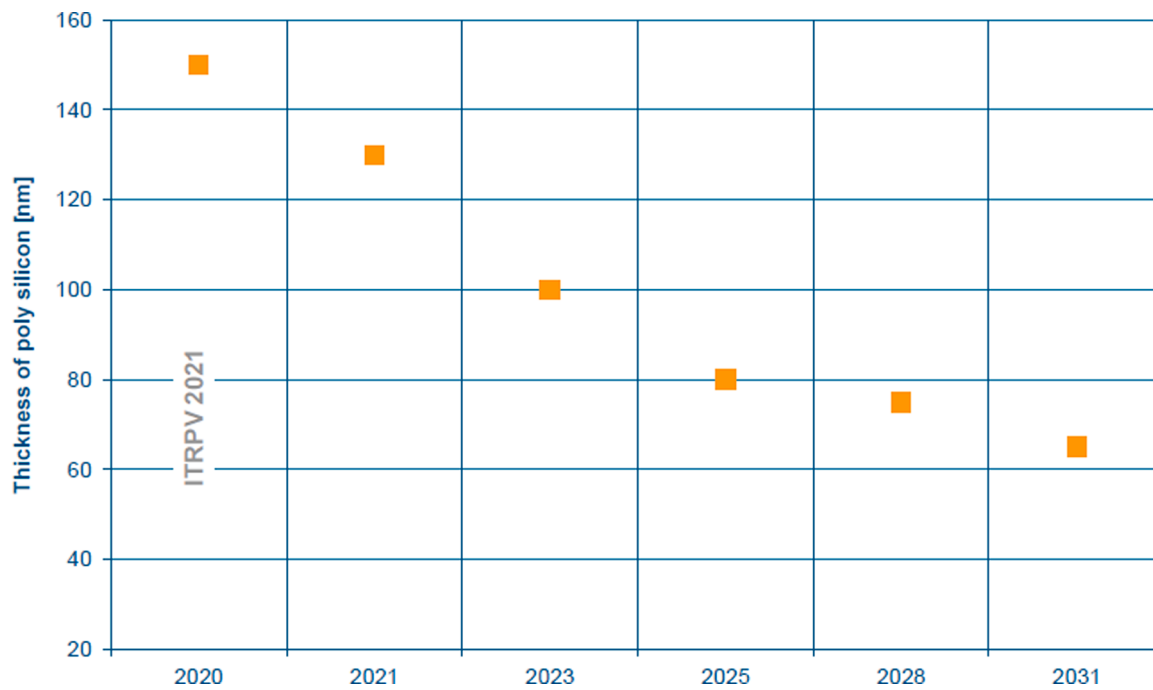


Fig. 27. Expected trend of poly-Si layer thickness for TOPCon contacts [19].

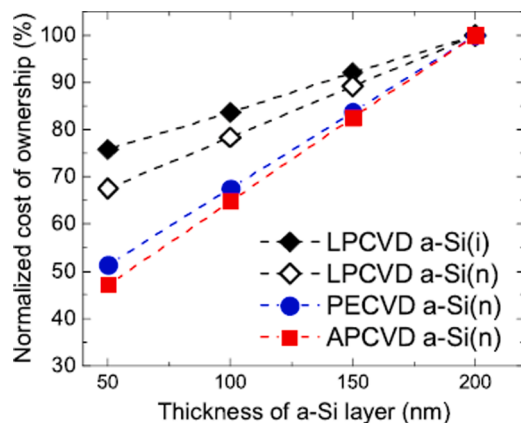


Fig. 28. Normalized COO calculated for various a-Si/poly-Si deposition technologies vs the thickness of the deposited layer. Here, two wafers per slot are assumed for LPCVD depositions. PECVD layer deposition is assumed for a batch type tool [127].

use of inline PECVD tool for the development of ultra-thin tunnel oxide layer and doped a-Si layer may provide an excellent conversion efficiency of as high as 22.8%; indicating the viability of using PECVD tool for the mass production of the doped a-Si layer [86]. Furthermore, as per ITRPV report, PECVD will gradually grab the market share of LPCVD process for the development of a-Si/poly-Si layer [19]. In recent times, Feldmann et al. demonstrated that screen-printing compatible a-Si(n) layers may be developed by using PECVD technology [128]. The recombination current density was found to be as low as  $\approx 3 \text{ fA/cm}^2$  in the passivated region whereas the value of  $J_0$  was almost  $200 \text{ fA/cm}^2$  in the metallized region. In the device level, the best cell featured a conversion efficiency of 22.95% with a  $V_{oc}$  of 700 mV,  $J_{sc}$  of  $41.2 \text{ mA/cm}^2$  and FF of 79.6%.

On the other hand, APCVD may also be a competitor to LPCVD and/or PECVD process due to its high deposition rate, facility of single-sided deposition, accessibility of *in-situ* doping etc. [127]. However, the industrial usage of APCVD process for the deposition of a-Si layer to form

the TOPCon structure is yet to be made. The comparative study of various a-Si/poly-Si deposition technologies has been summarized in the Table 11.

The other important aspect of the mass production of poly-Si layer is its thickness value for the cost-effectiveness and metallization purpose. According to the ITRPV 2021 edition, the gradual reduction of thickness of the poly-Si layer used in TOPCon solar cells has been anticipated [19]. Kafle et al. also investigated the dependence of the cost-effectiveness on the thickness of developed poly-Si layer by various routes [127]. The study showed that low thick poly-Si layer grown by APCVD may be the most effective tool in compared to its counterpart. However, improvement in the screen-printed metallization process is highly required to reduce the poly-Si layer thickness from the present value of 150–200 nm.

**(c) Metallization:** Metallization is one of the prime factors of realizing industrial scalable high efficiency and cost-effective TOPCon solar cells. Various factors such as recombination current density at metal/semiconductor interface, contact resistivity, rear side reflection (for monofacial cells only), firing temperature, cost-effectiveness, throughput etc. need to be considered during the rear-side metallization of large area TOPCon solar cells for mass production purpose. Other influencing parameters namely; thickness, doping concentration, surface morphology and uniformity of poly-Si layer must be taken care of before metallization [129]. As discussed in Section 6.4, for laboratorial or small scale research purpose the rear side metallization of TOPCon solar cell has been realized by various techniques such as thermal evaporation, PVD or electroplating etc. [20,91]. On the other hand, for large scale or mass production purpose the metallization has been mostly accomplished by screen printing and firing process for numerous advantages such as high throughput, low cost, probability of better rear side reflection of the evanescent light, simplicity etc. [43,86,115–117, 118–126]. Heraeus, the renowned paste making enterprise has recently announced that their “SOL7300 Pro” (Ag) paste may be very fruitful for realizing the metallization (especially rear side) of TOPCon solar cells as it offers low metal induced recombination, low contact resistivity even when fired at relatively low temperatures, excellent green strength and low possibility of damage to the ultra-thin poly-Si layer etc. [130]. However, the consumption of Ag paste needs to be reduced significantly

### Trend for remaining silver for metallization per cell (front + rear side)

(Values for 166.0 x 166.0 mm<sup>2</sup> cell size)

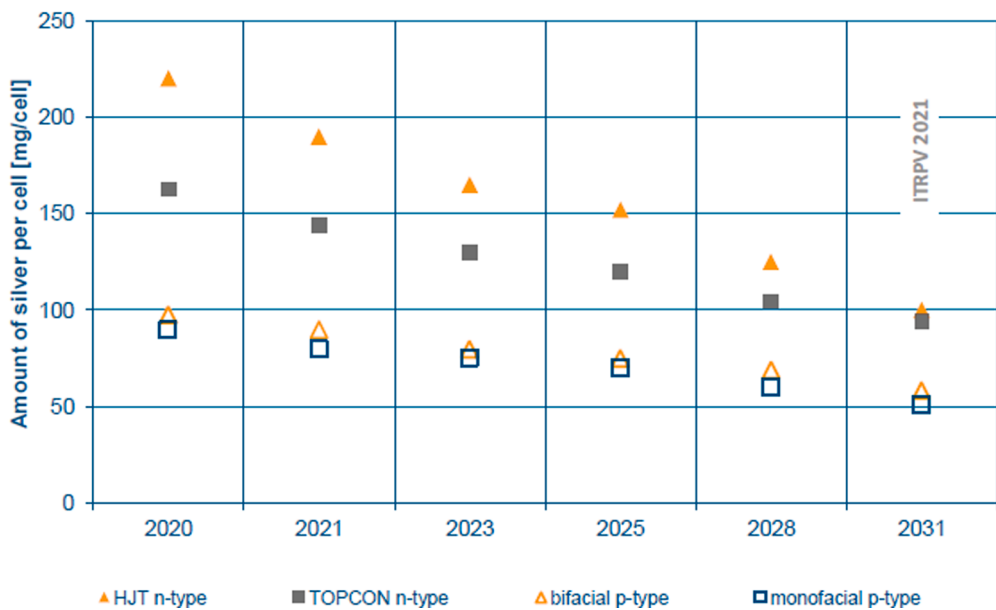


Fig. 29. Expected trend of silver consumption per cell for various cell concepts developed onto M6 wafers [19].

### Future trends in Si solar cell metallization materials

Lead free metallization pastes used for different technologies

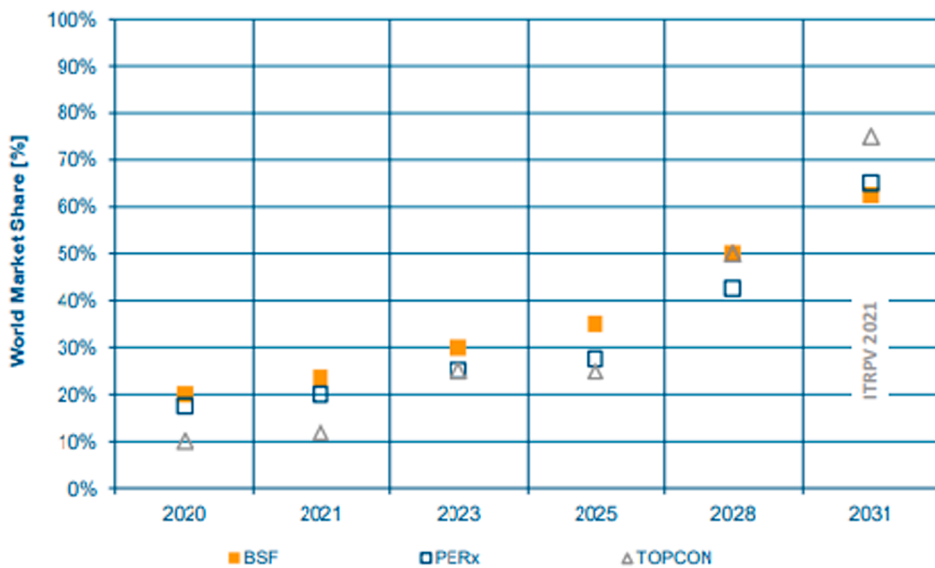


Fig. 30. Expected trend for implementation of lead free pastes for different cell technologies [19].

to facilitate the maximization of the annual solar module production rate from ~ 135 GW in 2020 to 3 TW in 2030 [131]. According to the report, the silver consumption must be kept within 2mg/W to achieve the desired module production rate. Surprisingly, the current consumption of silver for industrial PERC, TOPCon and SHJ solar cells is approximately 15.4mg/W, 25.6 mg/W, 33.9mg/W; respectively which is quite higher than the target value. The silver requirement for TOPCon and SHJ is more than its counterpart PERC due to its (Ag) requirement in

both front and the back side of the cells for metallization purpose. The other challenging issue associated with the Ag paste is its high volatility of the price which has been increasing significantly (To be specific, an increment of the price of Ag ≈ 50% was observed within one year) [19]. This concerning issue may be addressed by reducing the consumption of the Ag paste in the coming years and/or replacing it with some other less expensive materials such as copper. The silver consumption is being expected to be reduced to 8.5 mg/W, 13.8mg/W and 14.3 mg/W in the

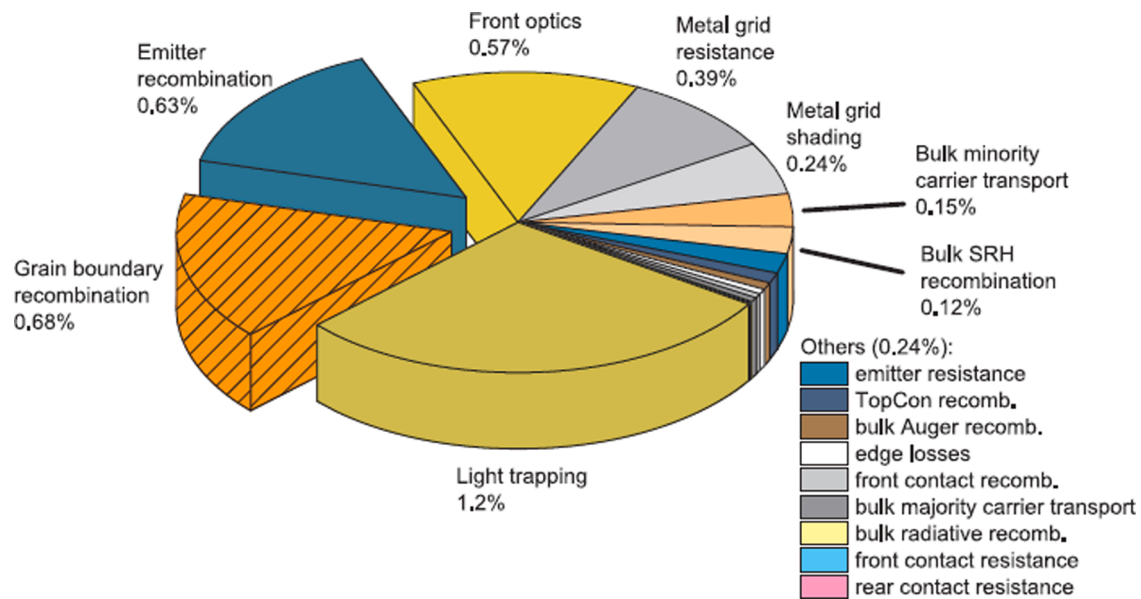


Fig. 31. Free energy loss analysis (FELA) of the record multi-crystalline Si solar cell [139].

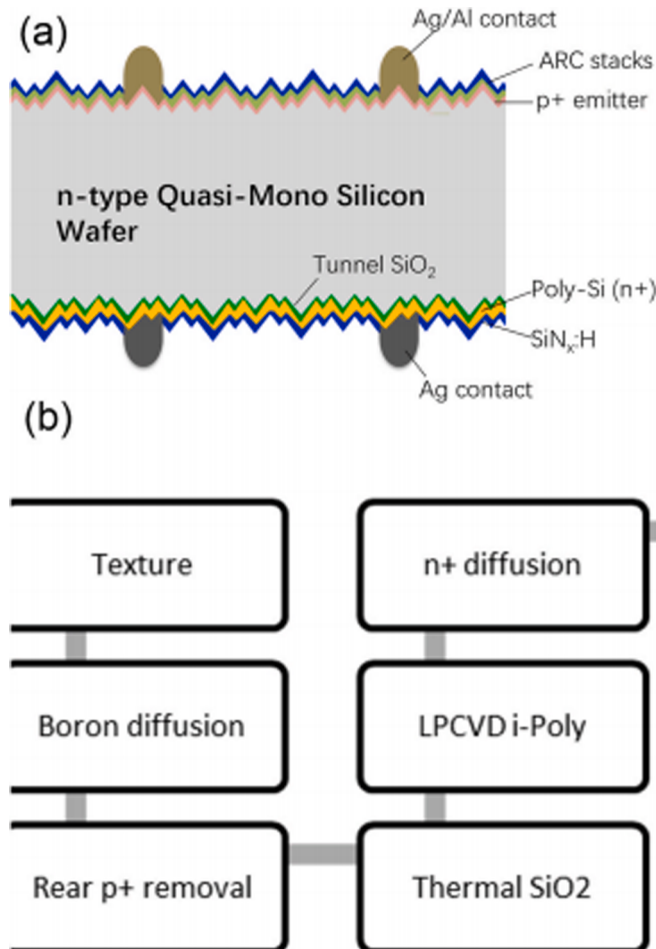


Fig. 32. (a) Schematic diagram and (b) process sequence of n-type quasi-mono silicon i-TOPCon bifacial solar cells [141].

coming decade i.e., by 2031 for PERC, TOPCon and SHJ solar cells; respectively [131]. Nevertheless, the expected consumption value is still quite higher than the target value of 2mg/W. However, silver will

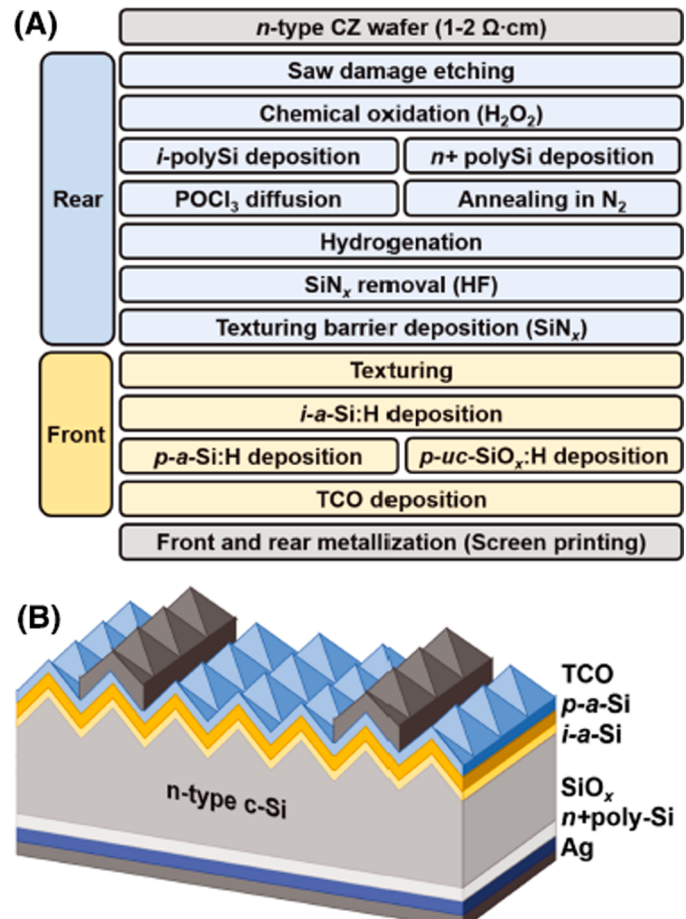


Fig. 33. (A) Procedure flow for the fabrication of hybrid solar cell and (B) the schematic of the final cell structure after the fabrication process [142].

remain an integral part for the metallization of TOPCon solar cells for the next few years and hence continuous improvement of the paste quality and breakthrough for the next generation cost-effective metallization material are much awaited. Besides, use of more lead free pastes

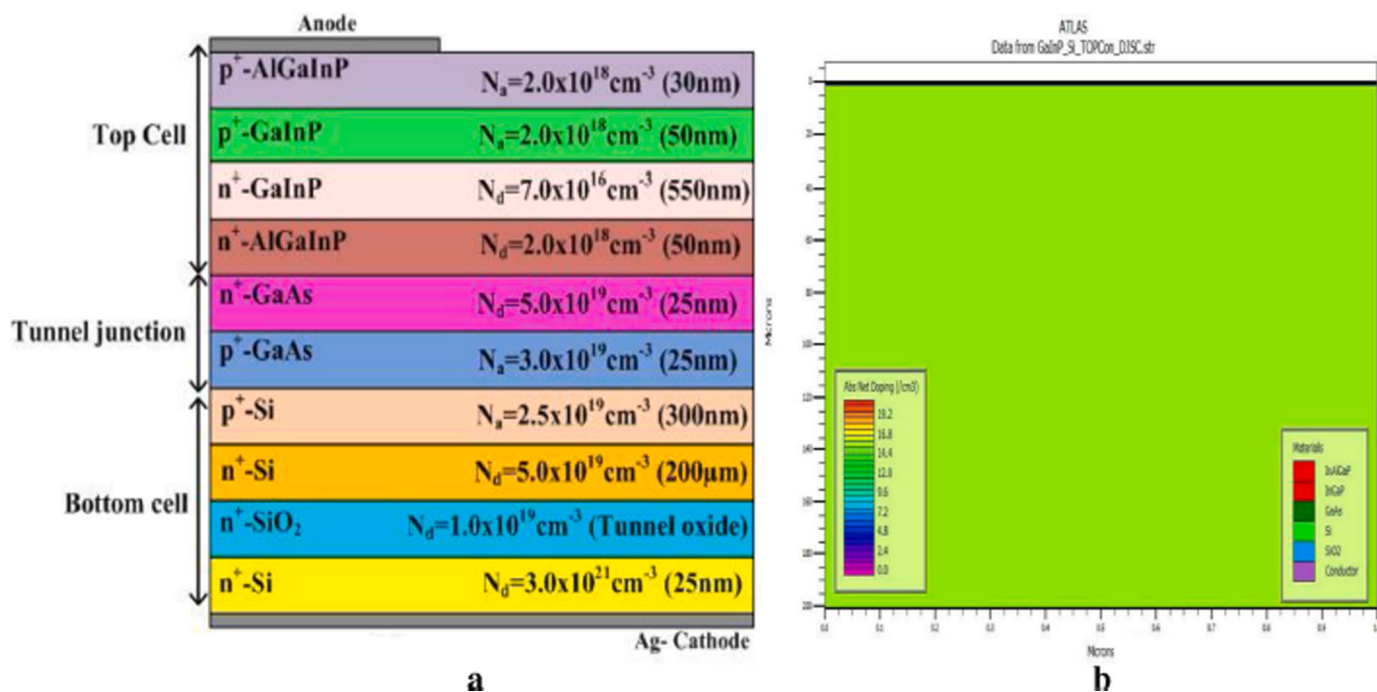


Fig. 34. (a) Schematic diagram and (b) simulated structure of GaInP/Si dual-junction solar cell [145].

during the metallization of industrial TOPCon solar cells may also be significantly effective to improve the cost/watt-peak [19].

#### 10. TOPCon solar cells based on multicrystalline silicon material

Improvement in the multicrystalline silicon material quality has been able to attract the researchers to develop high efficiency multicrystalline silicon based TOPCon solar cells [132–141]. Consequently, Schindler et al. used “efficiency limiting bulk recombination analysis” (ELBA) technique to predict the power conversion efficiency of these multicrystalline silicon based TOPCon solar cells [132]. The study revealed that the iso-textured n-type high performance multicrystalline silicon material may be used to develop TOPCon solar cells with a power conversion efficiency of beyond 20%. Nevertheless, according to the study, further improvement in the texturization of the samples may lead to maximize the efficiency potential of the solar cells. Eventually, the best practical solar cell based on n-type multicrystalline silicon demonstrated a conversion efficiency of 19.3% with  $V_{oc} = 663.01 \text{ mV}$ ,  $J_{sc} = 38.04 \text{ mA/cm}^2$ , and  $FF = 76.39\%$ . The reason for obtaining low FF may be attributed to the large series resistance value. Furthermore, in another contribution, Schindler et al. reported about the development of n-type multicrystalline silicon based TOPCon solar cells (active cell area =  $2 \times 2 \text{ cm}^2$ ) with a power conversion efficiency of 19.6% ( $V_{oc} = 663.7 \text{ mV}$ ,  $J_{sc} = 38.87 \text{ mA/cm}^2$ ,  $FF = 75.9\%$ ) [133]. The authors recommended that further enhancement in the power conversion efficiency may be realized by improving the optical confinement inside the solar cells and reducing the power losses occurring due to high value of series resistance. On the other hand, Riepe et al. reported that the crystal structure and the initial grain size have significant role on the power conversion efficiency of the multicrystalline silicon based TOPCon solar cells [134]. In the study, an efficiency prediction of about 20% was made, considering the use of multicrystalline silicon plate as seed material. However, proper texturization and selection of suitable seed may maximize the efficiency potential of n-type multicrystalline silicon based TOPCon solar cells. Two years later in 2017, Schindler et al. demonstrated an enhancement in the cell performance by improving the quality of multicrystalline silicon material and optimizing the base

resistivity along with the wafer thickness [135,136]. According to the reports, 21.9% efficient TOPCon solar cells with  $V_{oc} = 672.6 \text{ mV}$ ,  $J_{sc} = 40.8 \text{ mA/cm}^2$  and  $FF = 79.7\%$  based on n-type multicrystalline silicon substrate were developed. Additionally, “efficiency limiting bulk recombination analysis” (ELBA) also revealed an efficiency potential of 22.5% for n-type TOPCon solar cells based on multicrystalline silicon material. Concurrently, in 2017, Benick et al. reported that a conversion efficiency of 22.3% with  $V_{oc} = 674.2 \text{ mV}$ ,  $J_{sc} = 41.1 \text{ mA/cm}^2$  and  $FF = 80.5\%$  was achieved for n-type high performance multicrystalline silicon solar cells featuring TOPCon structure at the rear side and  $\text{Al}_2\text{O}_3$  passivated boron emitter on the front side [137]. The front side of the solar cell was textured by black silicon to reduce the reflection losses while maintaining low recombination current density ( $J_{0e}$ ) of  $\leq 60 \text{ mA/cm}^2$  for a  $90 \Omega/\text{sq}$  emitter.

On the other hand, different loss mechanisms involved in multicrystalline silicon based TOPCon solar cells were studied by Schindler et al. [139]. According to the report, the loss in  $J_{sc}$  may be attributed to the presence of larger number of structural crystal defects which act as carrier recombination centres. Besides, the study also revealed that recombination at the grain boundaries may be a major cause for obtaining lower FF in compared to FZ reference cells. In contrast, relatively low  $V_{oc}$  was realized due to the emitter-induced inhomogeneities. Besides, the loss analysis demonstrated that carrier recombination at grain boundaries and at the front emitter was mainly responsible for the electrical losses. However, the authors opined that improving the crystallization process, hydrogenation of the bulk and optimizing the boron emitter may lead to enhance the power conversion efficiency of multicrystalline silicon solar cells featuring TOPCon structure at the back.

In recent times, Liu et al. reported that a power conversion efficiency of 23.22% was obtained by applying industrial TOPCon (i-TOPCon) technology onto 157.4 mm × 157.4 mm quasi-mono n-type Si wafers [141]. Moreover, excellent surface passivating quality was observed at both front and rear side of the cell by applying this i-TOPCon technology which was originally developed for the fabrication of industrial grade TOPCon solar cells based on monocrystalline CZ Si wafers [118,120]. According to the report, significant power loss of almost 4% may be occurred due to the bulk recombination losses in quasi-mono Si wafers and hence enhancement in the power conversion efficiency may be

**Table 1**

Surface passivation quality of ultra-thin  $\text{SiO}_x$  layer grown by different routes on various types of wafers.

Type of Fabricated TOPCon Structure	Fabrication route	Wafer type	$iV_{oc}$ (mV)	Refs.
n-TOPCon	Wet chemical oxidation in hot $\text{HNO}_3$ atmosphere	n-type, planar FZ	720	[34]
		n-type, textured FZ	630	
	Oxidation in UV/ $\text{O}_3$ atmosphere	n-type, planar FZ	725	[35]
		n-type, textured FZ	715	
n-TOPCon	Wet chemical oxidation in hot $\text{HNO}_3$ atmosphere	n-type, planar FZ	> 720	[35]
		n-type, textured FZ	635	
	Oxidation in UV/ $\text{O}_3$ atmosphere	n-type, planar FZ	> 725	[35]
		n-type, textured FZ	> 710	
n-TOPCon	Oxidation in $\text{DIO}_3$ atmosphere	n-type, planar FZ	> 720	[37]
		n-type, textured FZ	~ 710	
	Wet chemical oxidation in hot $\text{HNO}_3$ atmosphere	n-type polished CZ	706–712	[37]
	Oxidation in CNS (Concentrated nitric and sulphuric) acid atmosphere	n-type polished CZ	714–718	
n-TOPCon	Wet chemical oxidation in hot $\text{HNO}_3$ atmosphere	n-type, solar grade CZ	727	[38]
	Plasma assisted oxidation in $\text{N}_2\text{O}$ atmosphere	n-type, solar grade CZ	730 (before hydrogenation) 747 (after hydrogenation)	
p-TOPCon	Wet chemical oxidation in hot $\text{HNO}_3$ atmosphere	n-type, solar grade CZ	718	[39]
	Plasma assisted oxidation in $\text{N}_2\text{O}$ atmosphere	n-type, solar grade CZ	703	
	Thermal oxidation in $\text{N}_2$ and $\text{O}_2$ atmosphere	n-type, solar grade CZ	722	[39]

**Table 2**

Thickness data measured by different methods on one identical sample without thermal annealing [42].

Method	Thickness average d (nm)	Thickness error (nm)
TEM	1.1	0.35
Ellipsometry	1.36	0.3
XPS 0°	0.61	0.15
XPS 70°	0.72	0.15
ToF-SIMS depth profiling	< 2	0.5

realized by improving the quality of bulk material. Nevertheless, further study demonstrated that reduction of  $J_0$  at the front emitter and rear side passivating contact may provide a  $V_{oc}$  of greater than 710 mV even with lower minority carrier lifetime inside the bulk.

## 11. Hybrid/heterojunction silicon solar cells with TOPCon structure

In 2019, Park et al. reported about the development of hybrid silicon solar cells featuring thin amorphous silicon layer as passivating hole contacts at the front and TOPCon structure as the passivating electron contacts at the back side of the cells [142]. The best cell featuring  $\mu\text{-SiO:H}$  layer as interfacial layer in between n-type base and p-a-Si:H front emitter demonstrated a power conversion efficiency of 21.8% ( $V_{oc} = 715$  mV,  $J_{sc} = 40.9 \text{ mA/cm}^2$ , and FF = 74.7%) with an effective cell area of  $4 \text{ cm}^2$ . In the cell structure, *in-situ* P-doped poly-Si layer served the purpose of rear side passivating contact. Furthermore, the authors performed a simulation study with the help of Quokka2 simulation tool and the study revealed that the power conversion efficiency may be enhanced up to 26% by improving the wafer quality and the passivation quality of the front and rear side passivating contacts.

On the other hand, Luderer et al. showed that  $p^+$  poly-Si/ $n^+$  poly-Si/ $\text{SiO}_x$  stack based on  $200 \mu\text{m}$ ,  $<100>$  oriented,  $1 \Omega\text{-cm}$ , n-type FZ Si wafers may feature very good junction properties with a combined junction resistance of less than  $10 \text{ m}\Omega\text{-cm}^2$ , subjected to the optimization of the necessary thermal treatment and the deposition parameters of a-Si layers [143]. Besides, the structure demonstrated an excellent surface passivation quality with an  $iV_{oc}$  of 726 mV. The authors further added that these results may be helpful to fabricate high-efficiency monolithic perovskite/silicon tandem solar cells featuring a c-Si bottom cell with  $p^+$  poly-Si/ $n^+$  poly-Si/ $\text{SiO}_x$  stack as a passivating front contact. Recently, Yoon et al. reported that highly transparent and less resistive 80 nm ITO layer was deposited onto TOPCon structure by means of DC magnetron sputtering at room temperature and at a power density of  $0.3 \text{ W/cm}^2$  to facilitate the development of high efficiency perovskite/silicon tandem solar cells [144]. In the contribution, firstly the single junction Si solar cells were developed based on n-type CZ Si wafers and the cells comprised of TOPCon structure at the front side and  $\text{Al}_2\text{O}_3/\text{SiN}_x$  passivated boron diffused  $p^+$  emitter at the rear side. A thermal treatment at a temperature of  $250^\circ\text{C}$  was carried out after ITO deposition to reduce any sputter induced damage. As a result, a very high  $iV_{oc}$  of  $684.7 \pm 11.3$  mV, a total  $J_0$  of  $49.2 \pm 14.8 \text{ fA/cm}^2$ , an iFF of  $81.9 \pm 0.8\%$  and a  $\rho_c$  of  $60\text{--}90 \text{ m}\Omega\text{-cm}^2$  were obtained for the ITO coated samples. Besides, the developed Si solar cells featuring a local metallic (Ag) contact to the rear emitter and ITO thin films as front-sided contact demonstrated a pseudo-efficiency of  $20.2 \pm 0.5\%$  with a  $V_{oc}$  of  $670.4 \pm 7$  mV, a  $J_{sc}$  of  $30.9 \text{ mA/cm}^2$  and a pseudo-FF of  $77.3 \pm 1.3\%$ . Finally, the authors claimed that the result was quite satisfactory to use sputter deposited ITO thin film as a recombination layer connecting perovskite top cell and Si bottom cell and a power conversion efficiency of 25% may be obtained for monolithic perovskite/Si tandem solar cells. On the other hand, with the help of Silvaco ATLAS TCAD tool and by using ASTM certified AM 1.5G spectrum, Verma and Mishra showed that a very high conversion efficiency of 35.32% may be achieved by applying TOPCon structure at the bottom cell of GaInP/Si dual-junction solar cell [145]. The applied TOPCon structure helped to minimize the carrier recombination losses at the rear side of the bottom cell and as a result, improvement in the external  $V_{oc}$  was observed. However, a decrement in the cell performance was noticed when the thickness of tunnelling  $\text{SiO}_2$  layer was increased beyond 0.2 nm. Reduced carrier transport through thicker  $\text{SiO}_2$  layer may be the reason for this phenomenon.

## 12. Future scope of work with possible challenges

So far we have observed how the intensified study has been conducted over the years to quantify the power output and simplify the commercialization process of TOPCon solar cells. Nevertheless, in accordance to the basic nature of research, there are still scopes of further explorations. Some of these have been pointed below:

### A. Improvement of PCE and cost-effectiveness

**Table 3**

I-V parameters of the developed TOPCon solar cells [43].

Thickness of SiO <sub>x</sub> layer (nm)	Nature of result	V <sub>oc</sub> (mV)	J <sub>sc</sub> (mA/cm <sup>2</sup> )	R <sub>ser</sub> (mΩ)	FF (%)	Efficiency (%)	Cell area (cm <sup>2</sup> )
1.55	Median	687.1	39.92	4.64	81.09	22.25	244.32
	Best	689.4	40	4.34	81.35	22.43	
1.43	Median	680.1	39.8	5.23	79.94	21.7	244.32
	Best	684	39.94	5.22	79.78	21.79	
1.25	Median	679	39.82	6.18	78.5	21.23	244.32
	Best	682.2	39.91	5.97	78.71	21.43	

**Table 4**

Impact of annealing temperature on oxide integrity and surface passivation quality [45].

T <sub>anneal</sub> (°C)	Oxide integrity (qualitative figure of merit)	iV <sub>oc</sub> (mV)	ρ <sub>c</sub> (mΩ·cm <sup>2</sup> )
800	High	715.5	3.9 ± 0.4
900	Medium	683.3	1.7 ± 0.3
950	Low, many pinholes	624.7	0.5 ± 0.1

Through the improvement of individual cell parameters i.e., V<sub>oc</sub>, J<sub>sc</sub> and FF the enhancement in PCE (Power conversion efficiency) of any solar cell structure may be realized. In the similar way, the power output of TOPCon solar cells can be maximized by quantifying the magnitude of different cell parameters. Now, the question should be how we can improve the cell parameters? In general, the open-circuit voltage (V<sub>oc</sub>) of any solar cell structure is highly limited by the various recombination mechanisms occurred inside the bulk layer and the junctions. In case of TOPCon solar cells, the magnitude of V<sub>oc</sub> may be improved by reducing the recombination current density at metal/semiconductor interface; specifically at the front side of the solar cells where TOPCon structure is generally not present due to its own demerits like parasitic absorption will take place. Therefore, the reduction of front sided recombination current density may be obtained by optimizing the metallized area fraction by means of optimizing the finger width [20]. The other way thorough which we can reduce the recombination current density at the front side is the implementation of selective emitter technology [25]. Besides, the bulk carrier recombination needs also to be reduced to attain higher V<sub>oc</sub> value. Bulk recombination may be minimized by improving the quality of the base wafer along with adopting proper cleaning procedure to decrease the defect density within the base material. Although excellent passivation quality has already been realized by TOPCon/POLO structure still continuous research must be carried on to realize even better passivation quality which in turn will provide higher V<sub>oc</sub> value.

The other major issue associated with the TOPCon structure is the parasitic absorption of light by doped poly-Si layer. In essence, the thickness and the doping concentration of doped poly-Si layer are two vital parameters to tune the parasitic absorption of light within it. To conquer the challenge of parasitic absorption of light, thinner poly-Si layer may be utilized with an additional capping layer such as ALD

Al<sub>2</sub>O<sub>3</sub> and/or PECVD SiN<sub>x</sub> layer. The use of these capping layers also helps to preserve the passivation quality of TOPCon structure by impeding hydrogen effusion during high temperature firing process [87]. Besides, use of wide band gap poly-SiC<sub>x</sub> layer instead of poly-Si layer may also open an effective way to realize lower parasitic absorption of light [78].

The improvement of cell performance is always welcome but the process and the used materials must be industrial feasible and cost-effective. The ultimate goal is to improve the cost/W<sub>peak</sub> and the simple way to achieve that goal is either reducing the processing and material cost or improving the power output or in the best cases, both should be attained. One of the most concerning issues associated with this high efficiency TOPCon solar cells is the use of expensive Ag paste for the metallization purpose in the both the sides of the cells. Therefore, minimization of the consumption of Ag paste is absolutely necessary to reduce the cost of the solar cells. In this regard, mass production of more bifacial solar cells may become helpful as in case of bifacial solar cells full area metallic contact is not required. Apart from this, the impact of using alternative metal (like Cu) on the contact properties may be investigated. Even, use of multilayer metallic contact such as Ag/Cu, Ag/Al etc. needs to promoted, subjected to the fulfillment of required contact properties for efficient carrier collection.

#### B. Development and light management of thin TOPCon solar cells

Undoubtedly, development of crystalline silicon solar cells based on thin wafers is a promising approach due to featuring various advantages such as low bulk impurities, low material consumption, flexibility, easy to handle etc. However, power conversion efficiency of these thin wafer based solar cells is usually lower than the conventional Si solar cells. This phenomenon may be ascribed to low light absorption due to possessing thin absorbing layer. Therefore, proper light management mechanisms need to be applied to triumph over this challenge.

To the best of our knowledge, an intensive study on the development of TOPCon solar cells based on thin Si wafers is yet to be made. However, there are certain areas where we should look into during the development process of thin TOPCon solar cells. Firstly, thin wafers are not commercially available. Therefore, proper etching methods (mainly chemical) must be applied to cut down the wafer thickness so that formation of cracks on the surface of the wafers can be avoided. Secondly, thin wafers must be handled very carefully during the cell fabrication

**Table 5**

Influence of ion energy, ion dose and annealing temperature on the passivating quality.

Features of wafers	Nature of deposited amorphous silicon layers prior to ion-implantation	Implanted material	Ion energy (KeV)	Ion dose ( $\times 10^{15} \text{ cm}^{-2}$ )	Annealing temperature (°C)	iV <sub>oc</sub> (mV)	Refs.
n-type FZ	Intrinsic amorphous Si layer	Phosphorous (p <sup>+</sup> )	2	1	800	720	[60]
		Boron (BF <sub>2</sub> )	2	5	800	694	
n-type FZ	Boron doped amorphous Si layer	Phosphorous	2	7.5	800	> 700	[61]
n-type FZ	Intrinsic amorphous Si layer	Phosphorous	2	1–5	800	725	[62]
	Boron doped amorphous Si layer	Phosphorous	2	7.5	800	720	
	Intrinsic amorphous Si layer	Boron (B)	1	5	800	640	
	Intrinsic amorphous Si layer	Boron (BF <sub>2</sub> )	2	5	800	690	
n-type FZ	Intrinsic amorphous Si layer	Phosphorous	2	1	850	733	[63]
	Intrinsic amorphous Si layer	Boron (BF)	2	1	850	696	

**Table 6**  
Reported passivation quality of n-TOPCon structure.

Features of base wafer	Ultra-thin SiO <sub>x</sub> layer deposition process	Amorphous-Si layer deposition process	Post-crystallization process	Obtained iV <sub>oc</sub> (mV)	Obtained J <sub>0</sub> (fA/cm <sup>2</sup> )	Refs.
n-type FZ, 1 Ω-cm	Wet chemical oxidation	PECVD	-	> 710	9	[20]
n-type FZ, 1 Ω-cm	Wet chemical oxidation	PECVD	RPHP	~720	7	[25]
n-type CZ, 1–3 Ω-cm	Concentrated nitric and sulphuric acid oxidation	PECVD	FGA + PECVD SiN <sub>x</sub>	724	6.9	[37]
p-type CZ, 1–3 Ω-cm	Oxidation in N <sub>2</sub> O plasma	PECVD	FGA + ALD Al <sub>2</sub> O <sub>3</sub>	742	3	[32]
n-type CZ, 3 Ω-cm	Oxidation in N <sub>2</sub> O plasma	PECVD	Insertion of AlO <sub>x</sub> /SiN <sub>x</sub> capping layer + annealing	747	2	[38]
n-type CZ, 0.5–2 Ω-cm	Thermal oxidation	LPCVD	ALD AlO <sub>x</sub> + PECVD SiN <sub>x</sub>	700	18	[43]
n-type CZ, 0.5–2 Ω-cm	Wet chemical oxidation	PECVD	Ozone oxidation	740	0.90	[46]
n-type CZ, 0.2–2 Ω-cm	Wet chemical oxidation	PECVD	-	730	6	[59]
n-type FZ, 1 Ω-cm	Wet chemical oxidation	LPCVD	RPHP	733	4.5	[63]
n-type CZ, 1–3 Ω-cm	Wet chemical oxidation	PECVD	ALD Al <sub>2</sub> O <sub>3</sub>	727	4.7	[66]
n-type FZ, 500 Ω-cm	Wet chemical oxidation	PECVD	PECVD SiN <sub>x</sub>	719	5.2	[72]
n-type CZ, 3–5 Ω-cm	Wet chemical oxidation	PECVD	Annealing in N <sub>2</sub> and water vapor atmosphere	≈ 730	3.8	[83]
n-type CZ, 1–7 Ω-cm	Wet chemical oxidation	PECVD	ALD Al <sub>2</sub> O <sub>3</sub> + PECVD SiN <sub>x</sub>	747	1.9	[84]
n-type CZ, 3.6 Ω-cm	Thermal oxidation	APCVD	AlO <sub>x</sub> /SiN <sub>x</sub>	730	6	[67]
n-type FZ, 100 Ω-cm	Thermal oxidation	-	ALD Al <sub>2</sub> O <sub>3</sub> + FGA	-	0.2	[88]
n-type CZ, 4 Ω-cm	Oxidation in UV/O <sub>3</sub> atmosphere	LPCVD	FGA	743	0.5	[89]
n-type CZ, 1–7 Ω-cm	Wet chemical oxidation	PECVD*	ALD Al <sub>2</sub> O <sub>3</sub> + thermal treatment	750	1.7	[78]
n-type CZ, 4–5 Ω-cm	Plasma assisted oxidation	PECVD	PECVD SiN <sub>x</sub>	730	3	[86]
n-type FZ, 1 Ω-cm	Thermal oxidation	PECVD	ALD AlO <sub>x</sub> + FGA	-	0.2 ± 0.4	[87]

\* In this case, doped poly-SiC<sub>x</sub> layer was used instead of doped poly-Si layer.

**Table 7**  
Reported passivation quality of p-TOPCon structure.

Features of base wafer	Ultra-thin SiO <sub>x</sub> layer deposition process	Amorphous-Si layer deposition process	Post-crystallization process	Obtained iV <sub>oc</sub> (mV)	Obtained J <sub>0</sub> (fA/cm <sup>2</sup> )	Refs.
n-type CZ, 3 Ω-cm	Thermal oxidation	PECVD	Annealing in N <sub>2</sub> and water vapor atmosphere + ALD AlO <sub>x</sub> :H	722	5.95	[39]
p-type FZ, 1 Ω-cm	Wet chemical oxidation	PECVD	RPHP	680	60	[60]
p-type FZ, 1 Ω-cm	Wet chemical oxidation	LPCVD	RPHP	696	22.0	[63]
n-type CZ, 3.6 Ω-cm	Thermal oxidation	APCVD	AlO <sub>x</sub> /SiN <sub>x</sub>	721	6	[67]
n-type CZ, 4 Ω-cm	Oxidation in UV/O <sub>3</sub> atmosphere	LPCVD	PECVD SiN <sub>x</sub>	734	3.8	[89]

**Table 8**  
Different large area monofacial TOPCon solar cells.

Cell area (cm <sup>2</sup> )	Features of wafer	Nature of the result	V <sub>oc</sub> (mV)	J <sub>sc</sub> (mA/cm <sup>2</sup> )	FF (%)	Efficiency (%)	Refs.
239	n-type, 5 Ω-cm, bulk lifetime > 3 ms, CZ	Average	673.6	39.5	79.1	21.1	[111]
		Best	674	39.6	80.0	21.4	
239	n-type, 5 Ω-cm, 200 μm, bulk lifetime > 2 ms, CZ	Average (5 cells)	678.5 ± 4.9	39.46 ± 0.2	78.6 ± 0.5	21.0 ± 0.2	[112]
		Best	683.4	39.66	78.1	21.2	
100	n-type, 1 Ω-cm, FZ	Best	694	40.8	81.0	22.9	[113]
100	n-type, 1 Ω-cm, 200 μm, FZ	Best	713	41.4	83.1	24.5	[114]
245.70	n-type, 4 Ω-cm, CZ	Best	691.2	40.4	80.7	22.5	[115]
239	n-type, 2 Ω-cm, 200 μm, CZ	Best	676	39.7	80.4	21.6	[116]
100		Best	682	39.9	80.8	22.0	

**Table 9**

Various large area bifacial TOPCon solar cells.

Cell area ( $\text{cm}^2$ )	Features of wafer	Nature of the result	$V_{\text{oc}}$ (mV)	$J_{\text{sc}}$ ( $\text{mA}/\text{cm}^2$ )	FF (%)	Efficiency (%)	Refs.
239	n-type, 5 $\Omega\text{-cm}$ , CZ	Best	675	38.8	79.1	20.72	[117]
244.3	n-type, 4–5 $\Omega\text{-cm}$ , CZ	Best	696	40.5	80.9	22.8	[86]
261.47	n-type, 0.2–2 $\Omega\text{-cm}$ , CZ	Median (20000 cells)	701.5	39.84	82.2	23.0	[118]
		Best (front)	716.7	40.14	82.0	23.57	
		Best (rear)	710.8	32.59	81.9	18.98	
246.21	n-type CZ	Average (300 cells)	701	40.66	80.80	23.04	[119]
		Best	703	40.53	81.25	23.15	
244.32	n-type, 0.5–1 $\Omega\text{-cm}$ , CZ	Median (9 cells)	712	40.80	82.23	23.91	[120]
		Best (front)	716.8	40.57	84.52	24.58	
		Best (rear)	711.8	33.06	82.77	19.48	
244.32	n-type, 0.5–1 $\Omega\text{-cm}$ , 180 $\mu\text{m}$ , CZ	Best	702.6	39.78	81.62	22.81	[122]
244.32	n-type, 0.5–1 $\Omega\text{-cm}$ , 180 $\mu\text{m}$ , CZ	Best	683.4	39.53	81.86	22.14	[123]
239	n-type, 2 $\Omega\text{-cm}$ , 180 $\mu\text{m}$ , CZ	Best	702	40.3	79.7	22.60	[124]
244.32 (M2)	n-type, 0.5–2 $\Omega\text{-cm}$ , 180 $\mu\text{m}$ , CZ	Median	687.1	39.92	81.09	22.25	[43]
		Best	689.4	40	81.35	22.43	
242.77 $\pm$ 0.35	n-type CZ	Best	719.8 $\pm$ 3.6	41.59 $\pm$ 0.395	83.83 $\pm$ 0.92	25.09 $\pm$ 0.35	[125]
267.4	n-type CZ	Best	-	-	-	25.25	[126]
244.3	n-type CZ	Average (20 cells)	688	39.4	79.7	21.6	[85]
		Best	691	39.5	80	21.8	
267.7 $\pm$ 1.1	n-type CZ	Best	714.6 $\pm$ 3.6	41.59 $\pm$ 0.411	83.43 $\pm$ 0.92	24.8	[110]

**Table 10**

Overview of oxidation technologies to form tunnel oxide layer. The symbols used are qualitative representation of: ‘√’ for favourable/possible with different degree, ‘×’ for not favourable/not-possible [127].

Characteristics/Technology	Thermal	UV-O <sub>3</sub>	Plasma	HNO <sub>3</sub>	DI-O <sub>3</sub>
Dry or wet processing	Dry	Dry	Dry	Wet	Wet
In-situ growth with poly-silicon deposition	√	×	√	×	×
Thermal stability	√√√	√√√	√√√	√	√√

**Table 11**

Overview of available a-Si/poly-Si deposition technologies and qualitative comparison based upon available literature. The symbols used represent: ‘√’ for favourable/possible with different degree, ‘×’ for not favourable/not-possible, and ‘-’ for work in progress/not yet demonstrated [127].

Characteristics/Technology	LPCVD	PECVD	APCVD	PVD	Evaporation
Single-sided deposition	×	√	√	√√	√√
In-situ doping	√	√√	√√	√	-
Availability of industrial tool	√√√	√√	√√	√√	-
Process demonstrated in lab-size cells	√√√	√√√	√	√√	-
Application in large area industrial cell	√√√	√√	-	-	-
Deposition mode (Batch/Inline)	Batch	Both	Inline	Inline	Batch

**Table 12**

TOPCon solar cells fabricated on multicrystalline silicon material.

Cell area ( $\text{cm}^2$ )	$V_{\text{oc}}$ (mV)	$J_{\text{sc}}$ ( $\text{mA}/\text{cm}^2$ )	FF (%)	Efficiency (%)	Refs.
4	663.01	38.04	76.39	19.3	[132]
4	663.7	38.87	75.9	19.6	[133]
4	672.6	40.8	79.7	21.9	[136]
4	674.2	41.1	80.5	22.3	[137]
247.79	41.14	711.9	79.29	23.22	[141]

process owing to its low mechanical strength. Thirdly, as the thermal resistivity is a function of wafer thickness, hence the optimized processing temperatures of thin wafer based solar cells may vary in comparison with the standard Si wafer based solar cells. Fourthly, advanced surface texturing and passivation process need to be implemented for

thin wafers. For example, the thickness of TOPCon structure may be required to be optimized to excel the surface passivation quality. Fifthly, incomplete absorption of light mainly in longer wavelength region may significantly reduce the value of  $J_{\text{sc}}$  and hence the conversion efficiency. Therefore, the optical path length of the incident light requires to be prolonged through advanced light trapping mechanisms such as incorporation of double-layer anti reflection coating at the front side of the cells and placing suitable material in between TOPCon structure and the rear side metallic contact to reflect back the evanescent light into the absorbing layers. Sixthly, mass production of thin wafer based TOPCon solar cells may become another challenge. To conquer this concern, we should direct our research in such a way so that minimal changes in the conventional production line have to be made. Besides, the module cost and utility LCOE (levelized cost of electricity) must be kept as low as possible.

#### C. Use of carrier selective contact layers as an alternative of doped poly-Si contacts

Carrier selective contact layers are widely used in various high efficiency solar cells due to their excellent surface passivation quality and efficient carrier extraction capability [146]. These carrier selective contact layers may also be used as an alternative of doped poly-Si layer in TOPCon structure, followed by a comparative study in the device level. Besides, improvement in the blue response in both-sided TOPCon solar cells may be realized by using wider band gap carrier selective contact layer instead of doped poly-Si layer. Nevertheless, the application of carrier selective contact layer to fabricate high efficiency TOPCon solar cells needs some cautious measures. Firstly, selection of suitable carrier selective contact layers is the first and foremost step. According to Feldmann et al., metal oxides with low work function may serve the purpose of contact layers to n-TOPCon where as dopant free high work function metal oxides such as MoO<sub>x</sub>, WO<sub>x</sub> may be used as contact layers to p-TOPCon [20]. Secondly, use of these transition metal oxides must provide excellent surface passivation quality, minimum contact resistivity and high thermal stability. Thirdly, suitable deposition method has to be adapted so that the uniformity and integrity of ultra-thin oxide layers do not get altered. Fourthly, optimization of metallization process may be required as the thermal stability of carrier selective metal oxides is not same as the doped poly-Si layer. Insertion of a capping layer such as SiN<sub>x</sub> may also be done prior to the metallization process to protect the carrier selective layer.

#### D. Incorporating TOPCon structure into PERC solar cells

In Ref. [107] we have seen how improvement in the efficiency potential may be realized by implementing TOPCon structures into industrial scalable p-PERC solar cells (based on CZ Si wafers). Specifically, simulation study revealed that the TOPCon upgraded solar cells demonstrated lower contact recombination losses compared to standard p-PERC solar cells. However, enhanced optical losses due to parasitic absorption of light by doped poly-Si layer partially compensated the electrical gains and hence a total efficiency gain of below 1% was realized. Still, the authors pointed out that the power output density of both conventional p-PERC solar cells and TOPCon upgraded p-PERC solar cells may be maximized by three ways: (i) reducing the width of the metallic fingers to minimize the carrier recombination losses at metal/semiconductor interfaces; (ii) improving the quality of phosphorous diffused front emitter to reduce the emitter recombination losses; and (iii) enhancing the minority carrier lifetime at the bulk by using high quality CZ c-Si wafers.

On the other hand, Mack et al. recently reported that a conversion efficiency of 21.2% was achieved with an active cell area was 244.32 cm<sup>2</sup> by introducing p-TOPCon structure instead of AlO<sub>x</sub> passivating layer at the rear side of the p-PERC solar cells [147]. However, the authors raised their concerns into some specific domains: (i) complex process sequence as the surface passivating quality of doped poly-Si layer depends upon the surface morphology of c-Si wafers; (ii) requirement of additional hydrogenation step such as implementation of sacrificial SiN<sub>x</sub>:H layer to regain the loss of hydrogen contents of the TOPCon structure during several processing steps; (iii) the doping concentration of boron within the poly-silicon layer is not kept very high to minimize the defect states and free carrier absorption; this may result in obtaining insufficient field to channelize the carriers efficiently through ultra-thin oxide layer; (iv) requirement of optimized metallization pastes to avoid the use of thicker poly-silicon layer (in this study the optimized thickness was 240 nm) because the use of thicker poly-Si layer helps to minimize the contact resistivity at a cost of increased free carrier absorbance; (v) necessity to address the throughput issue of doped poly-Si layer fabrication; and (vi) unavailability of required hardware set up to operate at full loads with homogeneous deposition. Nevertheless, the authors pointed out that some of these above mentioned worries may be overcome by providing some additional effort such as finding out the alternative metallization process or using p<sup>+</sup> polysilicon layer as rear emitter in n-type cells.

### 13. Conclusion

In essence, we may conclude that the merits and demerits of TOPCon solar cells have been explored by various researchers since its discovery. Simplified fabrication process, abundance of the raw material and higher power conversion efficiency are the major advantages of TOPCon solar cells. Till now, the highest reported efficiency has been 25.8% ( $V_{oc} = 725$  mV,  $J_{sc} = 42.5$  mA/cm<sup>2</sup> and FF = 83.3%) which is very close to theoretical efficiency limit as evaluated by Shockley-Queisser for a single junction crystalline silicon based solar cells. In addition, large area solar cells and modules have also been fabricated with higher power output than the present market dominating PERC solar modules. Concurrently, various industries have also developed bifacial TOPCon solar cells and modules where the highest reported front side conversion efficiency has been as high as 25.4%. Therefore, one can easily understand the importance of TOPCon solar cells in the PV industry. However, certain areas such as fabrication of thin TOPCon solar cells and enhancement of the reflection of the evanescent light from the back side of the cells by incorporating suitable interfacial layer in between doped poly-Si layer and rear side metallic (Ag) contact, impact of using metal oxide based carrier selective contact layer as an alternative of doped poly-Si layer, and simplification of the processing steps of the fabrication of TOPCon upgraded PERC solar cells need to be investigated.

### Declaration of Competing Interest

The authors declare the following financial interests/personal relationships which may be considered as potential competing interests:

Dr. Sumita Mukhopadhyay reports financial support was provided by MNRE, Govt. of India

### Acknowledgment

This work has been carried out in DST Solar PV Hub at IIEST Shibpur supported by Department of Science and Technology (DST/TM/CERI/D09(G) Govt. of India. One of the authors, Dibyendu Kumar Ghosh is acknowledging Ministry of New and Renewable Energy (MNRE), India for providing him the research fellowship.

### References

- [1] A.E. Becquerel, Recherches sur les effets de la radiation chimique de la lumiere solaire au moyen des courants electriques, *C. R. Acad. Sci.* 9 (1839) 145–149.
- [2] D.M. Chapin, C.S. Fuller, G.L. Pearson, A new silicon p-n junction photocell for converting solar radiation into electric power, *J. Appl. Phys.* 25 (1954) 676–677, <https://doi.org/10.1063/1.1721711>.
- [3] S.W. Glunz, R. Preu, D. Biro, Crystalline silicon solar cells-state-of-the-art and future developments, *Compr. Renew. Energy Book Chapter* (2012), <https://doi.org/10.1016/B978-0-08-087872-0.00117-7>.
- [4] A. Blakers, Development of the PERC solar cell, *IEEE J. Photovolt.* 9 (3) (2019) 629–635, <https://doi.org/10.1109/JPHOTOV.2019.2899460>.
- [5] J. Liu, Y. Yao, S. Xiao, X. Gu, Review of status developments of high-efficiency crystalline silicon solar cells, *J. Phys. D Appl. Phys.* 51 (2018), <https://doi.org/10.1088/1361-6463/aaac6d> article id: 123001.
- [6] R. Peibst, U. Römer, Y. Larionova, M. Rienäcker, A. Merkle, N. Folchert, S. Reiter, M. Turcu, B. Min, J. Krügener, D. Tetzlaff, E. Bugiel, T. Wietler, R. Brendel, Working principle of carrier selective poly-Si/c-Si junctions: is tunnelling the whole story? *Solar Energy Mater. Solar Cells* 158 (2016) 60–67, <https://doi.org/10.1016/j.solmat.2016.05.045>.
- [7] D. Adachi, J.L. Hernández, K. Yamamoto, Impact of carrier recombination on fill factor for large area heterojunction crystalline silicon solar cell with 25.1% efficiency, *Appl. Phys. Lett.* 107 (2015), <https://doi.org/10.1063/1.4937224> article id: 233506.
- [8] D.D. Smith, G. Reich, M. Baldrias, M. Reich, N. Boitnott, G. Bunea, Silicon solar cells with total area efficiency above 25%, in: *Proceedings of the IEEE 43rd Photovoltaic Specialists Conference (PVSC)*, 2016, pp. 3351–3355, <https://doi.org/10.1109/PVSC.2016.7750287>.
- [9] J. Nakamura, N. Asano, T. Hieda, C. Okamoto, H. Katayama, K. Nakamura, Development of heterojunction back contact Si solar cells, *IEEE J. Photovolt.* 4 (6) (2014) 1491–1495, <https://doi.org/10.1109/JPHOTOV.2014.2358377>.
- [10] K. Masuko, M. Shigematsu, T. Hashiguchi, D. Fujishima, M. Kai, N. Yoshimura, T. Yamanishi, Achievement of more than 25% conversion efficiency with crystalline silicon heterojunction solar cell, *IEEE J. Photovolt.* 4 (6) (2014) 1433–1435, <https://doi.org/10.1109/JPHOTOV.2014.2352151>.
- [11] K. Yoshikawa, H. Kawasaki, W. Yoshida, Silicon heterojunction solar cell with interdigitated back contacts for a photoconversion efficiency over 26%, *Nat. Energy* 2 (2017) 17032, <https://doi.org/10.1038/nenergy.2017.32>, article id.
- [12] K. Yoshikawa, W. Yoshida, T. Irie, H. Kawasaki, K. Konishi, H. Ishibashi, T. Asatani, D. Adachi, M. Kanematsu, H. Uzo, K. Yamamoto, Exceeding conversion efficiency of 26% by heterojunction interdigitated back contact solar cell with thin film Si technology, *Sol. Energy Mater. Sol. Cells* 173 (2017) 37–42, <https://doi.org/10.1016/j.solmat.2017.06.024>.
- [13] LONGi's Heterojunction Cell Efficiency Jumps To 26.30% Within A Week 29 (2021). <https://taiyangnews.info/technology/26-30-efficiency-for-longis-hjt-solar-cell/>.
- [14] <https://www.prnewswire.com/in/news-releases/longi-solar-sets-new-bifacial-mono-perc-solar-cell-world-record-at-24-06-percent-875820879.html>, "LONGi Solar sets new bifacial mono-PERC solar cell world record at 24.06 percent", 16 Jan, 2019.
- [15] A. Richter, J. Benick, F. Feldmann, A. Fell, M. Hermle, S.W. Glunz, n-Type Si solar cells with passivating electron contact: identifying sources for efficiency limitations by wafer thickness and resistivity variation, *Sol. Energy Mater. Sol. Cells* 173 (2017) 96–105, <https://doi.org/10.1016/j.solmat.2017.05.042>.
- [16] R. Goslich, 26.1 % record efficiency for p-type crystalline Si solar cells" by ISFH. <https://idw-online.de/de/news/688784>.
- [17] R. Peibst, M. Rienäcker, Y. Larionova, N. Folchert, F. Haase, C. Holleman, S. Wolter, J. Krügener, P. Bayerl, J. Bayer, M. Dzinnik, R.J. Haug, R. Brendel, Towards 28 %-efficient Si single-junction solar cells with better passivating POLO junctions and photonic crystals, *Sol. Energy Mater. Sol. Cells* 238 (2022), 111560, <https://doi.org/10.1016/j.solmat.2021.111560>.
- [18] High efficiency n-type cell technology: Development and prospects 15 (2021). <http://www.infolink-group.com/en/solar/analysis-trends/n-type-high-efficiency-cell-technology-development-and-prospect>. September.
- [19] International Technology Roadmap for Photovoltaic (ITRPV), Twelfth Edition, April 2021, <https://itrpv.vdma.org/web/itrpv/download>.

- [20] F. Feldmann, M. Bivour, C. Reichel, M. Hermle, S.W. Glunz, A passivated rear contact for high-efficiency n-type silicon solar cells enabling high VocS and FF>82%, in: Proceedings of the 28th European PV Solar Energy Conference and Exhibition, Paris, France, 2013, <https://doi.org/10.4229/28thEUPVSEC2013-2CO.4.4>, 30 September–4 October.
- [21] S.W. Glunz, F. Feldmann, A. Richter, M. Bivour, C. Reichel, H. Steinkemper, J. Benick, M. Hermle, The irresistible charm of a simple current flow pattern-25% with a solar cell featuring a full-area back contact, in: Proceedings of the 31st European Photovoltaic Solar Energy Conference and Exhibition, Hamburg, 2015, <https://doi.org/10.4229/EUPVSEC20152015-2BP.1.1>, September 2015.
- [22] Jolywood unveils 700 W TOPCon PV module 8 (2021). October.
- [23] Longi claims 25.19% efficiency for p-type TOPCon solar cell 21 (2021). <https://www.pv-magazine.com/2021/07/21/longi-claims-25-19-efficiency-for-p-type-topcon-solar-cell/>. July.
- [24] Longi unveils new 25.19% efficiency panel in p-type TOPCon cell panel 23 (2021). <http://agentfactor.net/solar-news-july-23rd-2021/>. July.
- [25] M. Hermle, F. Feldmann, J. Eisenlohr, J. Benick, A. Richter, B. Lee, P. Stradins, A. Rohatgi, S.W. Glunz, Approaching efficiencies above 25% with both sides-contacted silicon solar cells, in: Proceedings of the IEEE 42nd Photovoltaic Specialist Conference (PVSC), New Orleans, LA, 2015, pp. 1–3, <https://doi.org/10.1109/PVSC.2015.7356219>.
- [26] F. Feldmann, M. Simon, M. Bivour, C. Reichel, M. Hermle, S.W. Glunz, Efficient carrier-selective p- and n-contacts for Si solar cells, *Solar Energy Mater. Solar Cells* 131 (2014) 100–104, <https://doi.org/10.1016/j.solmat.2014.05.039>.
- [27] F. Feldmann, K-U Ritzau, M. Bivour, A. Moldovan, S. Modi, J. Templer, M. Hermle, S.W. Glunz, High and low work function materials for passivated contacts, in: Proceedings of the 5th International Conference on Silicon Photovoltaics, SiliconPV 2015, Energy Procedia 77, 2015, pp. 263–270, <https://doi.org/10.1016/j.egypro.2015.07.037>.
- [28] K. Tao, S. Jiang, R. Jia, Y. Zhou, P. Zhang, X. Dai, H. Sun, Z. Jin, X. Liu, The impact of indium tin oxide deposition and post annealing on the passivation property of TOPCon solar cells, *Sol. Energy* 176 (2018) 241–247, <https://doi.org/10.1016/j.solener.2018.10.034>.
- [29] M. Lozac'h, S. Nunomura, K. Matsubara, Double-sided TOPCon solar cells on textured wafer with ALD SiO<sub>x</sub> layer, *Sol. Energy Mater. Sol. Cells* 207 (2020), 110357, <https://doi.org/10.1016/j.solmat.2019.110357>.
- [30] M. Lozac'h, S. Nunomura, Role of silicon surface, polished <100> and <111> or textured, on the efficiency of double-sided TOPCon solar cells, *Prog. Photovolt. Res. Appl.* (2020), <https://doi.org/10.1002/pip.3304>.
- [31] A. Richter, J. Benick, R. Müller, F. Feldmann, C. Reichel, M. Hermle, S.W. Glunz, Tunnel oxide passivating electron contacts as full-area rear emitter of high-efficiency p-type silicon solar cells, *Prog. Photovolt. Res. Appl.* 26 (8) (2017) 579–586, <https://doi.org/10.1002/pip.2960>.
- [32] T. Gao, Q. Yang, X. Guo, Y. Huang, Z. Zhang, Z. Wang, M. Liao, C. Shou, Y. Zeng, B. Yan, G. Hou, X. Zhang, Y. Zhao, J. Ye, An industrially viable TOPCon structure with both ultra-thin SiO<sub>x</sub> and n<sup>+</sup>-poly-Si processed by PECDV for p-type c-Si solar cells, *Sol. Energy Mater. Sol. Cells* 200 (2019), 109926, <https://doi.org/10.1016/j.solmat.2019.109926> article id.
- [33] A. Richter, R. Müller, J. Benick, F. Feldmann, B. Steinhauser, C. Reichel, A. Fell, M. Bivour, M. Hermle, S.W. Glunz, Design rules for high-efficiency both-sides contacted silicon solar cells with balanced charge carrier transport and recombination losses, *Nat. Energy* 6 (4) (2021) 429–438, <https://doi.org/10.1038/s41560-021-00805-w>.
- [34] A. Moldovan, F. Feldmann, G. Krugel, M. Zimmer, J. Rentsch, M. Hermle, A Roth Fölsch, K. Kaufmann, C. Hagendorf, Simple cleaning and conditioning of silicon surfaces with UV/ozone sources, in: Proceedings of the 4th International Conference on Silicon Photovoltaics, SiliconPV 2014, Energy Procedia 55, 2014, pp. 834–844, <https://doi.org/10.1016/j.egypro.2014.08.067>.
- [35] A. Moldovan, F. Feldmann, K. Kaufmann, S. Richter, M. Wemer, C. Hagendorf, M. Zimmer, J. Rentsch, M. Hermle, Tunnel oxide passivated carrier-selective contacts based on ultra-thin SiO<sub>2</sub> layers grown by photo-oxidation or wet-chemical oxidation in ozonized water, in: Proceedings of the IEEE 42nd Photovoltaic Specialist Conference (PVSC), New Orleans, LA, 2015, pp. 1–6, <https://doi.org/10.1109/PVSC.2015.7356144>.
- [36] A. Moldovan, F. Feldmann, M. Zimmer, J. Rentsch, J. Benick, M. Hermle, Tunnel oxide passivated carrier-selective contacts based on ultra thin SiO<sub>2</sub> layers, *Solar Energy Mater. Solar Cells* 142 (2015) 123–127, <https://doi.org/10.1016/j.solmat.2015.06.048>.
- [37] H. Tong, M. Liao, Z. Zhang, Y. Wan, D. Wang, C. Quan, L. Cai, P. Gao, W. Guo, H. Lin, C. Shou, Y. Zeng, B. Yan, J. Ye, A strong-oxidizing mixed acid derived high-quality silicon oxide tunneling layer for polysilicon passivated contact silicon solar cell, *Sol. Energy Mater. Sol. Cells* 188 (2018) 149–155, <https://doi.org/10.1016/j.solmat.2018.09.001>.
- [38] Y. Huang, M. Liao, Z. Wang, X. Guo, C. Jiang, Q. Yang, Z. Yuan, D. Huang, J. Yang, X. Zhang, Q. Wang, H. Jin, M. Al-Jassim, C. Shou, Y. Zeng, B. Yan, J. Ye, Ultrathin silicon oxide prepared by in-line plasma-assisted N<sub>2</sub>O oxidation (PANO) and the application for n-type polysilicon passivated contact, *Sol. Energy Mater. Sol. Cells* 208 (2020), 110389, <https://doi.org/10.1016/j.solmat.2019.110389> article id.
- [39] X. Guo, M. Liao, Z. Rui, Q. Yang, Z. Wang, C. Shou, W. Ding, X. Luo, Y. Cao, J. Xu, L. Fu, Y. Zeng, B. Yan, J. Ye, Comparison of different types of interfacial oxides on hole-selective p<sup>+</sup>-poly-Si passivated contacts for high-efficiency c-Si solar cells, *Solar Energy Mater. Solar Cells* 210 (2020), 110487, <https://doi.org/10.1016/j.solmat.2020.110487>.
- [40] N.C. Mandal, S. Biswas, S. Acharya, T. Panda, S. Sadhukhan, J.R. Sharma, A. Nandi, S. Bose, A. Kole, G. Das, S. Maity, P. Chaudhuri, H. Saha, Study of the properties of SiO<sub>x</sub> layers prepared by different techniques for rear side passivation in TOPCon solar cells, *Mater. Sci. Semicond. Process.* 119 (2020), 105163, <https://doi.org/10.1016/j.jmssp.2020.105163>.
- [41] M. Lozac'h, S. Nunomura, H. Sai, K. Matsubara, Passivation property of ultrathin SiO<sub>x</sub>/h-a-Si:H stack layers for solar cell applications, *Sol. Energy Mater. Sol. Cells* 185 (2018) 8–15, <https://doi.org/10.1016/j.solmat.2018.05.004>.
- [42] S. Richter, K. Kaufmann, V. Naumann, M. Werner, A. Graff, S. Großer, A. Moldovan, M. Zimmer, J. Rentsch, J. Bagdahn, C. Hagendorf, High-resolution structural investigation of passivated interfaces of silicon solar cells, *Solar Energy Mater. Solar Cells* 142 (2015) 128–133, <https://doi.org/10.1016/j.solmat.2015.06.051>.
- [43] Q. Wang, W. Wu, N. Yuan, Y. Li, Y. Zhang, J. Ding, Influence of SiO<sub>x</sub> film thickness on electrical performance and efficiency of TOPCon solar cells, *Solar Energy Mater. Solar Cells* 208 (2020), 110423, <https://doi.org/10.1016/j.solmat.2020.110423>.
- [44] H. Kim, S. Bae, K.S. Ji, S.M. Kim, J.W. Yang, C.H. Lee, K.D. Lee, S. Kim, Y. Kang, H. S. Lee, D. Kim, Passivation properties of tunnel oxide layer in passivated contact silicon solar cells, *Appl. Surf. Sci.* 409 (2017) 140–148, <https://doi.org/10.1016/j.apsusc.2017.02.195>.
- [45] F. Feldmann, G. Nogay, P. Löper, D.L. Young, B.G. Lee, P. Stradins, M. Hermle, S. W. Glunz, Charge carrier transport mechanisms of passivating contacts studied by temperature-dependent J-V measurements, *Sol. Energy Mater. Sol. Cells* 178 (2018) 15–19, <https://doi.org/10.1016/j.solmat.2018.01.008>.
- [46] J.H. Baek, M.J. Jeong, W. Hu, H.S. Chang, Passivation improvement of nitric acid oxide by ozone post-treatment for tunnel oxide passivated contacts silicon solar cells, *Appl. Surf. Sci.* 489 (2019) 330–335, <https://doi.org/10.1016/j.apsusc.2019.05.369>.
- [47] K. Lancaster, S. Großer, F. Feldmann, V. Naumann, C. Hagendorf, Study of pinhole conductivity at passivated carrier-selected contacts of silicon solar cells, in: Proceedings of the 6th International Conference on Silicon Photovoltaics, SiliconPV 2016, Energy Procedia 92, 2016, pp. 116–121, <https://doi.org/10.1016/j.egypro.2016.07.040>.
- [48] S. Choi, K.H. Min, M.S. Jeong, J.I. Lee, M.G. Kang, H-E Song, Y. Kang, H.S. Lee, D. Kim, K.H. Kim, Structural evolution of tunneling oxide passivating contact upon thermal annealing, *Sci. Rep.* 7 (12853) (2017), <https://doi.org/10.1038/s41598-017-13180-y> article no.
- [49] D. Tetzlaff, J. Krügener, Y. Larionova, S. Reiter, M. Turcu, F. Haase, R. Brendel, R. Peibst, U. Höhne, J.D. Kähler, T.F. Wietler, A simple method for pinhole detection in carrier selective POLO-junctions for high efficiency silicon solar cells, *Sol. Energy Mater. Sol. Cells* 173 (2017) 106–110, <https://doi.org/10.1016/j.solmat.2017.05.041>.
- [50] T.F. Wietler, D. Tetzlaff, J. Krügener, M. Rienäcker, F. Haase, Y. Larionova, R. Brendel, R. Peibst, Pinhole density and contact resistivity of carrier selective junctions with polycrystalline silicon on oxide, *Appl. Phys. Lett.* 110 (2017) 461–466, <https://doi.org/10.1063/1.4986924>.
- [51] R. Peibst, U. Römer, K.R. Hofmann, B. Lim, T.F. Wietler, J. Krügener, N.P. Harder, R. Brendel, A simple model describing the symmetric I-V characteristics of p polycrystalline Si/n monocrystalline Si, and n polycrystalline Si/p monocrystalline Si junctions, *IEEE J. Photovolt.* 4 (3) (2014) 841–850, <https://doi.org/10.1109/JPHOTOV.2014.2310740>.
- [52] F. Feldmann, G. Nogay, J. Polzin, B. Steinhauser, A. Richter, A. Fell, A study on the charge carrier transport of passivating contacts, *IEEE J. Photovolt.* 8 (6) (2018) 1503–1509, <https://doi.org/10.1109/JPHOTOV.2018.2870735>.
- [53] R. Brendel, R. Peibst, Contact selectivity and efficiency in crystalline silicon photovoltaics, *IEEE J. Photovolt.* 6 (6) (2016) 1413–1420, <https://doi.org/10.1109/JPHOTOV.2016.2598267>. Nov.
- [54] M. Rienäcker, M. Bossmeyer, A. Merkle, U. Römer, F. Haase, J. Krügener, R. Brendel, R. Peibst, Junction resistivity of carrier-selective polysilicon on oxide junctions and its impact on solar cell performance, *IEEE J. Photovolt.* 7 (1) (2017) 11–18, <https://doi.org/10.1109/JPHOTOV.2016.2614123>. Jan.
- [55] N. Folchert, M. Rienäcker, A.A. Yeo, B. Min, R. Peibst, R. Brendel, Temperature-dependent contact resistance of carrier selective poly-Si on oxide junctions, *Sol. Energy Mater. Sol. Cells* 185 (2018) 425–430, <https://doi.org/10.1016/j.solmat.2018.05.046>.
- [56] A. Campa, F. Smole, N. Folchert, T. Wietler, B. Min, R. Brendel, M. Topić, Detailed analysis and understanding of the transport mechanism of poly-Si-based carrier selective junctions, *IEEE J. Photovolt.* 9 (6) (2019) 1575–1582, <https://doi.org/10.1109/JPHOTOV.2019.2943610>. Nov.
- [57] L. Galleni, M. Firt, H. Sivaramakrishnan Radhakrishnan, F. Duerinckx, L. Tous, J. Poortmans, Mechanisms of charge carrier transport in polycrystalline silicon passivating contacts, *Sol. Energy Mater. Sol. Cells* 232 (2021), 111359, <https://doi.org/10.1016/j.solmat.2021.111359>.
- [58] Z. Yang, Z. Liu, M. Cui, J. Sheng, L. Chen, L. Lu, W. Guo, X. Yang, Y. Zhao, W. Yang, J.C. Greer, Y. Zeng, B. Yan, J. Ye, Charge-carrier dynamics for silicon oxide tunneling junctions mediated by local pinholes, *Cell Rep. Phys. Sci.* 2 (12) (2021), 100667, <https://doi.org/10.1016/j.xcrp.2021.100667>.
- [59] Z. Zhang, Y. Zeng, C.S. Jiang, Y. Huang, M. Liao, H. Tong, M. Al-Jassim, P. Gao, C. Shou, X. Zhou, B. Yan, J. Ye, Carrier transport through the ultrathin silicon-oxide layer in tunnel oxide passivated contact (TOPCon) c-Si solar cells, *Sol. Energy Mater. Sol. Cells* 187 (2018) 113–122, <https://doi.org/10.1016/j.solmat.2018.07.025>.
- [60] F. Feldmann, R. Müller, C. Reichel, M. Hermle, Ion implantation into amorphous Si layers to form carrier-selective contacts for Si solar cells, *Phys. Status Solidi RRL* 8 (9) (2014) 767–770, <https://doi.org/10.1002/pssr.201409312>.
- [61] C. Reichel, F. Feldmann, R. Müller, A. Moldovan, M. Hermle, S.W. Glunz, Interdigitated back contact silicon solar cells with tunnel oxide passivated

- contacts formed by ion implantation", in: Proceedings of the 29th European PV Solar Energy Conference and Exhibition, Amsterdam, The Netherlands, 2014, pp. 22–26, <https://doi.org/10.4229/EUPVSEC2014-2CO.1.1>. September.
- [62] C. Reichel, F. Feldmann, R. Müller, R.C. Reedy, B.G. Lee, D.L. Young, P. Stradins, M. Hermle, S.W. Glunz, Tunnel oxide passivated contacts formed by ion implantation for applications in silicon solar cells, *J. Appl. Phys.* 118 (1–9) (2015), 205701, <https://doi.org/10.1063/1.4936223>.
- [63] F. Feldmann, C. Reichel, R. Müller, M. Hermle, The application of poly-Si/SiO<sub>x</sub> contacts as passivated top/rear contacts in Si solar cells, *Solar Energy Mater. Solar Cells* 159 (2017) 265–271, <https://doi.org/10.1016/j.solmat.2016.09.015>.
- [64] B. Steinhäuser, J.I. Polzin, F. Feldmann, M. Hermle, S.W. Glunz, Excellent surface passivation quality on crystalline silicon using industrial-scale direct-plasma TOPCon deposition technology, *Sol. RRL* (2018), 1800068, <https://doi.org/10.1002/solr.201800068>.
- [65] J.I. Polzin, F. Feldmann, B. Steinhäuser, M. Hermle, S. Glunz, Realization of TOPCon using industrial scale PECDV equipment, in: Proceedings of the AIP Conference Proceedings1999, 2018, 040018, <https://doi.org/10.1063/1.5049281>.
- [66] Q. Yang, M. Liao, Z. Wang, J. Zheng, Y. lin, X. Guo, Z. Rui, D. Huang, L. Lu, M. Feng, P. Cheng, C. Shou, Y. Zeng, B. Yan, J. Ye, *In-situ* phosphorus-doped polysilicon prepared using rapid-thermal anneal (RTA) and its application for polysilicon passivated-contact solar cells, *Solar Energy Mater. Solar Cells* 210 (2020), 110518, <https://doi.org/10.1016/j.solmat.2020.110518>.
- [67] A. Merkle, S. Seren, H. Knauss, B. Min, J. Steffens, B. Terheiden, Atmospheric pressure chemical vapor deposition of *in-situ* doped amorphous silicon layers for passivating contacts, in: Proceedings of the 35th European Photovoltaic Solar Energy Conference and Exhibition Brussels, Belgium, 2018, pp. 785–791, <https://doi.org/10.4229/35thEUPVSEC20182018-2DV.3.49>.
- [68] J.F. Mousumi, G. Gregory, J.P. Ganesan, C. Nunez, K. Provancha, S. Seren, H. Zunft, T. Jurca, P. Banerjee, A. Kar, R. Kumar, K.O. Davis, Process–structure–properties relationships of passivating, electron-selective contacts formed by atmospheric pressure chemical vapor deposition of phosphorus-doped polysilicon, *Phys. Status Solidi (RRL)-Rapid Res. Lett.* (2022), 2100639, <https://doi.org/10.1002/pssr.202100639>.
- [69] D. Yan, A. Cuevas, S.P. Phang, Y. Wan, D. Macdonald, 23% efficient p-type crystalline silicon solar cells with hole-selective passivating contacts based on physical vapor deposition of doped silicon films, *Appl. Phys. Lett.* 113 (6) (2018), 061603, <https://doi.org/10.1063/1.5037610>.
- [70] L. Nasebandt, S. Hübner, B. Min, C. Hollemann, T. Dippell, P. Wohlfart, R. Peibst, R. Brendel, Fired-only passivating poly-Si on oxide contacts with dc-sputtered *in-situ* phosphorous-doped silicon layers", in: Proceedings of the 37th European Photovoltaic Solar Energy Conference and Exhibition, 2020, pp. 184–187.
- [71] S. Masuda, K. Gotoh, I. Takahashi, K. Nakamura, Y. Ohshita, N. Usami, Impact of boron incorporation on properties of silicon solar cells employing p-type polycrystalline silicon grown by aluminum-induced crystallization, *Jpn. J. Appl. Phys.* 57 (2018), <https://doi.org/10.7567/JJAP.57.08RB12>, 08RB12.
- [72] G.C. Wilkes, A.D. Upadhyaya, A. Rohatgi, M.C. Gupta, Laser crystallization and dopant activation of a-Si:H carrier-selective layer in TOPCon Si solar cells, *IEEE J. Photovolt.* 10 (5) (2020) 1283–1289, <https://doi.org/10.1109/JPHOTOV.2020.3006273>.
- [73] B. Nemeth, D. Young, M. Page, V. LaSalvia, S. Johnston, R. Reedy, P. Stradins, Polycrystalline silicon passivated tunneling contacts for high efficiency silicon solar cells, *J. Mater. Res.* 31 (6) (2016) 671–681, <https://doi.org/10.1557/jmr.2016.77>.
- [74] G. Nogay, J. Stuckelberger, P. Wyss, E. Rucavado, C. Allebé, T. Koida, M. Morales-Masis, M. Despeisse, F-J Haug, P. Löper, C. Ballif, Interplay of annealing temperature and doping in hole selective rear contacts based on silicon-rich silicon-carbide thin films, *Sol. Energy Mater. Sol. Cells* 173 (2017) 18–24, <https://doi.org/10.1016/j.solmat.2017.06.039>.
- [75] Q. Li, K. Tao, Y. Sun, R. Jia, S.M. Wang, Z. Jin, X.Y. Liu, Replacing the amorphous silicon thin layer with microcrystalline silicon thin layer in TOPCon solar cells, *Solar Energy* 135 (2016) 487–492, <https://doi.org/10.1016/j.solener.2016.06.012>.
- [76] K. Tao, Q. Li, C. Hou, S. Jiang, J. Wang, R. Jia, Y. Sun, Y. Li, Z. Jin, X. Liu, Application of a-Si/ $\mu$ -Si hybrid layer in tunnel oxide passivated contact n-type silicon solar cells, *Sol. Energy* 144 (2017) 735–739, <https://doi.org/10.1016/j.solener.2017.01.061>.
- [77] S. Choi, O. Kwon, K.H. Min, M.S. Jeong, K.T. Jeong, M. Kang, S. Park, K.K. Hong, H. Song, K. Kim, Formation and suppression of hydrogen blisters in tunnelling oxide passivating contact for crystalline silicon solar cells, *Sci. Rep.* (2020), <https://doi.org/10.1038/s41598-020-66801-4>.
- [78] Y. Lin, Z. Yang, Z. Liu, J. Zheng, M. Feng, Y. Zhi, L. Lu, M. Liao, W. Liu, D. Ma, Q. Han, H. Cheng, Q. Zeng, Z. Yuan, B. Yan, Y. Zeng, J. Ye, Dual-functional carbon-doped polysilicon films for passivating contact solar cells: regulating physical contacts while promoting photoelectrical properties, *Energy Environ. Sci.* 14 (2021) 6406–6418, <https://doi.org/10.1039/DIEE02011K>.
- [79] J. Zheng, Z. Yang, L. Lu, M. Feng, Y. Zhi, Y. Lin, M. Liao, Y. Zeng, B. Yan, J. Ye, Blistering-free polycrystalline silicon carbide films for double-sided passivating contact solar cells, *Sol. Energy Mater. Sol. Cells* 238 (2022), 111586, <https://doi.org/10.1016/j.solmat.2022.111586>.
- [80] F. Feldmann, M. Nicolai, R. Müller, C. Reichel, M. Hermle, Optical and electrical characterization of poly-Si/SiO<sub>x</sub> contacts and their implications on solar cell design, in: Proceedings of the 7th International Conference on Silicon Photovoltaics 124, 2017, pp. 31–37, <https://doi.org/10.1016/j.egypro.2017.09.336>. Silicon PV, 2017, Energy Procedia.
- [81] H. Park, H. Park, S.J. Park, S. Bae, H. Kim, J.W. Yang, J.Y. Hyun, C.H. Lee, S. H. Shin, Y. Kang, H.S. Lee, D. Kim, Passivation quality control in poly-Si/SiO<sub>x</sub>/c-Si passivated contact solar cells with 734 mV implied open circuit voltage, *Sol. Energy Mater. Sol. Cells* 189 (2019) 21–26, <https://doi.org/10.1016/j.solmat.2018.09.013>.
- [82] S. Chowdhury, G. Chavan, S. Kim, D. Oh, Y. Kim, E.C. Cho, Y. Cho, J. Yi, Analysis of passivation property using thin Al<sub>2</sub>O<sub>3</sub> layer and simulation for realization of high-efficiency TOPCon cell, *Infrared Phys. Technol.* (2020), <https://doi.org/10.1016/j.infrared.2020.103436>.
- [83] Z. Zhang, M. Liao, Y. Huang, X. Guo, Q. Yang, Z. Wang, T. Gao, C. Shou, Y. Zeng, B. Yan, J. Ye, Improvement of surface passivation of tunnel oxide passivated contact structure by thermal annealing in mixture of water vapor and nitrogen environment, *Sol. RRL* (2019), 1900105, <https://doi.org/10.1002/solr.201900105>.
- [84] Z. Zhang, Y. Zeng, Y. Huang, X. Guo, Z. Wang, Q. Yang, C. Shou, B. Yan, J. Ye, Improvement of passivating quality by post-crystallization treatments with different methods for high quality tunnel oxide passivated contact c-Si solar cells, in: Proceedings of the IEEE 46th Photovoltaic Specialists Conference (PVSC), Chicago, IL, USA, 2019, pp. 2215–2218, <https://doi.org/10.1109/PVSC40753.2019.8980516>.
- [85] P. Padhamnath, J. Wong, B. Nagarajan, J.K. Buatis, L.M. Ortega, N. Nandakumar, A. Khanna, V. Shanmugam, S. Duttagupta, Metal contact recombination in monoPoly™ solar cells with screen-printed & fire-through contacts, *Sol. Energy Mater. Sol. Cells* 192 (2019) 109–116, <https://doi.org/10.1016/j.solmat.2018.12.026>.
- [86] N. Nandakumar, J. Rodriguez, T. Kluge, T. Große, L. Fondop, P. Padhamnath, N. Balaji, M. König, S. Duttagupta, Approaching 23% with large-area monoPoly cells using screen-printed and fired rear passivating contacts fabricated by inline PECDV, *Prog. Photovolt. Res. Appl.* 27 (2019) 107–112, <https://doi.org/10.1002/pip.3097>.
- [87] J.I. Polzin, B. Hammann, T. Niewelt, W. Kwapił, M. Hermle, F. Feldmann, Thermal activation of hydrogen for defect passivation in poly-Si based passivating contacts, *Sol. Energy Mater. Sol. Cells* 230 (2021), 111267, <https://doi.org/10.1016/j.solmat.2021.111267> article id.
- [88] B. Steinhäuser, T. Niewelt, A. Richter, R. Eberle, J. Polzin, F. Feldmann, M. C. Schubert, M. Hermle, Life(time) at the limits – very high lifetimes in crystalline silicon measured by photoconductance and photoluminescence, in: Proceedings of the 38th European Photovoltaic Solar Energy Conference and Exhibition, 2021.
- [89] R. Peibst, Y. Larionova, S. Reiter, M. Turcu, R. Brendel, D. Tetzlaff, J. Krügener, T. Wietler, U. Höhne, J.D. Kähler, H. Mehlich, S. Frigge, Implementation of N<sup>+</sup> and P<sup>+</sup> polo junctions on front and rear side of souble-side contacted industrial silicon solar cells", in: Proceedings of the 32nd European Photovoltaic Solar Energy Conference and Exhibition, 2016, pp. 323–327, <https://doi.org/10.4229/EUPVSEC20162016-2BO.3.2>.
- [90] L. Tutsch, F. Feldmann, M. Bivour, W. Wolke, M. Hermle, J. Rentsch, Integrating transparent conductive oxides to improve the infrared response of silicon solar cells with passivating rear contacts, in: Proceedings of the AIP Conference Proceedings1999, 2018, 040023, <https://doi.org/10.1063/1.5049286>.
- [91] B. Grübel, G. Cimotti, V. Arya, T. Fellmeth, F. Feldmann, B. Steinhäuser, S. Kluska, T. Kluge, D. Landgraf, M. Glathhaar, Plated Ni/Cu/Ag for TOPCon solar cell metallization", in: Proceedings of the 36th European PV Solar Energy Conference and Exhibition, Marseille, France, 2019, 9–13 September.
- [92] J. Eisenlohr, B.G. Lee, J. Benick, F. Feldmann, M. Drießen, N. Milenkovic, B. Bläsi, J.C. Goldschmidt, M. Hermle, Rear side sphere gratings for improved light trapping in crystalline silicon single junction and silicon-based tandem solar cells, *Solar Energy Mater. Solar Cells* 142 (2015) 60–65, <https://doi.org/10.1016/j.solmat.2015.05.043>.
- [93] S. Reiter, N. Koper, R. Reineke-Koch, Y. Larionova, M. Turcu, J. Krügener, D. Tetzlaff, T. Wietler, U. Höhne, J.D. Kähler, R. Brendel, R. Peibst, Parasitic absorption in polycrystalline Si-layers for carrier-selective front junctions, *Energy Proced.* 92 (2016) 199–204, <https://doi.org/10.1016/j.egypro.2016.07.057>.
- [94] M. Singh, R. Santbergen, L. Mazzarella, A. Madrampazakis, G. Yang, R. Vismara, Z. Remes, A. Weeber, M. Zeman, O. Isabella, Optical characterization of poly-SiO<sub>x</sub> and poly-SiCx carrier-selective passivating contacts, *Sol. Energy Mater. Sol. Cells* 210 (2020), 110507, <https://doi.org/10.1016/j.solmat.2020.110507>.
- [95] Z. Xu, K. Tao, S. Jiang, R. Jia, W. Li, Y. Zhou, Z. Jin, X. Liu, Application of polycrystalline silicon carbide thin films as the passivating contacts for silicon solar cells, *Solar Energy Mater. Solar Cells* 206 (2020), 110329, <https://doi.org/10.1016/j.solmat.2019.110329>.
- [96] F. Feldmann, M. Bivour, C. Reichel, H. Steinkemper, M. Hermle, S.W. Glunz, Tunnel oxide passivated contacts as an alternative to partial rear contacts, *Solar Energy Mater. Solar Cells* 131 (2014) 46–50, <https://doi.org/10.1016/j.solmat.2014.06.015>.
- [97] A. Rohatgi, B. Rounsville, Y.W. Ok, A.M. Tam, F. Zimbardi, A.D. Upadhyaya, Y. Tao, K. Madani, A. Richter, J. Benick, M. Hermle, Fabrication and modeling of high-efficiency front junction N-type silicon solar cells with tunnel oxide passivating back contact, *IEEE J. Photovolt.* 7 (5) (2017) 1236–1243, <https://doi.org/10.1109/JPHOTOV.2017.2715720>.
- [98] C.W. Chen, M. Hermle, J. Benick, Y. Tao, Y.W. Ok, A. Upadhyaya, A.M. Tam, A. Rohatgi, Modeling the potential of screen printed front junction CZ silicon solar cell with tunnel oxide passivated back contact, *Prog. Photovolt. Res. Appl.* (2016), <https://doi.org/10.1002/pip.2809>.
- [99] S. Lindekugel, T. Rachow, N. Milenkovic, A. Richter, J. Benick, S. Janz, S. Reber, Emitters grown by rapid vapour-phase direct doping for high efficiency solar cells", in: Proceedings of the 31st European PV Solar Energy Conference and

- Exhibition, Hamburg, Germany 14–18, 2015, p. 2015, <https://doi.org/10.4229/EUPVSEC2015-2CO.4.5>. September.
- [100] S. Kühnhold-Pospischil, B. Steinhauser, A. Richter, E. Gust, S. Janz, Rapid vapor-phase direct doping for high-efficiency solar cells, *IEEE J. Photovolt.* 8 (6) (2018) 1421–1428, <https://doi.org/10.1109/JPHOTOV.2018.2861713>.
- [101] Y. Zeng, H. Tong, C. Quan, L. Cai, Z. Yang, K. Chen, Z. Yuan, C.H Wu, B. Yan, P. Gao, J. Ye, Theoretical exploration towards high-efficiency tunnel oxide passivated carrier-selective contacts (TOPCon) solar cells, *Sol. Energy* 155 (2017) 654–660, <https://doi.org/10.1016/j.solener.2017.07.014>.
- [102] N. Anand, P. Kale, Optimization of TOPCon structured solar cell using AFORS HET, *Trans. Electr. Electron. Mater.* 22 (2021) 160–166, <https://doi.org/10.1007/s42341-020-0220-0>.
- [103] M. Verma, S. Routray, G.P. Mishra, Extensive study on effect of pinhole induced electric field in Si CS-TOPCon solar cell, in: Proceedings of the 4th IEEE Electron Devices Technology & Manufacturing Conference (EDTM), Penang, Malaysia, 2020, pp. 1–4, <https://doi.org/10.1109/EDTM47692.2020.9117863>.
- [104] S. Mitra, H. Ghosh, H. Saha, K. Ghosh, Recombination analysis of tunnel oxide passivated contact solar cells, *IEEE Trans. Electron Devices* 66 (3) (March 2019) 1368–1376, <https://doi.org/10.1109/TED.2018.2890584>.
- [105] C. Quan, Y. Zeng, D. Wang, M. Liao, H. Tong, Z. Yang, Z. Yuan, P. Gao, B. Yan, K. Chen, J. Ye, Computational analysis of a high-efficiency tunnel oxide passivated contact (TOPCon) solar cell with a low-work-function electron-selective-collection layer, *Sol. Energy* 170 (2018) 780–787, <https://doi.org/10.1016/j.solener.2018.06.008>.
- [106] T. Sugiura, S. Matsumoto, N. Nakano, Numerical analysis of p-type and n-type based carrier-selective contact solar cells with tunneling oxide thickness and bulk properties, *Jpn. J. Appl. Phys.* 59 (2020), <https://doi.org/10.35848/1347-4065/ab6a2c>. SGGF03.
- [107] C. Messmer, A. Fell, F. Feldmann, N. Wöhrlé, J. Schön, M. Hermle, Efficiency roadmap for evolutionary upgrades of PERC solar cells by TOPCon: impact of parasitic absorption, *IEEE J. Photovolt.* 10 (2) (2020) 335–342, <https://doi.org/10.1109/JPHOTOV.2019.2957642>.
- [108] A. Richter, J. Benick, F. Feldmann, A. Fell, B. Steinhauser, N.Tucher J.I.Polzin, J. N. Murthy, M. Hermle, S.W. Glunz, Both sides contacted silicon solar cells: options for approaching 26% efficiency”, in: Proceedings of the 36th European PV Solar Energy Conference and Exhibition, Marseille, France 9–13, 2019, <https://doi.org/10.4229/EUPVSEC20192019-2BP>. September.
- [109] Y. Zeng, Q. Yang, Y. Wan, Z. Yang, M. Liao, Y. Huang, Z. Zhang, X. Guo, Z. Wang, P. Gao, C.H Wu, B. Yan, J. Ye, Numerical exploration for structure design and free-energy loss analysis of the high-efficiency polysilicon passivated-contact p-type silicon solar cell, *Sol. Energy* 178 (2019) 249–256, <https://doi.org/10.1016/j.solener.2018.12.044>.
- [110] P. Zheng, J. Yang, Z. Wang, L. Wu, H. Sun, S. Chen, Y. Guo, H. Xia, S.P. Phang, E. C. Wang, J. Stuckelberger, H.C. Sio, X. Zhang, D. Macdonald, H. Jin, Detailed loss analysis of 24.8% large-area screen-printed n-type solar cell with polysilicon passivating contact, *Cell Rep. Phys. Sci.* 2 (10) (2021) 100603, <https://doi.org/10.1016/j.xrpp.2021.100603> article id.
- [111] Y. Tao, V. Upadhyaya, Y. Huang, C.W. Chen, K. Jones, A. Rohatgi, Carrier selective tunnel oxide passivated contact enabling 21.4% efficient large-area N-type silicon solar cells, in: Proceedings of the 43rd IEEE Photovoltaic Specialists Conf.(PVSC), 2016, <https://doi.org/10.1109/PVSC.2016.7750103>.
- [112] Y. Tao, V. Upadhyaya, C-W Chen, A. Payne, E.L. Chang, A. Upadhyaya, A. Rohatgi, Large area tunnel oxide passivated rear contact n-type Si solar cells with 21.2% efficiency, *Prog. Photovolt. Res. Appl.* 24 (2016) 830–835, <https://doi.org/10.1002/pip.2739>.
- [113] F. Feldmann, B. Steinhauser, V. Arya, A. Büchler, A.A. Brand, S. Kluska, M. Hermle, S.W. Glunz, Evaluation of TOPCon technology on large area solar cells”, in: Proceedings of the 33rd European Photovoltaic Solar Energy Conference and Exhibition, 2017, pp. 465–467, <https://doi.org/10.4229/EUPVSEC2017-2DO.3.3>.
- [114] B. Steinhauser, F. Feldmann, J-I Polzin, L. Tutsch, V. Arya, B. Grübel, A. Fischer, A. Moldovan, J. Benick, A. Richter, A.A. Brand, S. Kluska, M. Hermle, Large area TOPCon technology achieving 23.4% efficiency, in: Proceedings of the IEEE 7th World Conference on Photovoltaic Energy Conversion (WCPEC) (A Joint Conference of 45th IEEE PVSC, 28th PVSEC & 34th EU PVSEC), Waikoloa Village, HI, 2018, pp. 1507–1510, <https://doi.org/10.1109/PVSC.2018.8547683>.
- [115] F. Feldmann, T. Fellmeth, B. Steinhauser, H. Nagel, D. Ourinson, S. Mack, E. Lohmüller, J. Polzin, J. Benick, A. Richter, A. Moldovan, M. Bivour, F. Clement, J. Rentsch, M. Hermle, S.W. Glunz, Large area TOPCon cells realized by a PECVD tube process”, in: Proceedings of the 36th European PV Solar Energy Conference and Exhibition, Marseille, France 9–13, 2019, <https://doi.org/10.4229/EUPVSEC20192019-2EO.1.4>. September.
- [116] Y.Y. Huang, Y.W. Ok, A.D. Upadhyaya, V.D. Upadhyaya, K. Madani, A. Rohatgi, Large area 21.6% efficiency front junction N-type cell with screen printed tunnel oxide passivated poly-Si rear contact, in: Proceedings of the IEEE 46th Photovoltaic Specialists Conference (PVSC), Chicago, IL, USA, 2019, pp. 1120–1123, <https://doi.org/10.1109/PVSC40753.2019.8980527>.
- [117] M.K. Stodolny, M. Lenes, Y. Wu, G.J.M. Janssen, I.G. Romijn, J.R.M. Luchies, L. J. Geerlings, n-Type polysilicon passivating contact for industrial bifacial n-type solar cells, *Sol. Energy Mater. Sol. Cells* 158 (2016) 24–28, <https://doi.org/10.1016/j.solmat.2016.06.034>.
- [118] Y. Chen, D. Chen, C. Liu, Z. Wang, Y. Zou, Y. He, Y. Wang, L. Yuan, J. Gong, W. Lin, X. Zhang, Y. Yang, H. Shen, Z. Feng, P.P. Altermatt, P.J. Verlinden, Mass production of industrial tunnel oxide passivated contacts (i-TOPCon) silicon solar cells with average efficiency over 23% and modules over 345 W, *Prog. Photovolt. Res. Appl.* (2019) 1–8, <https://doi.org/10.1002/pip.3180>.
- [119] W. Wu, J. Bao, L. Ma, C. Chen, R. Liu, Z. Qiao, J. Chen, Z. Liu, Development of industrial n-type bifacial TOPCon solar cells and modules”, in: Proceedings of 36th European Photovoltaic Solar Energy Conference and Exhibition, Marseille, France 9–13, 2019, <https://doi.org/10.4229/EUPVSEC20192019-2BP.1.5>. September.
- [120] D. Chen, Y. Chen, Z. Wang, J. Gong, C. Liu, Y. Zou, Y. He, Y. Wang, L. Yuan, W. Lin, R. Xia, L. Yin, X. Zhang, G. Xu, Y. Yang, H. Shen, Z. Feng, P.P. Altermatt, P.J. Verlinden, 24.58% total area efficiency of screen-printed, large area industrial silicon solar cells with the tunnel oxide passivated contacts (i-TOPCon) design, *Sol. Energy Mater. Sol. Cells* 206 (2020), 110258, <https://doi.org/10.1016/j.solmat.2019.110258>.
- [121] Y. Chen, D. Chen, P.P. Altermatt, G. Xu, Z. Wang, C. Liu, Y. Zou, Y. He, Y. Wang, J. Gong, L. Yuan, W. Liu, Y. Chen, M. Deng, Y. Hu, S. Chen, J. Xiang, H. Shen, S. Zhang, L. Wang, X. Zhang, Y. Yang, Z. Feng, P.J. Verlinden, >25% large-area industrial silicon solar cell: learning from history and future perspective”, in: Proceedings of the 36th European Photovoltaic Solar Energy Conference and Exhibition, Marseille, France, 2019, pp. 9–13. September.
- [122] Y. Zhou, K. Tao, A. Liu, R. Jia, J. Bao, Y. Sun, S. Yang, Q. Wang, Q. Zhang, S. Yang, Y. Cao, H. Qu, The impacts of LPCVD wrap-around on the performance of n-type tunnel oxide passivated contact c-Si solar cell, *Curr. Appl. Phys.* 20 (2020) 911–916, <https://doi.org/10.1016/j.cap.2020.03.021>.
- [123] Y. Zhou, K. Tao, A. Liu, R. Jia, S. Jiang, J. Bao, S. Yang, Y. Cao, H. Qu, Study of boron diffusion for p<sup>+</sup> emitter of large area N-type TOPCon silicon solar cells, *Appl. Phys. A* 126 (9) (2020) 671, <https://doi.org/10.1007/s00339-020-03851-5>, article id.
- [124] Y.Y Huang, Y.W. Ok, K. Madani, W. Choi, A.D. Upadhyaya, V.D. Upadhyaya, A. Rohatgi, Fully screen-printed bifacial large area 22.6% N-type Si solar cell with lightly doped ion-implanted boron emitter and tunnel oxide passivated rear contact, *Solar Energy Mater. Solar Cells* 214 (2020), 110585, <https://doi.org/10.1016/j.solmat.2020.110585>.
- [125] <https://taiyangnews.info/technology/longi-reports-25-09-n-type-topcon-cell-efficiency/>, “LONGI Achieves 25.09% Power Conversion Efficiency For Monocrystalline Bifacial N-Type TOPCON Solar Cell; Germany’s ISFH Confirms”, April 30, 2021.
- [126] <https://www.pv-magazine.com/2021/05/31/jinkosolar-improves-efficiency-of-n-type-monocrystalline-topcon-solar-cell-by-0-35/>, JinkoSolar improves efficiency of n-type monocrystalline TOPCon solar cell by 0.35%, MAY 31, 2021.
- [127] B. Kafle, B.S. Goraya, S. Mack, F. Feldmann, S. Nold, J. Rentsch, TOPCon-technology options for cost efficient industrial manufacturing, *Sol. Energy Mater. Sol. Cells* 227 (2021), 111100, <https://doi.org/10.1016/j.solmat.2021.111100> article id.
- [128] F. Feldmann, B. Steinhauser, T. Pernau, H. Nagel, T. Fellmeth, S. Mack, D. Ourinson, E. Lohmüller, J. Polzin, A. Moldovan, M. Bivour, F. Clement, J. Rentsch, M. Hermle, S.W. Glunz, Industrial TOPCon solar cells realized by a PECVD tube process, in: Proceedings of the 37th European Photovoltaic Solar Energy Conference and Exhibition, 2020, <https://doi.org/10.4229/EUPVSEC2020202-2AO.6.3>.
- [129] <https://www.saurenergy.com/solar-energy-articles/heraeus-advanced-metallization-pastes-for-high-efficiency-solar-cells-using-poly-silicon-passivated-contacts/>, “Heraeus Advanced Metallization Pastes For High Efficiency Solar Cells using Poly-Silicon Passivated Contacts”, September 26th, 2018.
- [130] [https://www.heraeus.com/en/hpt/press\\_media\\_photovoltaics/photovoltaic\\_news\\_2021/sneec\\_2021.html](https://www.heraeus.com/en/hpt/press_media_photovoltaics/photovoltaic_news_2021/sneec_2021.html), “For SNEC 2021, Heraeus Photovoltaics delivers next generation of high-performance, high-efficiency metallization pastes for solar cell manufacturers”.
- [131] Dependence on Silver Could Hamper Terawatt Scale Solar Module Production: Report, Sep 30 2021. <https://mercomindia.com/dependence-on-silver-could-hamper/>.
- [132] F. Schindler, B. Michl, P. Krenckel, S. Riepe, F. Feldmann, J. Benick, W. Warta, M. C. Schubert, Efficiency potential of p- and n-type high performance multicrystalline silicon, in: Proceedings of the 5th International Conference on Silicon Photovoltaics 77, 2015, pp. 633–638. SiliconPV 2015, Energy Procedia.
- [133] F. Schindler, J. SchöN, B. Michl, S. Riepe, P. Krenckel, J. Benick, F. Feldmann, M. Hermle, S.W. Glunz, W. Warta, M.C. Schubert, High efficiency multicrystalline silicon solar cells: potential of n-type doping, in: Proceedings of the IEEE 42nd Photovoltaic Special Conference (PVSC), New Orleans, LA, 2015, pp. 1–3, <https://doi.org/10.1109/PVSC.2015.7355619>.
- [134] S. Riepe, P. Krenckel, F. Schindler, C. Schmid, T. Strauch, J. Benick, M. C. Schubert, Development of multicrystalline silicon for 20% efficient n-type solar cells”, in: Proceeding of the 31st European Photovoltaic Solar Energy Conference and Exhibition, September 2015, Hamburg, 2015.
- [135] F. Schindler, B. Michl, P. Krenckel, S. Riepe, J. Benick, R. Müller, A. Richter, S. W. Glunz, M.C. Schubert, Optimized multicrystalline silicon for solar cells enabling conversion efficiencies of 22%, *Sol. Energy Mater. Sol. Cells* 171 (2017) 180–186, <https://doi.org/10.1016/j.solmat.2017.06.005>.
- [136] F. Schindler, B. Michl, P. Krenckel, S. Riepe, J. Benick, R. Müller, A. Richter, S. W. Glunz, M.C. Schubert, How to achieve efficiencies exceeding 22% with multicrystalline n-type silicon solar cells, in: Proceeding of the 7th International Conference on Silicon Photovoltaics, SiliconPV, 2017,Energy Procedia 124, 2017, pp. 777–780, <https://doi.org/10.1016/j.egypro.2017.09.086>.
- [137] J. Benick, R. Müller, F. Schindler, A. Richter, H. Hauser, F. Feldmann, P. Krenckel, S. Riepe, M.C. Schubert, M. Hermle, S.W. Glunz, Approaching 22% efficiency with multicrystalline n-type silicon solar cells”, in: Proceeding of the 33rd European PV Solar Energy Conference and Exhibition, Amsterdam, The Netherlands, 2017, 25–29 September.

- [138] J. Benick, A. Richter, R. Müller, H. Hauser, F. Feldmann, P. Krenckel, S. Riepe, F. Schindler, M.C. Schubert, M. Hermle, A.W. Bett, S.W. Glunz, High-efficiency n-Type HP mc silicon solar cells, *IEEE J. Photovolt.* 7 (5) (2017) 1171–1175, <https://doi.org/10.1109/JPHOTOV.2017.2714139>.
- [139] F. Schindler, A. Fell, Müller R, J. Benick, A. Richter, F. Feldmann, P. Krenckel, S. Riepe, M.C. Schubert, S.W. Glunz, Towards the efficiency limits of multicrystalline silicon solar cells, *Sol. Energy Mater. Sol. Cells* 185 (2018) 198–204, <https://doi.org/10.1016/j.solmat.2018.05.006>.
- [140] M.C. Schubert, F. Schindler, J. Schön, W. Kwaplil, J. Benick, R. Müller, F.D. Heinz, A. Fell, S. Riepe, A. Morishige, Limiting defects in n-type multicrystalline silicon solar cells, *Phys. Status Solidi A* 216 (2019), 1900331, <https://doi.org/10.1002/pssa.201900331>.
- [141] C. Liu, D. Chen, Y. Chen, Y. Ling, Y. Zou, Y. Wang, J. Gong, Z. Feng, P. P. Altermatt, P.J. Verlinden, Industrial TOPCon solar cells on n-type quasi-mono Si wafers with efficiencies above 23%, *Sol. Energy Mater. Sol. Cells* 215 (2020), 110690 <https://doi.org/10.1016/j.solmat.2020.110690>.
- [142] H. Park, Y. Lee, S.J. Park, S. Bae, S. Kim, D. Oh, J. Park, Y. Kim, H. Guim, Y. Kang, H.S Lee, D. Kim, J. Yi, Tunnel oxide passivating electron contacts for high-efficiency n-type silicon solar cells with amorphous silicon passivating hole contacts, *Prog. Photovolt. Res. Appl.* (2019) 1–11, <https://doi.org/10.1002/pip.3190>.
- [143] C. Luderer, C. Reichel, F. Feldmann, M. Bivour, M. Hermle, Passivating and low-resistive poly-Si tunneling junction enabling high-efficiency monolithic perovskite/silicon tandem solar cells, *Appl. Phys. Lett.* 115 (2019), 182105, <https://doi.org/10.1063/1.5120552>.
- [144] W. Yoon, D. Scheiman, Y.W Ok, Z. Song, C. Chen, G. Jernigan, A. Rohatgi, Y. Yan, P. Jenkins, Sputtered indium tin oxide as a recombination layer formed on the tunnel oxide/poly-Si passivating contact enabling the potential of efficient monolithic perovskite/Si tandem solar cells, *Sol. Energy Mater. Sol. Cells* 210 (2020), 110482, <https://doi.org/10.1016/j.solmat.2020.110482>.
- [145] M. Verma, G.P. Mishra, An integrated GaInP/Si dual junction solar cell with enhanced efficiency using TOPCon technology, *Appl. Phys. A* 126 (2020) 661, <https://doi.org/10.1007/s00339-020-03840-8>, article id.
- [146] J. Melskens, B.W.H. van de Loo, B. Macco, L.E. Black, S. Smit, W.M.M. Kessels, Passivating contacts for crystalline silicon solar cells: from concepts and materials to prospects, *IEEE J. Photovolt.* 8 (2) (2018) 373–388, <https://doi.org/10.1109/JPHOTOV.2018.2797106>. March.
- [147] S. Mack, D. Herrmann, M. Lenes, M. Renes, A. Wolf, Progress in p-type tunnel oxide-passivated contact solar cells with screen-printed contacts, *Sol. RRL* (2021), 2100152, <https://doi.org/10.1002/solr.202100152> article id.